

UNIVERSITY OF COPENHAGEN

DEPARTMENT OF GEOSCIENCES AND NATURAL RESOURCES MANAGEMENT



## Master Thesis

Lotte Snedker Jensen

# Simulation of Flow and Transport at Field Site Faardrup

Submitted 10<sup>th</sup> of August 2020

Supervisor: Karsten Høgh Jensen (KU)

Co. Supervisors: Sachin Karan (GEUS) and Annette Rosenbom (GEUS)

**Geological Survey of Denmark and Greenland**

*Ministry of Energy, Utilities and Climate*



  
**GEUS**

*Name of department:* Department of Geosciences and Natural Resources Management (KU)

*Author:* Lotte Snedker Jensen (vsl219)

*Title:* Simulation of flow and transport at field site Faardrup

*Topic description:* The thesis project focuses on the simulation of flow and transport at a field site, which is part of the Danish Pesticide Leaching Assessment Program (PLAP), which is run by GEUS. A unique database is available from the site consisting of nearly 20 years of monitoring data, including climatic data, soil moisture, temperature, drain flow, groundwater levels, as well as a tracer, pesticide, and isotope concentrations. In addition, the site has been subject to a detailed geological characterization, and important hydraulic parameters have been measured. For simulating flow and transport, a complex simulation code HydroGeoSphere will be used. This code allows for consideration of all important flow and transport processes, including macropore and fractured flows, which are of relevance for this site. The code will be calibrated using the inverse code PEST. Supplementary field investigations will be carried out, including infiltration and permeameter tests and soil cores will be excavated for measurements of soil hydraulic parameters in the lab.

*Supervisor:* Karsten Høgh Jensen  
(IGN, Department of Geosciences and Natural Resources Management)

*Co. Supervisors:* Sachin Karan (GEUS, Geological Survey of Denmark and Greenland)  
Annette Rosenbom (GEUS, Geological Survey of Denmark and Greenland)

*Submission date:* 10<sup>th</sup> of August 2020

*ECTS:* 60

*Number of Characters:* 115,625

**Abstract**

Five different models were developed in HydroGeoSphere to simulate variably saturated flow and solute transport at Faardrup field site. Faardrup field site is located 8.5 km south of Slagelse in Denmark and is part of The Danish Pesticide Leaching Assessment Program (PLAP). PLAP is run by GEUS, who also provided data for this project. Four of the models are single-domain models, and one model is a dual-domain model with the second domain representing macropores. Three of these models were calibrated using the inverse calibration tool PEST. The accuracy of the models has been assessed by comparing simulated data against observed data for saturation, pressure head, and drain outflow. The models reached simulated saturation values closest to the observed values, but simulated pressure head and drain outflow values proved more problematic and did not reach a close resemblance. The dual-domain model needs further work to simulate the anticipated data. None of the models fall within any of the decided uncertainty limits and are not accurate enough for any form of practical use without further work.

## Table of content

1 Introduction .....	6
2 The Danish Pesticide Leaching Assessment Program (PLAP) .....	7
2.1 Faardrup field site .....	9
2.1.1 Geology.....	9
2.1.2 Technical installations .....	11
2.1.3 MACRO.....	14
3 Theory .....	15
3.1 Subsurface waters .....	15
3.1.1 Hydraulic head .....	16
3.1.2 Porous media .....	17
3.1.3 Soil water retention.....	19
3.2 Variably saturated flow .....	20
3.2.1 Preferential flow.....	21
3.2.2 Solute transport .....	22
3.3 Calibration.....	23
3.3.1 PEST.....	27
3.4 HydroGeoSphere .....	28
3.4.1 Water budget.....	28
3.4.2 Subsurface flow .....	29
3.4.3 Precipitation .....	31
3.4.4 Evapotranspiration .....	31
3.4.5 Free drainage and drains .....	33
3.4.6 Solute transport .....	34
3.4.7 Dual-continuum subsurface coupling.....	35
4 Method.....	37
4.1 Data .....	37
4.2 Model set-up .....	38
4.2.1 Validation .....	43
4.2.2 Solute transport .....	43
4.2.3 Dual-domain .....	43
4.3 Inverse calibration .....	44
5 Results.....	47

5.1 Model A - Manual calibrated.....	48
5.2 Model B - Inverse calibrated.....	53
5.3 Model C - Inverse calibrated (not completed).....	57
5.3.1 Model C - Validation.....	61
5.3.2 Model C - Solute transport.....	63
5.4 Model D - Inverse calibrated (not completed).....	66
5.5 Model E - Dual-domain.....	70
6 Fieldwork.....	72
7 Discussion.....	74
8 Conclusion.....	80
9 Future work.....	81
Acknowledgments.....	82
References.....	83
Appendix.....	85
Appendix 1 - Model A.....	85
Appendix 2 - Model B.....	88
Appendix 3 - Model C.....	92
Appendix 4 - Model D.....	95
Appendix 5 - Model E.....	99
Appendix 6 - Fieldwork.....	102
Appendix 7 - Input files to HydroGeoSphere.....	105

## 1 Introduction

The purpose of this thesis is to develop a model in the program HydroGeoSphere (HGS) (Therrien, McLaren, Sudicky, & Panday, 2010) to simulate water flow and transport at the Faardrup field site (Figure 1) in Denmark. Field site Faardrup is one of 6 fields that make up the Pesticide Leaching Assessment Program (PLAP). PLAP is run by GEUS and was established in 1998. The purpose of PLAP is to monitor if pesticides used in farming, or their degradation products, leach to the groundwater in concentrations that could endanger the groundwater resource (Lindhardt, et al., 2001). In Denmark, drinking water is extracted exclusively from groundwater (Miljøstyrelsen, 2020), and it is, therefore, essential to protect it from pollution by pesticides used in agriculture. PLAP is used to identify these pesticides and is an essential instrument since laboratory experiments are not always adequate (Lindhardt, et al., 2001).

The PLAP project contains a database of nearly 20 years of monitoring data, including climatic data, soil moisture, temperature, drain flow, groundwater levels, as well as bromide tracer experiments, pesticide, and isotope concentrations. For each of the PLAP fields, geological investigations were conducted, which resulted in detailed geological descriptions of each field.

In this project, the data from the Faardrup field site has been used to develop a variably saturated flow model in the modeling program HydroGeoSphere, representing this field.

HydroGeoSphere was developed by Dr. Edward Sudicky, Dr. Peter Forsyth, and Dr. Rene Therrien and is a fully-integrated 3D surface and subsurface flow simulator. The HydroGeoSphere code accounts for all important mechanisms of the hydrologic cycle (Therrien, McLaren, Sudicky, & Panday, 2010).

HydroGeoSphere allows for the integration of a second domain, that could represent macropores and thereby allow the simulation of preferential flow. This is important for the Faardrup field site due to its clayey till soils with many macropores.

The tool PEST (Doherty, 2018) was used to inverse calibrate the HydroGeoSphere model. The HydroGeoSphere model has then been evaluated against observed data for drain flow, pressure head, and saturation at different depths.

## 2 The Danish Pesticide Leaching Assessment Program (PLAP)

In Denmark, The Danish National Groundwater Monitoring Program (GRUMO) has the task of monitoring the quality of danish groundwater (Thorling & Kjøller, 2020). This is done by collecting water samples from more than 1,000 monitoring wells throughout the country. These water samples are, among other things, examined for pollution by pesticides. GRUMO results have shown that pesticides or their degradation products are present in approximately 30% of the monitoring wells. The Pesticide Leaching Assessment Program (PLAP) was established in 1998 to better understand the characterization of the leaching that might occur under actual field conditions. The objective of PLAP is to monitor if pesticide or their degradation products, if applied as permitted by the law, leach to the groundwater under actual field conditions. The results are compared to the criterium for drinking water quality of 0.1 µg/l (Lindhardt, et al., 2001). PLAP is used as an early warning system for unacceptable concentrations of pesticide leaching. It warns against specific pesticides, which could cause a threat to the groundwater quality even if used as permitted (Rosenbom, et al., 2017).

PLAP consists of 6 fields that were selected in 1999, with monitoring initiated between May 1999 and April 2000. The locations of the selected fields are shown in Figure 1. The original field in Slaeggerup has since been shut down, and a new field in Lund was added in 2017 (Lindhardt, et al., 2001).

The field in PLAP was selected based on various parameters to ensure the field is representative of the climate conditions and dominant soil types in Denmark. The most important parameters controlling that pesticide leaching is considered to be soil type and climate conditions. Parameters such as size, site access, and the drainage system, needed to be considered for practical reasons (Lindhardt, et al., 2001). It was important that the drainage system was established years prior since digging to establish a new system could destroy existing structures in the soil (Nimmo, 2004). The chosen fields had to have a shallow groundwater table to ensure rapid detection. The cultivation of the fields is done by conventional agricultural practice in the surrounding area, and the pesticides were used in maximum doses according to regulations (Lindhardt, et al., 2001).

For each PLAP field, a hydrological model of the variably-saturated zone was set up in the program MACRO (Larsbo, Roulier, Stenemo, Karsteel, & Jarvis, 2005) and is used to describe the soil water dynamics at each location (Lindhardt, et al., 2001).

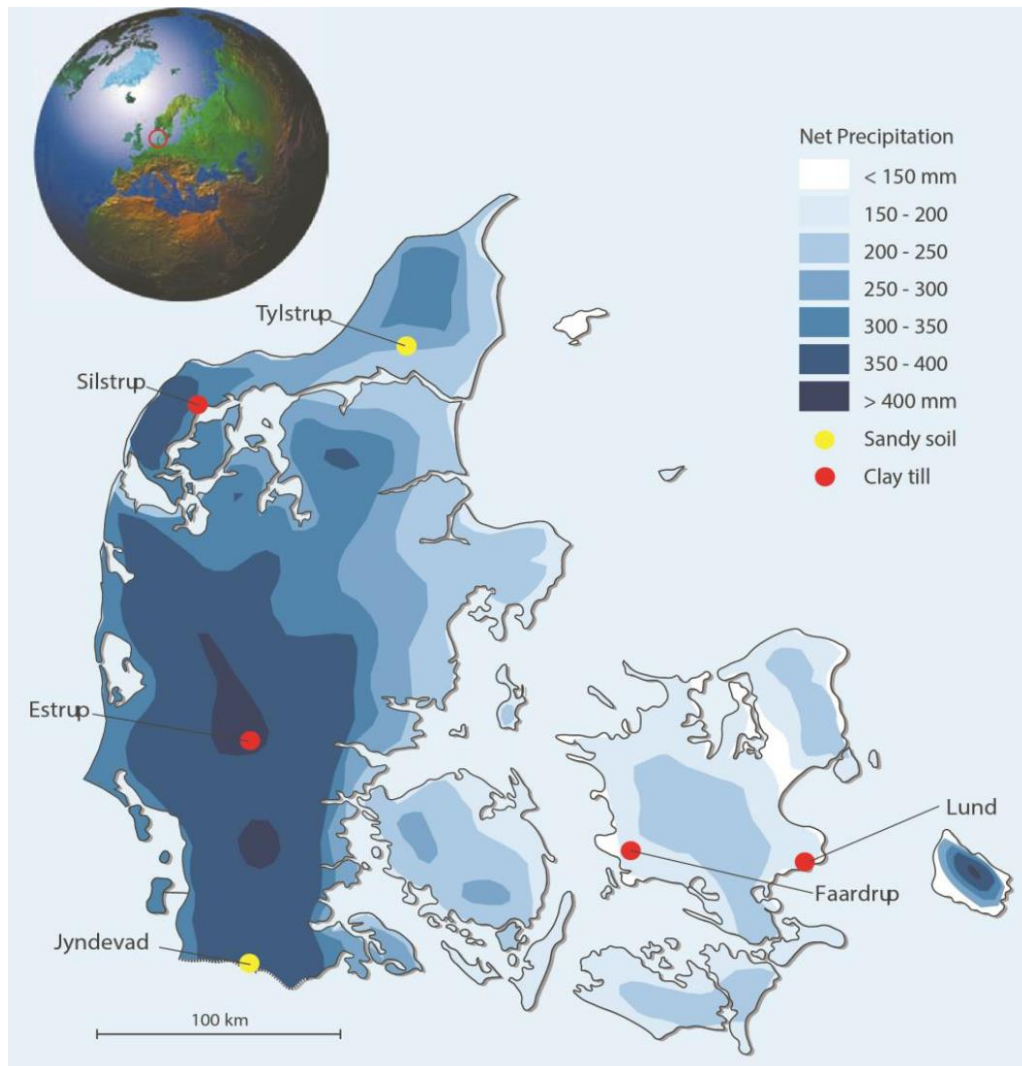


Figure 1: Geographical location of the PLAP fields and net precipitation in Denmark. The fields Tylstrup (sandy), Silstrup (clayey till), Estrup (clayey till), Jydevad (sandy), Faardrup (clayey till), and Lund (clayey till) added in 2017 was selected to represent the different span of net precipitation across the country. (Rosenbom, et al., 2017)

## 2.1 Faardrup field site

The Faardrup test field is located 8.5 km south of Slagelse on Zealand. The land registration no. is 6a, Fårdrup By, Fårdrup. The land is privately owned and leased by the Danish Institute of Agricultural Sciences (DIAS). The field covers an area of 150 x 160 m (2.3 ha) and has a buffer zone between 11 m and 17 m in all directions (Rosenbom, et al., 2017). Before the PLAP project, the field was used as conventional farmland since 1940 (Lindhardt, et al., 2001).

### 2.1.1 Geology

At the Faardrup test field, the geology is dominated by Weichselian deposits of clay till to a depth of more than 18 m. The term till or glacial till is used to describe unsorted material deposited by glacial ice (Larsen & Sand-Jensen, 2017). The regional meltwater aquifer is located approx. 15-25 m b.g.s. The ground is covered by 0.3-0.4 m clayey topsoil characterized as sandy loam with many worm-holes and root channels. The saturated hydraulic conductivity is ranging from  $10^{-6}$ - $10^{-3}$  m/s.

The upper part of the till (approx. 0.4-1.8 b.g.s.) has a clay content of about 12 % and is classified as sandy-clayey till. The till contains sand lenses and is non-calcareous. This upper part of the till is very weathered, bioturbated, and fractured. The numerous desiccation cracks decrease with depth, as well as the number of borrow and root channels also decrease in number with depth. The saturated hydraulic conductivity is ranging from  $10^{-5}$ - $10^{-3}$  m/s.

From 2-4.2 m b.g.s. the clayey till is oxidized and calcareous. At this level, the till is dominated by many horizontal to sub-horizontal fractures and a few large fractures which penetrate as deep as 5 m b.g.s. and possible further. The saturated hydraulic conductivity is ranging from  $10^{-6}$ - $10^{-5}$  m/s for the upper 1.5 m while  $10^{-9}$  m/s in the lower part.

From 4-18 m b.g.s. the calcareous clay till is reduced and contains sand lenses and layers of sandy till. There are few large fractures both in a sub-horizontal direction and a vertical direction. The saturated hydraulic conductivity at 5.0 m b.g.s.  $10^{-9}$  is m/s.

Information from boreholes around the field shows that even though the area is dominated by clayey till it also contains meltwater clay and sand (see Figure 2) from small channels or basins interbedded in the till but also as a large structure crossing the field (Lindhardt, et al., 2001).

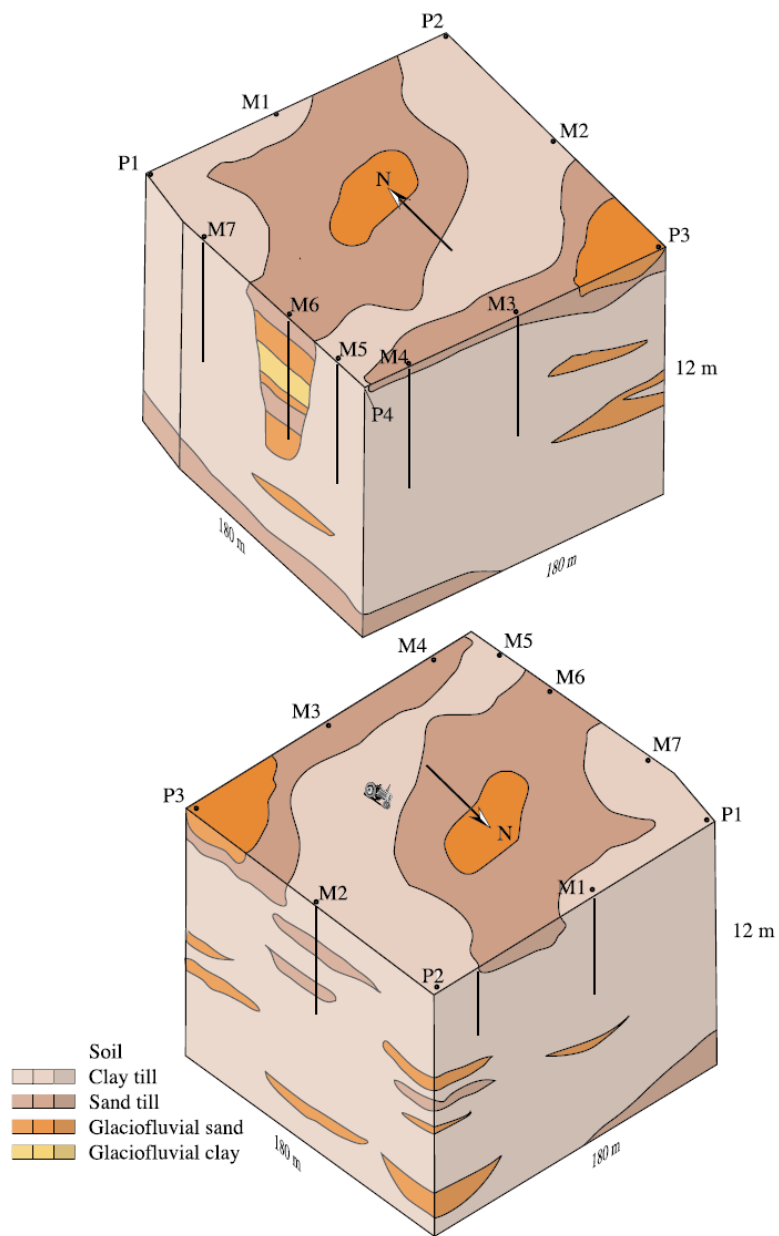


Figure 2: A geological model for the Faardrup field site. The geological model was built from borehole information. The location of the borehole/wells are shown in Figure 3 (Lindhardt, et al., 2001)

### 2.1.2 Technical installations

All construction work on the field was done during April and May 1999, and all installations can be seen in Figure 3.

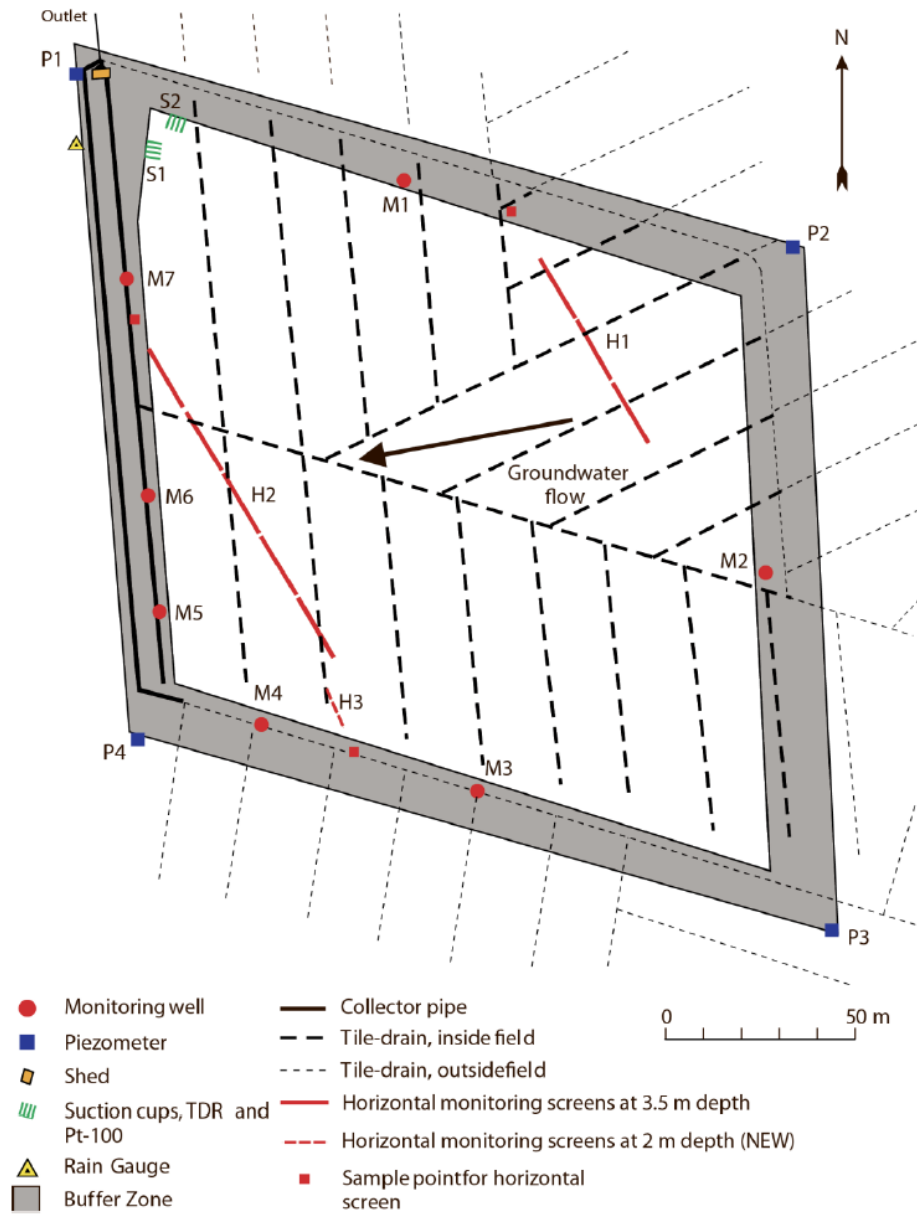


Figure 3: Overview of the technical installations at the Faardrup field site. The direction of the groundwater flow is shown with an arrow (Lindhardt, et al., 2001).

The existing traditional drainage system was installed in 1944. When the field was selected for the PLAP project, the drainage system was sealed off to isolate the drain water from the field. The drain water led to the monitoring chamber in the northwestern corner of the field by a collector pipe. Drain water from outside the field is led around this system. The drains are placed 1.1 m b.g.s.

In each corner of the fields buffer zone, four clusters of piezometers were installed (see Figure 4). The clusters consist of three screens of 0.5 m distributed over depths from 1.5-13.2 m b.g.s. (see Table 1).

Measurements from these piezometers are done manually once a month. In summer 1999, data showed that the groundwater flow direction was towards the west (Lindhardt, et al., 2001).

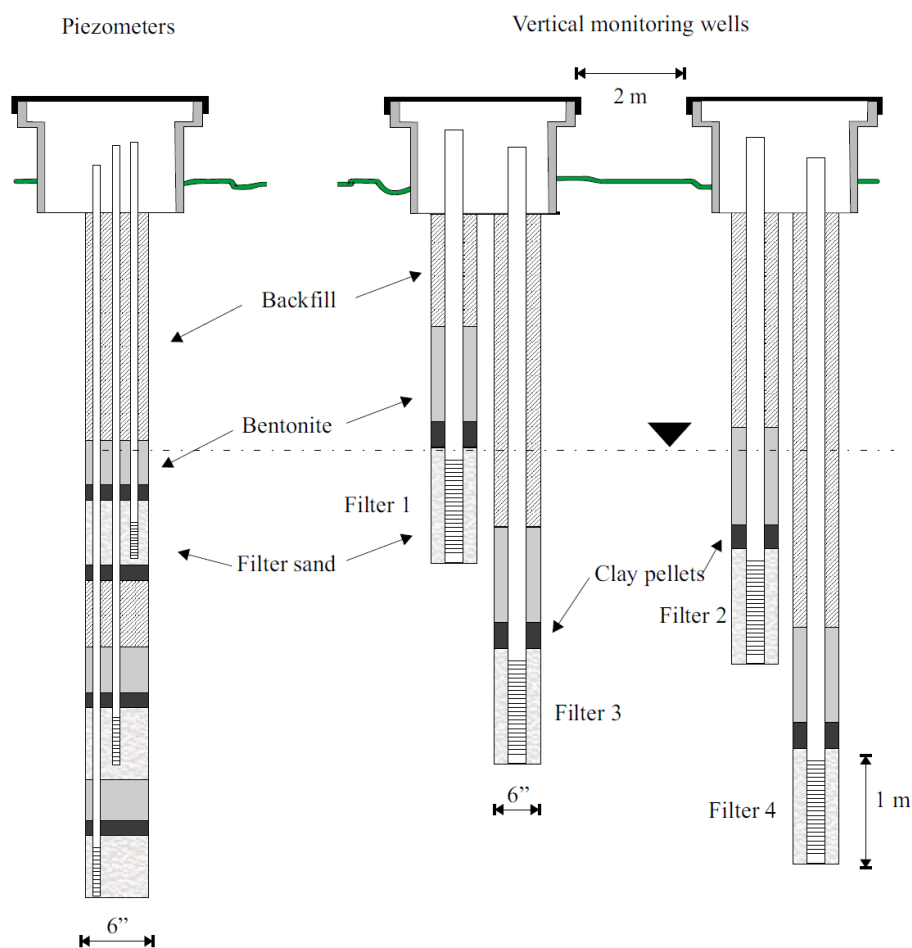


Figure 4: Construction set-up of a multiple-level piezometer and monitoring well at the Faardrup field site. (Lindhardt, et al., 2001)

Table 1: Name of piezometers and depth of screens at the Faardrup field site (Lindhardt, et al., 2001).

Piezometer	DGU no.	Upper screen m b.g.s.	Middle screen m b.g.s.	Lower screen m b.g.s.
P1	215. 920	2.5–3.0	6.5–7.0	10.5–12.0
P2	215. 963	3.0–3.5	5.5–6.0	9.3–9.8
P3	215. 964	2.5–3.0	6.2–6.7	12.7–13.2
P4	215. 965	3.0–3.5	5.5–6.0	11.6–11.9

The monitoring wells are grouped into seven clusters of four, and most wells are placed downstream. The monitoring wells have 1 m screens and each cluster have a screen in 1.5-2.5 m b.g.s., 2.5-3.5 m b.g.s, 3.5-4.5 m b.g.s and 4.5-5.5 m b.g.s. (see Table 1). At Faardrup also two horizontal monitoring wells were installed because the sandy lenses seen in Figure 1 can cause lateral flow.

In the unsaturated zone, the soil water is under tension and cannot flow to a well as it does in the saturated zone. Soil water monitoring in the unsaturated zone, therefore, requires the use of suction cups. At two different locations, eight suction cups were installed, four at 1 m b.g.s. and four 2 m b.g.s. This was done from two excavation pits at the edge of the field.

The soil water content is measured in the depths of 0.25, 0.6, 0.9, 1.1, 1.9, and 2.1 m b.g.s. This is done using the CR10X-controlled Time Domain Reflectometry (TDR) system. The accuracy of these measurements is around  $\pm 1$  vol %. Also, the soil temperature is measured in different depths in the same two locations as the TDR and suction cups (Lindhardt, et al., 2001).

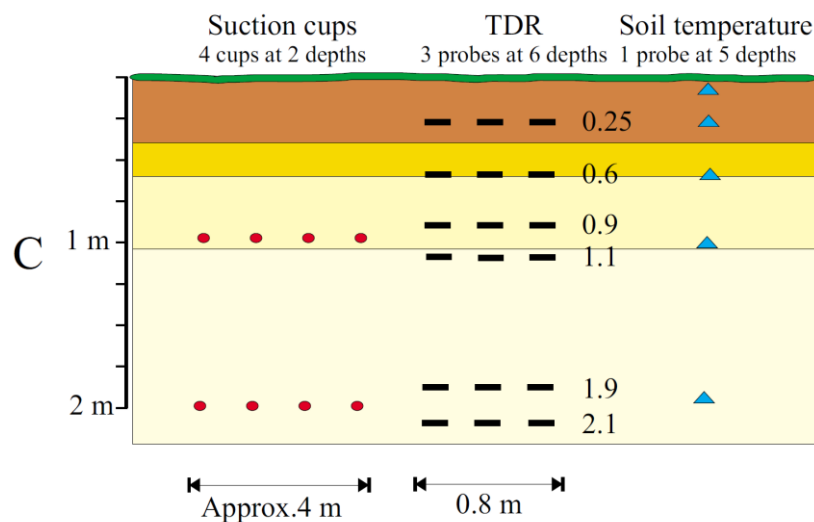


Figure 5: A plan view of an excavation wall indicating the location of suction cups, TDR, and temperature probes installed at the PLAP fields (Lindhardt, et al., 2001).

### **2.1.3 MACRO**

The data from the PLAP project test fields were used in the numerical model MACRO (Larsbo, Roulier, Stenemo, Karsteel, & Jarvis, 2005) to simulate the water flow in the variably-saturated zone and establish an annual water balance. At Faardrup, the model was set up for the period September 1999 - June 2016 with a soil profile down to 5 m b.g.s.

The model was calibrated for the period 1999 - 2004 and validated for the period 2004 - 2016 using the time series for observed groundwater table measured in piezometers, the water content in the depths 25, 60, and 110 cm b.g.s. and measured drainage (Rosenbom, et al., 2017).

### 3 Theory

#### 3.1 Subsurface waters

The subsurface waters are separated into two primary categories: the unsaturated zone and the saturated zone (Figure 6). The two zones are separated by the water table, which is technically defined as the surface where the pore water pressure is equal to atmospheric pressure (Fitts, 2012). The unsaturated zone, also called the vadose zone, lies above the water table, and the pores between the grains are only partially filled with water. The remaining pore space is filled with the gaseous phase (Šimůnek & van Genuchten, 2017). The water in the unsaturated zone is called soil water. In the saturated zone, the mineral surfaces attract the water by capillary forces causing the water pressure to be less than atmospheric pressure. The saturated zone, which lies below the water table, the pores are fully saturated with water, and the water pressure is greater than atmospheric pressure. The capillary fringe is a saturated zone above the water table, which can occur primarily in media with a small pore size due to capillary forces (Fitts, 2012).

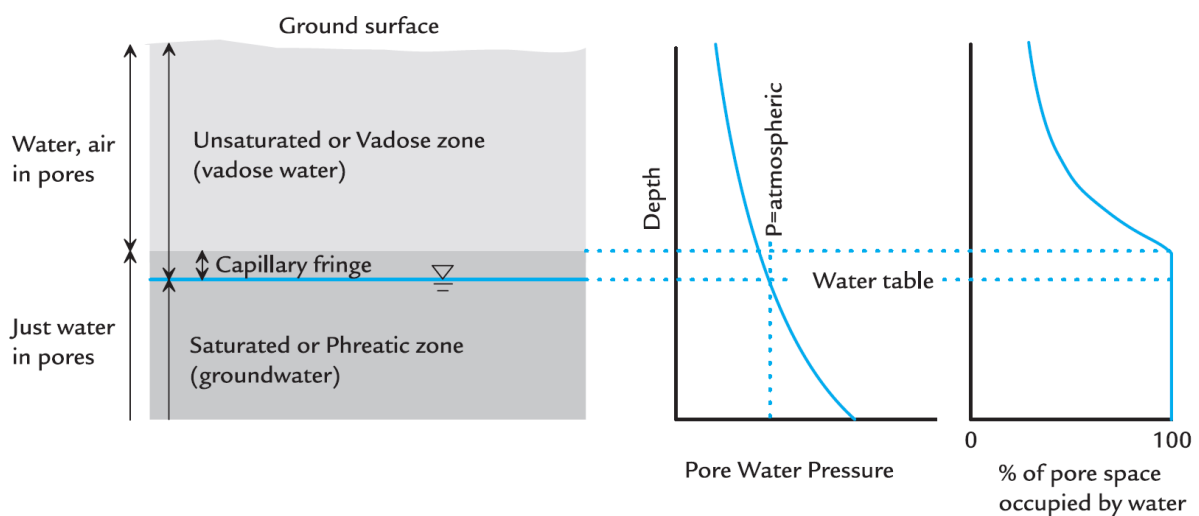


Figure 6: A vertical cross-section of the subsurface showing the terms used to describe subsurface waters (Fitts, 2012).

Water enters the unsaturated zone by precipitation or irrigation on fields (Figure 7). Not all of the rainfall enters the soil because of interception from plant and evapotranspiration. If the infiltration capacity is lower than the rainfall and irrigation intensity, the excess water will be removed by runoff or evaporate. Water in the unsaturated zone, which is not removed by plant roots may percolate deeper down and reach the saturated zone (Šimůnek & van Genuchten, 2017).

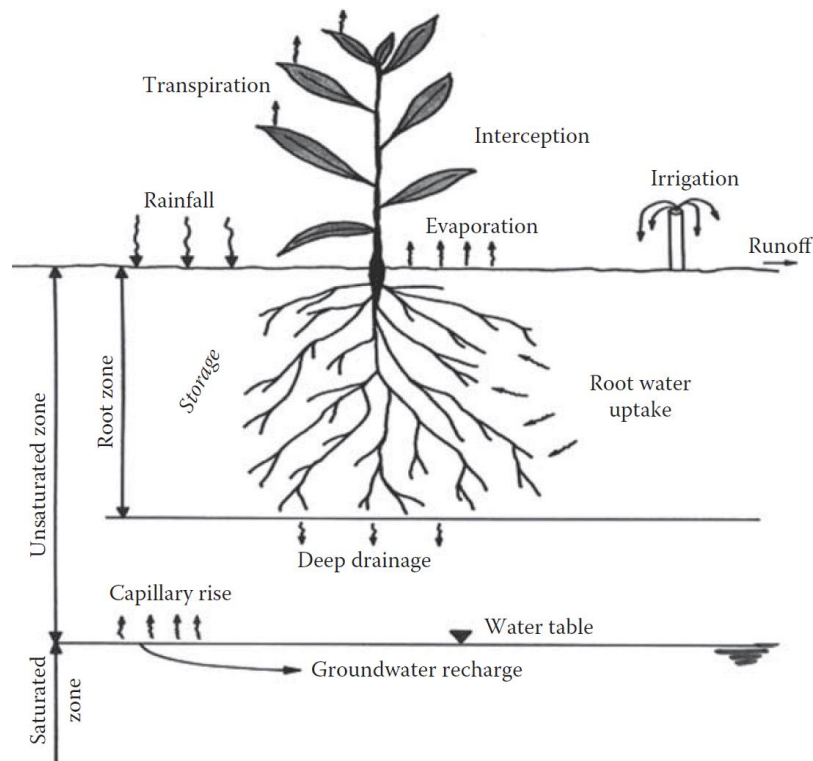


Figure 7: Conceptual schematic showing the water fluxes and various hydrological components in the unsaturated zone (Šimůnek & van Genuchten, 2017).

### 3.1.1 Hydraulic head

In the saturated zone, the hydraulic head equals the sum of the elevation head and the pressure head (Figure 8):

$$h = z + \frac{p}{\rho g} \quad (1)$$

where  $z$  is the elevation head [L] and  $\frac{p}{\rho g}$  is the pressure head [L]. The pressure head consists of the pressure  $p$  divided by water density  $\rho$  and acceleration due to gravity  $g$  (Hendriks, 2010). At a free air/water interface in the ground, the pressure head is defined as zero, and therefore the pressure head is zero at the water table if it establishes itself freely (Hendriks, 2010). In hydrostatic conditions, the hydraulic head can be measured directly in a well or a piezometer (Fitts, 2012).

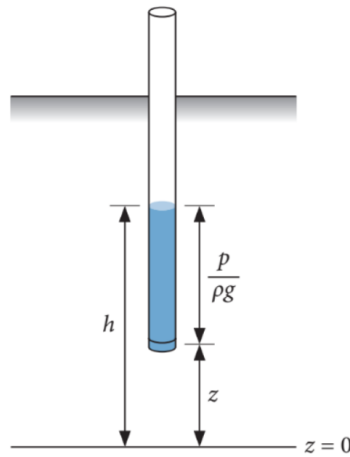


Figure 8: Schematic showing how hydraulic head  $h$ , pressure head  $\frac{p}{\rho g}$ , and elevation head  $z$  are defined in a piezometer (Hendriks, 2010).

### 3.1.2 Porous media

In porous media, the porosity of the soil,  $n$ , is pore space fraction of the total volume of material:

$$n = \frac{V_v}{V_t} \tag{2}$$

Where  $V_v$  is the volume of voids and  $V_t$  is the total volume of material. In a material like sand, the porosity is mostly dominated by the pore space between the mineral grains. Different geological materials have different porosity (Table 2). In unconsolidated clayey soils fractures though the medium is also a very important component of the porosity because even though the fracture porosity may be small, most of the water flow may occur in these fractures (Fitts, 2012).

Table 2: Typical values of porosity in different geological materials (Fitts, 2012)

Typical values of porosity	
Material	n [%]
Narrowly graded silt, sand, gravel	30-50
Widely graded silt, sand, gravel	20-35
Clay, clay-silt	35-60
Sandstone	5-30
Limestone, dolomite	0-40
Shale	0-10
Crystalline rock	0-10

Grain size is the key characteristic when determining the name of the material (Table 3). In general, most soils consist of a mixture of different materials, and the texture can then be determined by the percentage of clay, silt, and sand (Figure 9) (Haverkamp, Debionne, Angulo-Jaramillo, & de Condappa, 2017).

Table 3: U.S. Department of Agriculture grain size definitions (Fitts, 2012).

Material	Grain size range [mm]
Clay	< 0.002
Silt	0.002 - 0.05
Sand	0.05 - 2.0
Gravel	> 2.0

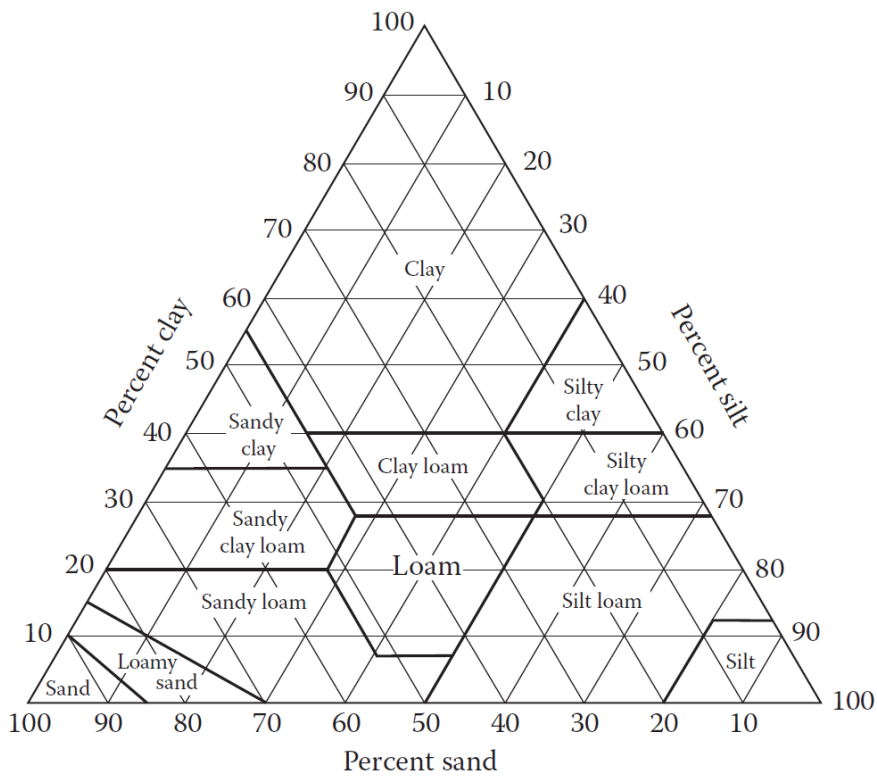


Figure 9: U.S. Department of Agriculture soil textural classification chart showing the percentages of clay, silt, and sand (Haverkamp, Debionne, Angulo-Jaramillo, & de Condappa, 2017).

The water content is the fraction of water occupied space:

$$\theta = \frac{V_w}{V_t} \quad (3)$$

Where  $V_w$  is the volume of water and  $V_t$  is the total material volume. If the soil is saturated, then the water content will be equal to the porosity (Fitts, 2012).

### 3.1.3 Soil water retention

Soil water characteristic or water retention curves define the relationship between water content ( $\theta$ ) and soil matric potential, also called matric suction ( $\psi$ ) (Benson & Sawangsuriya, 2014). When adding water to dry soil, the smaller pores will suck water first (at high suction), and later the larger pores will fill with water (at low suction) when the soil becomes quite wet. Likewise, the water in wet soil will drain from the larger pores first (at low suction) and the smaller pores later (at high suction). This is because smaller pores have a larger suction power than the larger pores and therefore have a better hold on the water. The water held in a specific soil at different matric pressures, therefore, depends on the pore size distribution and is strongly affected by soil texture and structure (Hendriks, 2010) (Nimmo, *Vadose Water*, 2009) (Tuller & Or, 2005).

The matric potential ( $\psi$ ) is equivalent to the pressure head (with a negative sign) in saturated soils. Water retention curves for different soil types are shown in Figure 10 (Tuller & Or, 2005).

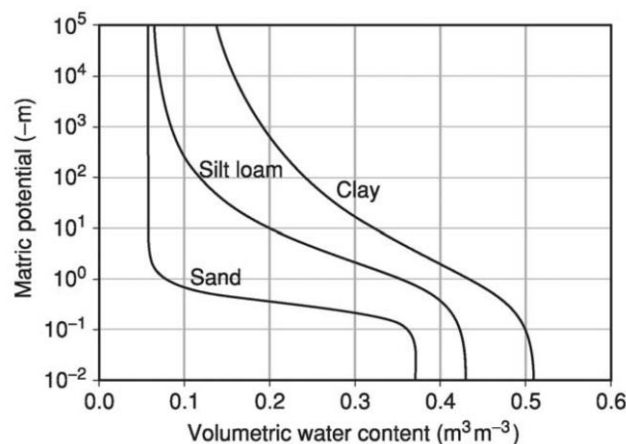


Figure 10: Typical soil-water characteristic (retention) curves for soils of different texture (sand, silt loam, and clay) (Tuller & Or, 2005).

Figure 10 shows that clay soils have a higher matric potential or suction than sandy soils with the same water content have. This is due to different water binding forces in the two soil types and because clay has a higher porosity and larger pore size distribution than, for example, well-sorted sand (Hendriks, 2010).

The shape of the water retention curves seen in Figure 10 are generally defined using Van Genuchten's equation (Benson & Sawangsuriya, 2014):

$$\theta(\psi) = \theta_r + \frac{\theta_s - \theta_r}{[1 + (\alpha\psi)^n]^{1-1/n}} \quad (4)$$

Where  $\theta(\psi)$  is the water retention curve,  $\theta_s$  is the saturated water content,  $\theta_r$  is the residual water content,  $\alpha$  is related to the inverse of the air entry suction, and  $n$  (also called  $\beta$ ) describes the slope of the curve (Benson & Sawangsuriya, 2014).  $\alpha$  and  $\beta$  are Van Genuchten fitting parameters that determine the shape of the curve and the values for  $\alpha$  and  $\beta$  are estimated through laboratory testing. Commonly used model values for  $\alpha$  and  $\beta$  for different soil types can be found in (Carsel & Parrish, 1988). Soils with larger pores have larger  $\alpha$  and soils with broader distribution of pore size have lower  $\beta$  (Benson & Sawangsuriya, 2014). So, for clayey soil, generally, both  $\alpha$  and  $\beta$  would be lower than for sandy soil (Carsel & Parrish, 1988).

### 3.2 Variably saturated flow

Traditionally the variably saturated flow in soils is described by Richards equation that combines the Darcy-Buckingham equation for fluid flow with a mass balance equation. For water flow in variably saturated soil, the mass balance equation is often formulated:

$$\frac{\partial \theta}{\partial t} = -\frac{\partial q_i}{\partial x_i} - S \quad (5)$$

Where  $\theta$  is the water content,  $t$  is time,  $x_i$  is the spatial coordinate,  $q_i$  is the flux density, and  $S$  is a general sink/source term, for example, to account for root water uptake. Equation 5 states that a change in water content or storage in a given volume happens because of spatial changes in the water flux. These changes can be fluxes in or out of the system or sinks or sources within the system. The mass equation has to be combined with an equation describing the volumetric flux density ( $q$ ),

to produce a governing equation for variably saturated flow. For uniform flow, this could be the extension of Darcy's law, the Darcy-Buckingham equation (Hendriks, 2010) (Šimůnek & van Genuchten, 2017):

$$q_i = -K(h) \left( K_{ij}^A \frac{\partial h}{\partial x_i} + K_{iz}^A \right) \quad (6)$$

Where  $K$  is the unsaturated hydraulic conductivity [ $LT^{-1}$ ] and  $K_{ij}^A$  are components of a dimensionless anisotropy tensor  $K^A$  (which reduces to the unit matrix when the medium is isotropic). In Darcy's equation  $K(h)$  is a constant equal to the saturated hydraulic conductivity,  $K_s$ , but in Darcy-Buckingham (equation 6)  $K(h)$  (unsaturated hydraulic conductivity) is a nonlinear function of the pressure head (Šimůnek & van Genuchten, 2017).

Combined equation 5 and 6 leads to the general Richards equation:

$$\frac{\partial \theta(h)}{\partial t} = \frac{\partial}{\partial x_i} \left[ K(h) \left( K_{ij}^A \frac{\partial h}{\partial x_i} + K_{iz}^A \right) \right] - S(h) \quad (7)$$

which is the partial differential equation governing variably saturated flow in the vadose zone (Šimůnek & van Genuchten, 2017).

### 3.2.1 Preferential flow

The Richards equation (equation 7) typically periodic uniform water flow patterns, but many field soils are not consistent with this uniform flow pattern (Šimůnek & van Genuchten, 2017). In Richards equation (equation 7), only matrix flow is considered, but in reality, large parts of the water flow through vertical preferential pathways. These pathways can consist of cracks, root holes, or worm-holes, which effectively causes the water to bypass the soil matrix as it infiltrates to the groundwater (Hendriks, 2010). Preferential flow causes irregular wetting of the soil profile because water moving faster in some areas of the soil profile. Preferential flow causes water and solutes to infiltrate deeper and faster than it can be predicted with Richards equation describing uniform flow. Macropores are one of the most important causes of preferential flow (Šimůnek & van Genuchten, 2017). Macropores

are pores with a diameter larger than 30  $\mu\text{m}$  can be caused by biological activity like root channels or wormholes or by geological forces causing cracks and fracturing (Hendriks, 2010). Preferential pathways usually only make up a small fraction of the total matrix but can participate in large parts of the water flow. This can reduce the potential of the soil to absorb and degrade pollutants and thereby make the groundwater more vulnerable to pollution (Hendriks, 2010).

### 3.2.2 Solute transport

For water flow, the mathematical formulation for solute transport are usually based on a mass balance equation:

$$\frac{\partial C_t}{\partial t} = -\frac{\partial J_{Ti}}{\partial x_i} - \phi \quad (8)$$

Where  $C_t$  is the total concentration of the chemical in all forms [ $\text{ML}^{-3}$ ],  $t$  is time,  $x_i$  is the spatial coordinate and  $J_{Ti}$  is the total chemical mass flux density (mass flux per unit area per unit time) [ $\text{ML}^{-2}\text{T}^{-1}$ ]. The reaction term  $\phi$  is the rate of change of mass per unit volume [ $\text{ML}^{-3}\text{T}^{-1}$ ] by reactions that lead to a loss or gain of chemical in the soil system (Šimůnek & van Genuchten, 2017).

If a solute is present in both the gaseous and liquid phase, the various transport processes contribute to the total chemical flux:

$$J_T = J_l + J_g \quad (9)$$

Where  $J_l$  represent the transport processes in the liquid phase and  $J_g$  represent the transport processes in the gaseous phase. (Šimůnek & van Genuchten, 2017)

Three main solute transport processes can be active in both the gaseous and liquid phases: diffusion, dispersion, and advection. Diffusion is the random motion of chemical molecules that causes the solute to move from a place with a high concentration to a place with a lower concentration. Dispersion is caused by uneven water flow velocities within and between soil pores and results in an uneven dispersion of a solute. Advection is the processes where solutes are being transported with the water movements (Fitts, 2012) (Šimůnek & van Genuchten, 2017). In both the Gaseous and liquid phase  $J_l$  and  $J_g$  are equal to the sum of these three processes:

$$J_l = J_{lc} + J_{ld} + J_{lh} \tag{10}$$

$$J_g = J_{gc} + J_{gd} + J_{gh}$$

Where  $c$  is advection,  $d$  is diffusion, and  $h$  is the dispersion (Šimůnek & van Genuchten, 2017).

### 3.3 Calibration

Manual calibration, also called trial-and-error estimation, is more or less random and is done by manually changing the parameter values. The simulated values are then compared to the observed data. How good this form of calibration work depends, among other things, on the modeler's knowledge and experience. This method can give the modeler an idea of in what direction the parameters have to be moved to get at a better result. But a systematic manual calibration can, depending on the number of parameters, require numerous model runs and long simulation time because each model has to run and be compared to observed data manually.

Inverse calibration is an automatic calibration method used to carry out automatic optimizations of selected parameters. The inverse calibration has many advantages as it automatically finds the parameter values which gives the best fit between simulated and observed data. It also gives information about the quality of the calibration, calculates confidence intervals of the estimated parameters, and identifies parameter correlation and sensitivity of each parameter (Sonnenborg & Henriksen, 2005). Inverse calibration can be illustrated, as shown in Figure 11.

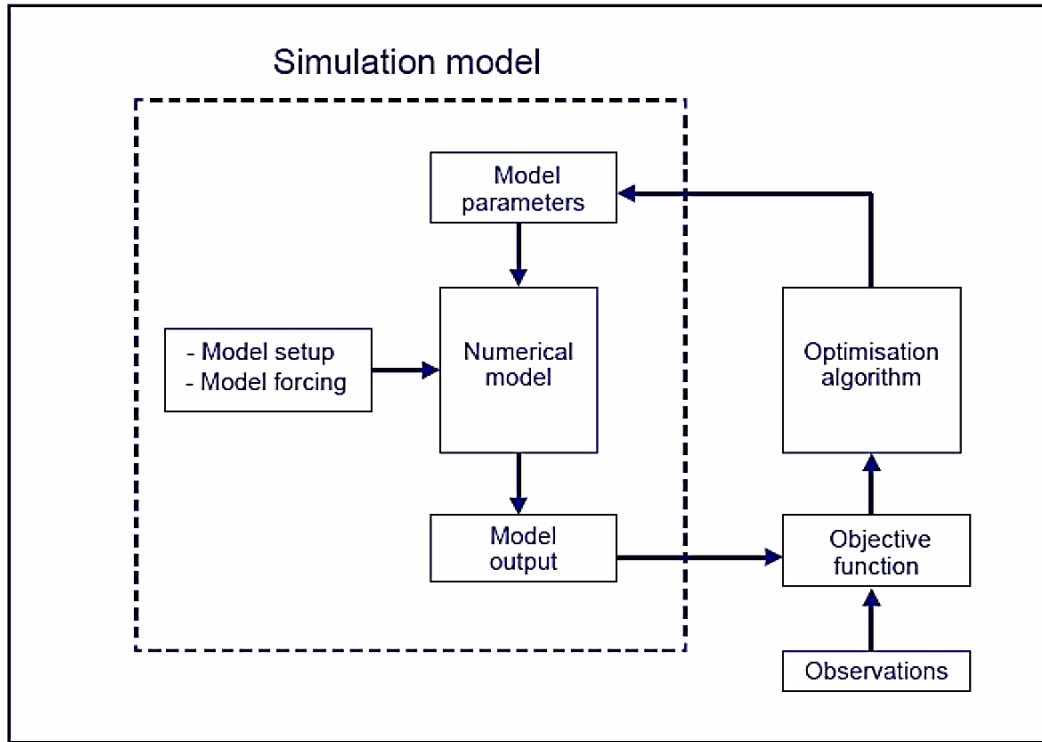


Figure 11: Schematic of the inverse calibration process (Sonnenborg & Henriksen, 2005).

Figure 11 shows how the simulation model and the optimization algorithm are connected during inverse calibration. The simulation model consists of the numerical model, in this case HGS, which contains model set-up and model forcing. In this case, the model set-up is the boundary conditions and conceptual model, and the model forcing is input data like observed ET and precipitation. The model parameters are the parameters that the model is allowed to change to get a better fit between simulated and observed data.

In the parameter estimation, the objective function,  $G$ , is a measurement for the deviation between the simulated and observed values. The difference between a measurement and a model output for this specific measurement is called a residual.  $G$  is the weighted sum of the squared of the residuals  $r_i = \psi_{obs,i} - \psi_{sim,i}$  where  $\psi_{sim,i}$  is the simulated value and  $\psi_{obs,i}$  is the observed value.  $\Psi$  is a variable from the model.  $G$  is defined as:

$$G(\underline{b}) = \sum_{i=1}^n w_i r_i^2 \tag{11}$$

Where  $\underline{b}$  is the vector of the calibration parameters and  $w_i$  is the weight of the individual residual (Sonnenborg & Henriksen, 2005).

The weight of data can be done both within the same data group or between data groups. The weighing of data within a data group, it is possible to optimize the model by assigning a higher weight to measurements with low uncertainty and a lower weight to measurements of high uncertainty. With the inverse calibration is possible to weight the data within the same group based on the uncertainties is by appointing the residuals a weight that is inversely proportional to the variance of the error on the residuals,  $\sigma^2$ :

$$w_i = \frac{1}{\sigma_i^2} \quad (12)$$

There is often more than one type of observed measurement to calibrate against, and if all measurements in all groups are weighted the same, then the group with the most measurements will dominate the optimization.

If there are two types of measurements, the two groups can be assigned an equal weight by:

$$G = v_1 G_1 + v_2 G_2 \quad (13)$$

Where  $G_1$  and  $G_2$  are objective function for each group and  $0 \leq v_i \leq 1$  and  $\sum v_i = 1$ . Estimation of the weight for each group can be done by weighing with the number of observations available within the various data types:

$$v_i = \frac{N_i}{N} \quad (14)$$

Where  $N_i$  is the number of observations of data type  $i$  and  $N$  is the total number of observations.

When doing the inverse calibration, it is possible to perform a sensitivity analysis. This is an analysis of the simulation results sensitivity due to changes in the calibration parameters. It shows which parameters have the most significant impact on the simulation results. The sensitivity analysis also gives a correlation matrix. The correlation matrix shows the correlation coefficient between all the model parameters. If two parameters have a close to 1 or -1, it can be difficult for the inverse

calibration to give a unique value for the correlated parameters, and it can cause problems when running the calibration. A guideline rule says that when two parameters have a correlation coefficient higher than 0.95, one of the parameters should be taken out of the calibration. Which one can be determined by looking at the sensitivity analysis where the parameter with the lowest sensitivity of the two should be left out of the calibration (Sonnenborg & Henriksen, 2005).

When evaluating how good a model is, different performance criteria can be used besides the visual comparison of the observed and simulated data. The RMSE (root mean squared error) is the most commonly used term to determine the fit between simulated and observed data. RMSE is defined as:

$$RMSE = \sqrt{\frac{1}{n} \sum_{i=1}^n (\psi_{obs,i} - \psi_{sim,i})^2} \quad (15)$$

Where  $\psi_{sim,i}$  is the simulated values and  $\psi_{obs,i}$  is the observed values.  $n$  is the number of observations, and  $r$  is the residuals for a given datatype (Sonnenborg & Henriksen, 2005).

To evaluate the model's ability to simulate average drain output  $F_{bal}$  (%) can be calculated:

$$F_{bal} = 100 \frac{\overline{Q_o} - \overline{Q_s}}{\overline{Q_o}} \quad (17)$$

Where  $Q_o$  and  $Q_s$  the average flow for the observed and simulated data (Sonnenborg & Henriksen, 2005).

### 3.3.1 PEST

The modeling code PEST (parameter estimation) can be used to carry out inverse calibrations. PEST expedites the process of model calibration, and model parameters are automatically back-calculated by fitting simulated data to observed data. In the calibration, PEST seeks to minimize the objective function. PEST operates independently of the model and interacts with the model through the model's output and input files. This makes PEST useful in this case where the model is built in HGS. When running in parameter estimation mode or computing sensitivities, it runs the model many times. PEST is run from the master folder and has several subfolders from where each model is run. Each subfolder runs one model at the time, but the number of subfolders is limited to computer processing power. The inverse calibration can be controlled by using the command prompt window (in Windows) where also HGS is controlled from. Before running the inverse calibration, PEST is also used to assign a weight to the different data groups. In the control file (.pst), the observed data is inserted, and the weight of each observed data point is also shown there. To assign weights, the command `pwtadj1` is used. The control file is also where the model parameters are listed together with initial values and boundaries for each parameter. The first number in the eighth line of the control file is called NOPTMAX. NOPTMAX determines the maximum number of iterations PEST is allowed to do in a particular parameter estimation run. If the NOPTMAX is set to 0 PEST, only does one model run, and it can be used to compute objective function components and residuals from the initial parameter values. If NOPTMAX is set to -1, it computes sensitivities and covariance matrix. PEST also requires template files for each of the model's input files where model parameters are defined and instruction files for each of the relevant model output files. The PEST output run record file (.rec) shows the record of the inverse calibration and the estimated parameters. It also shows the correlation matrix. The PEST output sensitivity file (.sen) gives the sensitivity of each parameter (Doherty, 2018).

### 3.4 HydroGeoSphere

The HydroGeoSphere (HGS) program is developed by Dr. Edward Sudicky, Dr. Peter Forsyth, and Dr. Rene Therrien. HGS is a fully-integrated 3D surface and subsurface flow simulator. The HGS code allows simulations with fully integrated hydrologic and subsurface flow, as well as water quality and solute transport. HGS is set up to account for all the important mechanisms of the hydrologic cycle, and for each time step simultaneously calculate surface solutions and variably-saturate subsurface flow regimes (Therrien, McLaren, Sudicky, & Panday, 2010).

When building a model in HGS, the pre-processor *grok* is used to create the necessary input files for HGS, and then HGS is run to solve the problem and create the output files. The post processor *hsplot* can be used to generate output files to ParaView and other programs (Therrien, McLaren, Sudicky, & Panday, 2010).

#### 3.4.1 Water budget

For each given timestep, HGS solves the surface and subsurface flow together with mass and energy transport equations and gives complete water budgets. The total hydrologic budget combining both the surface water budget and the subsurface water budget can be written as:

$$P = (Q_{S2} + Q_{S1}) + (Q_{G2} + Q_{G1}) + (ET_S + ET_G) + (Q_S^W + Q_G^W) + (\Delta S_S + \Delta S_G) / \Delta t \quad (18)$$

$P$  is the net precipitation (actual precipitation – interception),  $Q_S$  are the inflow and outflow of surface water,  $Q_G$  is the inflow and outflow of subsurface water,  $ET$  is the evapotranspiration from the surface and subsurface flow system,  $Q^W$  is the surface and subsurface water withdrawal, and  $S\Delta$  is the surface and subsurface water storage over time step  $\Delta t$  (Figure 12) (Therrien, McLaren, Sudicky, & Panday, 2010).

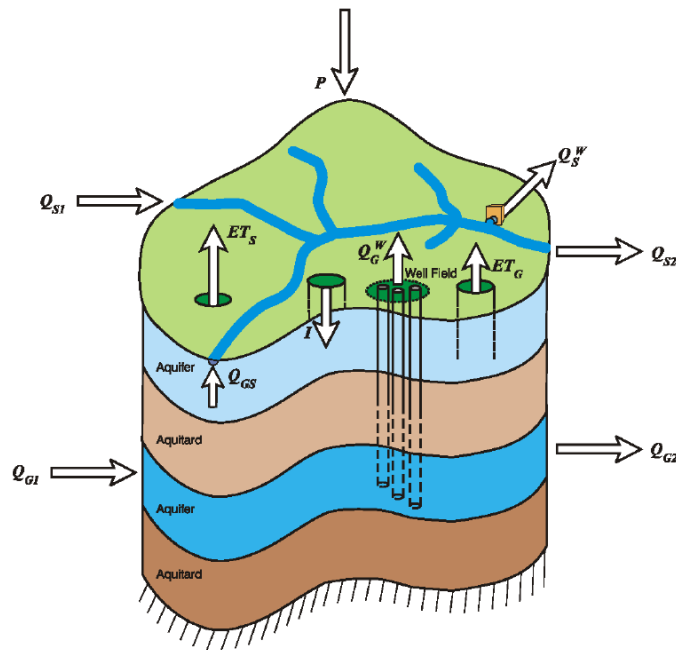


Figure 12: Regional hydrologic cycle involving the components included in the water budget. (Therrien, McLaren, Sudicky, & Panday, 2010)

### 3.4.2 Subsurface flow

The subsurface flow equation used in HGS can be expanded to include discrete fractures, a second interacting porous continuum, wells, drain, and surface flow.

HGS makes the following assumptions for subsurface flow: the fluid is essentially incompressible, the porous medium and fractures/macropores are non-deformable, the system is under isothermal conditions, and the air phase is infinitely mobile.

In HGS, a modified version of Richards' equation is used to describe the three-dimensional transient subsurface flow in a variably-saturated porous medium:

$$-\nabla \cdot (w_m q) + \sum \Gamma_{ex} \pm Q = w_m \frac{\partial}{\partial t} (\theta_s S_w) \quad (19)$$

Where  $w_m$  is the volumetric fraction of the total porosity occupied by the porous medium and is always equal to 1 unless a second continuum is used in a simulation, for example, when a dual continuum is used to simulate fractures or macropores.  $\Gamma_{ex}$  is the internal rate of fluid exchange (e.g.,

drains, wells, and surface water), whereas  $Q$  is the external fluid outside the simulation domain and represents a source (positive) or a sink (negative) to the porous medium system.  $\theta_s$  is the saturated water content, which is assumed equal to the porosity, and  $S_w$  is the degree of saturation (Therrien, McLaren, Sudicky, & Panday, 2010).

The fluid flux  $q$  [ $L T^{-1}$ ] is given by:

$$q = -K \cdot k_r \nabla(\psi + z) \quad (20)$$

where  $k_r = k_r(S_w)$  represents the relative permeability of the medium in connection to the degree of water saturation  $S_w$ .  $\psi$  is the pressure head [L], and  $z$  is the elevation head [L].

$K$  is the hydraulic conductivity tensor [ $L T^{-1}$ ] and is given by:

$$K = \frac{\rho g}{\mu} k \quad (21)$$

where  $g$  is the gravitational acceleration [ $L T^{-2}$ ],  $\rho$  is the density of water [ $M L^{-3}$ ],  $\mu$  is the viscosity of water [ $M L^{-1} T^{-1}$ ], and  $k$  is the permeability of the porous medium.

The water saturation  $S_w$  is connected to the water content  $\theta$  through:

$$S_w = \frac{\theta}{\theta_s} \quad (22)$$

The pressure head  $\psi$  is the primary variable for the solution of the flow equation (equation 19), and therefore relations are made to relate the unknown  $\psi$  to the secondary values  $S_w$  and  $k_r$ . Based on work by Mualem (1967), Van Genuchten (1980) proposed this saturation-pressure relation:

$$\begin{aligned} S_w &= S_{wr} + (1 - S_{wr})(1 + |\alpha\psi|^\beta)^{-v} & \text{for } \psi < 0 \\ S_w &= 1 & \text{for } \psi \geq 0 \end{aligned} \quad (23)$$

With the relative permeability given by:

$$k_r = S_e^{(lp)} \left[ 1 - \left( 1 - S_e^{\frac{1}{v}} \right)^v \right]^2 \quad (24)$$

Where  $v = 1 - \frac{1}{\beta}$  when  $\beta > 1$ .  $S_{wr}$  is the residual water saturation,  $\alpha$  [L<sup>-1</sup>] is the inverse of the air-entry pressure head, and  $\beta$  is the pore-size distribution. The values for  $\alpha$  and  $\beta$  are generally found from a fit of equation 23 and 24 to experimental results.  $S_e$  is effective saturation and is given by  $S_e = (S_w - S_{wr}) / (1 - S_{wr})$ .  $lp$  is the pore connectivity parameter and is estimated to be 0.5 for most soils (Therrien, McLaren, Sudicky, & Panday, 2010).

### 3.4.3 Precipitation

Some amount of precipitation is intercepted by leaves, branches, and stems of vegetation and on its way down and never reaches the soil surface. This process is called interception and is simulated by the bucket model, where only precipitation, which is not in interception storage or evaporated from interception, reached the soil surface. The interception storage capacity  $S_{int}^{Max}$  dependent on the vegetation type and its development stage:

$$S_{int}^{Max} = c_{int} LAI \quad (25)$$

where LAI is the leaf area index and  $c_{int}$  is the canopy storage parameter [L]. LAI represents how much of the ground surface the leaves cover and is dependent on the plant growth rate time (Therrien, McLaren, Sudicky, & Panday, 2010).

### 3.4.4 Evapotranspiration

In HGS, the evapotranspiration (ET) is modeled with the combination of evaporation and plant transpiration and therefore affects both the surface and subsurface flow domains. The transpiration from vegetation happens in the root zone in the subsurface domain, and the rate of transpiration  $T_p$  is estimated through the following relationship which distributes transpiration net capacity along with multiple factors [Kristensen and Jensen, 1975]:

$$T_p = f_1(LAI)f_2(\theta)RDF[E_p - E_{can}] \quad (26)$$

The model assumes that evaporation occurs if the reference evaporation  $E_p$  has not been removed by the processes of canopy evaporation  $E_{can}$  and plant transpiration.

The function  $f_1$  correlates the  $T_p$  with the LAI linearly. The function for the leaf area index  $f_1(LAI)$  is defined as:

$$f_1(LAI) = \max\{0, \min[1, (C_2 + C_1LAI)]\} \quad (27)$$

and the time-varying root distribution function  $RDF$  is defined as:

$$RDF = \frac{\int_{z_1'}^{z_2'} r_F(z') dz'}{\int_0^{L_r} r_F(z') dz'} \quad (28)$$

The function of nodal water content, which is a moisture content dependent term is expressed as:

$$f_2(\theta) = \begin{cases} 0 & \text{for } 0 \leq \theta \leq \theta_{wp} \\ f_3 & \text{for } \theta_{wp} \leq \theta \leq \theta_{fc} \\ 1 & \text{for } \theta_{fc} \leq \theta \leq \theta_o \\ f_4 & \text{for } \theta_o \leq \theta \leq \theta_{an} \\ 0 & \text{for } \theta_{an} \leq \theta \end{cases} \quad (29)$$

where:

$$f_3 = 1 - \left[ \frac{\theta_{fc} - \theta}{\theta_{fc} - \theta_{wp}} \right]^{C_3} \quad (30)$$

$$f_4 = \left[ \frac{\theta_{an} - \theta}{\theta_{an} - \theta_o} \right]^{C_3} \quad (31)$$

The parameters  $C_1$ ,  $C_2$  and  $C_3$  are fitting parameters,  $L_r$  is the effective root length [L],  $z'$  is the depth coordinate from the soil surface [L] and  $r_F(z')$  is the root extraction function [ $L^3 T^{-1}$ ], which usually varies logarithmically with depth.  $\theta_{fc}$  is the moisture content at field capacity,  $\theta_{wp}$  is the moisture content at the wilting point,  $\theta_o$  is the moisture content at the oxic limit and  $\theta_{an}$  is the moisture content at the anoxic limit (Therrien, McLaren, Sudicky, & Panday, 2010).

### 3.4.5 Free drainage and drains

The free drainage feature is often chosen as a boundary condition for unsaturated flow models. It assumes that there is a unit hydraulic gradient along the vertical direction, and this results in a volumetric flow rate out of the domain:

$$Q_i = K_{zz} k_{rw} A_i \quad (32)$$

Where  $A_i$  is the outflow area associated with the node  $i$  where free drainage occurs,  $k_{rw}$  represents the relative permeability and  $K_{zz}$  is the vertical saturated hydraulic conductivity of the underlying porous media.

Drain nodes are used to simulate flow out of the model domain but, at the same time, not allowing inflow. The drain flow rate for a chosen drain node  $i$  is given by:

$$\begin{aligned} Q_i &= C_{DR}(h_i - h_{DR}) & h_i &> h_{DR} \\ Q_i &= 0 & h_i &\leq h_{DR} \end{aligned} \quad (33)$$

Where  $C_{DR}$  is an equivalent conductance [ $L^2 T^{-1}$ ] for the drain node and  $h_{DR}$  is the drain hydraulic head.  $h_i$  is the hydraulic head for the drain node (Therrien, McLaren, Sudicky, & Panday, 2010).

### 3.4.6 Solute transport

In HGS the three-dimensional transport of solutes in a variably-saturated porous medium is described:

$$-\nabla \cdot w_m(qC - \theta_S S_w D \nabla C) + [w_m \theta_S S_w R \lambda C]_{par} + \sum \Omega_{ex} \pm Q_c = w_m \left[ \frac{\partial(\theta_S S_w R C)}{\partial t} + \theta_S S_w R \lambda C \right] \quad (34)$$

Where  $C$  is solute concentrations [ $M L^{-3}$ ], and  $\lambda$  is the first-order decay constant [ $L$ ].  $Q_c$  is the exchange of solute with the outside of the simulation domain [ $M L^{-3} T^{-1}$ ] and represents a source or a sink.  $\Omega_{ex}$  is the mass exchange rate of solutes [ $M L^{-3} T^{-1}$ ] between the subsurface and the other domains in the model.

The retardation factor is represented by:

$$R = 1 + \frac{\rho_b}{\theta_S S_w} K' \quad (35)$$

where  $\rho_b$  is the bulk density of the porous medium [ $M L^{-3}$ ], and  $K'$  is the equilibrium distribution coefficient and is describing as a linear Freundlich adsorption isotherm [ $L^{-3} M$ ].

The hydrodynamic dispersion tensor  $D$  is given by:

$$\theta_S S_w D = (\alpha_l - \alpha_t) \frac{qq}{|q|} + \alpha_t |q| \mathbf{I} + \theta_S S_w \tau D_{free} \mathbf{I} \quad (36)$$

where  $\alpha_l$  is longitudinal dispersivity [ $L$ ] and  $\alpha_t$  is transverse dispersivity [ $L$ ].  $|q|$  is the magnitude of the Darcy flux,  $\tau$  is the tortuosity, and  $\mathbf{I}$  is the identity tensor.  $D_{free}$  are the free-solution diffusion coefficient [ $L^2 T^{-1}$ ] and the product  $\tau D_{free}$  representing the effective diffusion coefficient for the matrix.

In the unsaturated zone, the tortuosity varies with the water saturation given by the Millington-Quirk relationship (Therrien, McLaren, Sudicky, & Panday, 2010):

$$\tau = \frac{(\theta_s S_w)^{7/3}}{\theta_s^2} \quad (37)$$

### 3.4.7 Dual-continuum subsurface coupling

In HGS, it is possible to run a dual continuum model. This is done by having two different continua. The first is always porous medium and is represented by the modified version of Richards' equation for three-dimensional transient subsurface flow in a variably-saturated porous medium (equation 19). The second continuum could be fractures or macropores and simulate such in the porous medium. The second continuum is given by the same equation (equation 19) with the difference that the notation d represents the dual continuum:

$$-\nabla \cdot (w_d q_d) - \Gamma_d \pm Q_d = w_d \frac{\partial}{\partial t} (\theta_{sd} S_{wd}) \quad (38)$$

In the same way, both equation 20 and 21 are identical for the dual continuum except for the notation d:

$$q_d = -K_d \cdot k_{rd} \nabla (\psi_d + z_d) \quad (39)$$

$$K_d = \frac{\rho g}{\mu} k_d \quad (40)$$

In HGS the fluid exchange between the subsurface porous medium and the dual continuum (e.g., macropores) can only be simulated with the dual node approach. It uses a Darcy flux relation to transfer water to one domain from another. The Darcy is simulated by the hydraulic head difference between the two domains. It is assumed that the two domains are separated by a thin layer of porous material where the water exchange can happen across.

The first (porous medium) and second continuum (e.g., macropores) are coupled by a fluid exchange term. With the dual node method, the exchange term can be defined as (Gerke and Van Genuchten, 1993):

$$\Gamma_d = \alpha_{wd} K_a k_{ra} (\psi_d - \psi) \quad (41)$$

where:

$$\alpha_{wd} = \frac{\beta_d}{a} \left[ \frac{\gamma_w}{a} \right] \quad (42)$$

$K_a$  is the hydraulic conductivity of the interface between the two domains [ $L T^{-1}$ ] and  $k_{ra}$  is the relative permeability of the interface between the two domains.  $\beta_d/a$  is the surface area of the macropores per unit total volume of the medium [ $L T^{-1}$ ],  $\beta_d$  is a geometrical shape factor,  $a$  is the fracture-matrix skin thickness [ $L$ ] over which the flow exchange will occur and  $\gamma_w$  is an empirical coefficient (Therrien, McLaren, Sudicky, & Panday, 2010).

## 4 Method

### 4.1 Data

Data for this model was provided by Annette Rosenbom (GEUS) and originates from the Faardrup test site and the Faardrup MACRO model (Larsbo, Roulier, Stenemo, Karsteel, & Jarvis, 2005). The data set contains observed data from 01-01-2000 to 31-12-2009. The observed data consist of time series for precipitation, evapotranspiration, drainage, depth to the groundwater table, water content in the depths of 25, 60, 93, 110, 190, and 210 cm b.g.s. and bromide concentrations in the drain, suction cups, and wells. The data also contain crop data, including root depth and LAI. The input data from the MACRO model, which is used to build the initial model in HGS, is shown in Table 4.

Table 4: Input data from the MACRO model used to develop the HGS model.

<b>MACRO Input data</b>			
<b>Soil properties</b>	<b>Zone 1</b>	<b>Zone 2</b>	<b>Zone 3</b>
<i>Depth interval [cm b.g.s.]</i>	0-32	32-110	110-500
<i>Saturated water content [%]</i>	42	36	31
<i>Wilting point [%]</i>	14	17	9
<i>Residual water content [%]</i>	0	0	0
<i>Bulk density [kg/cm<sup>3</sup>]</i>	0.00151	0.00167	0.00182
<i>Saturated hydraulic conductivity [cm/day]</i>	1615.2	2668.8	62.4
<i>Van Genuchten's beta [-]</i>	1.14	1.1	1.12
<i>Van Genuchten's alfa [cm<sup>-1</sup>]</i>	0.1	0.1	0.02
<i>Pore size distribution factor (macropores) [-]</i>	4	4	4
<i>Torosity factor (micropores) [-]</i>	0.5	0.5	0.5
<i>Effective diffusion pathlength [cm]</i>	2.5	2.0	5.0
<i>Clay [%]</i>	14.6	17.05	18.7
<i>Silt [%]</i>	25	33.87	26.95
<i>Sand [%]</i>	60.4	49.08	54.35
<i>pH [-]</i>	6.68	7.26	7
<i>Org. C [%]</i>	3	0.1595	0.087
<i>Texture</i>	Sandy loam	Loam	Sandy loam

When evaluating if the model data fit the observed data, it is crucial that all data the same units. The model gives results in saturation, but the original observed data is given as water content. Therefore the observed data for water content is converted to saturation by dividing with the porosity. For the depths of 190 cm b.g.s. and 210 cm b.g.s, it resulted in saturations above 1. This is impossible, and therefore a small correction was made in the observed porosity value for zone 3. When changing the porosity in zone 3 from 31% to 35%, it was possible to convert the water content data to useful

saturation data. The observed ET and precipitation data were converted from mm/day to cm/day, and the observed drainage data was converted from mm/day to cm<sup>3</sup>/day.

Data about the groundwater table was given as the depth to the groundwater table from the ground surface. This was converted to match the pressure head data from HGS. The screen in the piezometer (P1) where these data was measured is placed 250-300 cm b.g.s. It is assumed that the screen is placed 275 cm b.g.s. to do this conversion. The observed depth to the groundwater table is subtracted from 275 to calculate the pressure head at a depth of 275 cm b.g.s. On the 4<sup>th</sup> of January, the depth to the groundwater table was measured to 90 cm b.g.s, and when subtracting this from 275 cm, the resulting pressure head is 185 cm.

#### **4.2 Model set-up**

The dimensions of the HGS model are 10 cm (x-direction) x 10 cm (y-direction) x 500 cm (z-direction) with the discretization of 1 in both x and y direction and 500 in the y-direction. This column represents the soil at Faardrup from the ground surface to 500 cm b.g.s. With the model reaching down to a depth of 500 cm b.g.s. all the measurements of the groundwater table are within the model with a good margin. The model is divided into 3 zones with different soil properties, according to Figure 13. Zone 1 ranges from the ground surface to 32 cm b.g.s, zone 2 ranges from 32-110 cm b.g.s and zone 3 ranges from 110-500 cm b.g.s. Because of some set-up difficulties, the model was set up so that the z value is 500 at the top of the model and 0 at the bottom of the model. This does not make any difference to the results, and it just means that all depth values are recalculated to fit this set-up, so they correspond to the accurate b.g.s. values.

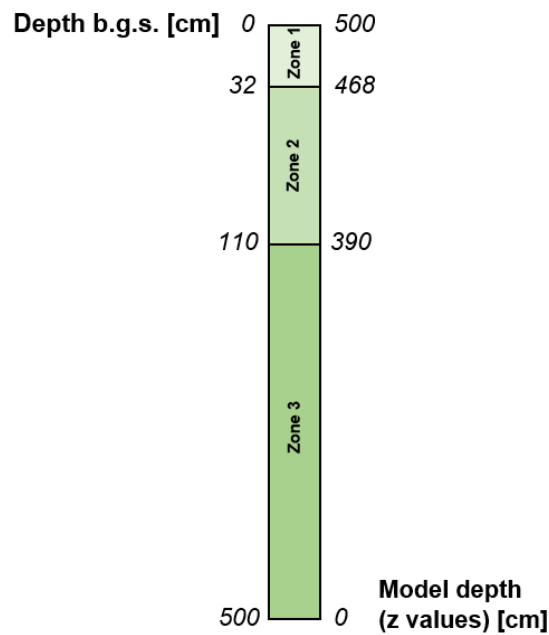


Figure 13: Conceptual schematic of the column build in HGS. The three zones are shown together with the depth b.g.s. and the model depth to each of the zone boundaries.

The initial model has been set up for three years from 01-01-2000 to 31-12-2002.

The general simulation parameters for the model include transient flow, unsaturated conditions, pressure head input (which causes all head input data to be treated as pressure head instead of hydraulic heads), and finite difference mode (Aquanty, 2015). The units are set to kilogram-centimeter-day. All these conditions are specified in the *grok* file. The *grok* file is the main file that contains most of the model information. Using the domain type *porous media*, the physical boundaries for the three zones are specified in the *grok* file while the soil properties are specified in the *mprops* file. Using the domain type *surface*, both the observed values for precipitation and evapotranspiration are set as a boundary condition at the top of the column. The observed precipitation is set as the type *rain*, and the observed evapotranspiration is set as the type *potential evapotranspiration* which sets the input to be a specified flux boundary condition and converts the fluxes to nodal volumetric fluxes by multiplying by the contributing area of the chosen face (Aquanty, 2015). To include the observed evapotranspiration data in the model, it was necessary to create a surface domain where the overland flow properties are specified in the *oprops* file. The properties for evapotranspiration are specified in the *etprops* file under the domain type *et*. The transpiration fitting parameter C1, c2, and C3 are estimated from (Kristensen & Jensen, 1975). The root depth is set to a maximum of 90 cm because the crop data from the field shows this as the maximum root depth, and the function *edf*

*quadratic decay function* is used to stimulate root growth (Aquanty, 2015). The LAI is defined with a table done from the crop data to define when the crop has leaves and when the crop is harvested.

At the bottom of the model, a boundary condition is set using the type *free drainage*, and this allows water to exit the model through the bottom.

The model set-up results in an influx of water only through the top of the model by precipitation and outflux of water from the model happens by ET, drains, and through the bottom of the model as free drainage.

The initial head in the model is set using the type *Funktion z initial head*, which uses linear interpolation between two chosen nodes in the z-direction and the assigned head values. The initial head value is determined from pressured head observed data from the first day, and the top node of the model is assigned the value -90 cm, and the bottom node of the model is assigned 410 cm.

At Faardrup, the drains are set in a depth of 110 cm b.g.s. but this coincides with the boundary between zone 2 and zone 3, and therefore the drains are moved up 10 cm to a depth of 100 cm b.g.s. so they lie within zone 2.

The drains are added to the model in the depth of 100 cm b.g.s. using the type *simple drain*. The drain nodes only allow water to flow out of the system when the head in the drain node is higher than the selected drain head value. With the drain head value set to 0, the drains only remove water from the model when the groundwater table lies higher than the drain node (Aquanty, 2015).

The model is set up to create output files for every second day when running *hsplot*, which creates output files to other post-processing programs, in this case, to Paraview. Output files directly from HGS contains data for each day. This is done to save simulation time.

Multiple observation points were set in different depths to create output files in the specific depths. The observation points *sat1*, *sat2*, *sat3*, *sat4*, *sat5*, and *sat6* were set in depths corresponding to the water content measurements in 25, 60, 90, 110, 190, and 210 cm b.g.s. One observation point (*GWT*) was set in 275 cm to correspond to the screen in well P1. The observation point *drain* was set in 100 cm b.g.s. to correspond to the drain's placement. Observation points SC1 and SC2 were set in 100 and 200 cm b.g.s. together with observation point *HWS* in 350 cm b.g.s. to trace bromide concentrations. SC1 and SC2 correspond to the suction cups placement, and *HWS* is the horizontal wells.

To avoid problems with convergence, a copy of the model was moved to a subfolder, and the command *generate tables from unsaturated functions* were used in the *.mporps* file. This instruction generates tables for pressure saturation and saturation-relative permeability, and by linking to these

tables from the model run in the main folder, the model does not have the same problems with convergence error. The tables need to be adapted before the model can read it and for that Sachin Karan (GEUS) developed a python script to be run before running the HGS model. This script was necessary so the tables could be generated automatically in preparation for the inverse calibration.

Using the data provided in Table 4, it was not possible to get the initial HGS model to converge. By the trial and error method, it was discovered that a significant decrease of the k-values (hydraulic conductivity) in all zones and an increase of the Van Genuchten parameter beta in all zones resulted in the model converging. New parameter values for Van Genuchten's alpha and beta was used from (Carsel & Parrish, 1988) and determined from soil type. In Table 5, all input data for the HGS model is shown.

Table 5: HGS model input data. The table includes data from the mprops file (matrix properties), etprops file (evapotranspiration properties), and oprops file (overland properties).

<b>HGS model input data</b>			
<b>Material properties (mprops)</b>	<b>Zone 1</b>	<b>Zone 2</b>	<b>Zone 3</b>
Hydraulic conductivity [cm/day]	10	10	0.05
Porosity [%]	42	36	35
Residual water content [%]	0.01	0.01	0.01
Bulk density [kg/cm <sup>3</sup> ]	0.00151	0.00167	0.00182
Torosity factor (micropores) [-]	1	1	1
Specific storage[cm <sup>-1</sup> ]	1e-7	1e-7	1e-7
Van Genuchten's beta [-]	1.89	1.56	1.89
Van Genuchten's alfa [cm <sup>-1</sup> ]	0.075	0.036	0.075
Drain [cm <sup>3</sup> / day]		10	
<b>ET properties (etprops)</b>			
Evaporation depth [cm]		100	
Root depth [cm]		90	
Wilting point		0.2	
Field capacity		0.32	
Oxic limit		0.76	
Anoxic limit		0.9	
Transpiration fitting parameter C1		0.34	
Transpiration fitting parameter C2		0.15	
Transpiration fitting parameter C3		1	
LAI		See table in etprops	
<b>Overland flow properties (oprops)</b>			
X friction		10	
y friction		10	
Rill storage height		0.01	
Obstruction storage height		0	
Coupling length		10	

#### 4.2.1 Validation

Validation is used in site-specific models to determine if the model can produce useful results from data not used in the calibration (Sonnenborg & Henriksen, 2005). In this case, the model has been extended with three years (the same length as the calibration period), and the results for the whole period was compared to the observed data. This is called a split-sample test (Sonnenborg & Henriksen, 2005) where one half of the data are used in the calibration, and the other half are used as the validation period.

#### 4.2.2 Solute transport

At Faardrup, 30 kg/ha potassium (KBr) was added on the field on the 5<sup>th</sup> of October 1999. The model was extended to begin on the 1<sup>st</sup> of October 1999, to simulate the transport of bromide at this time. The concentration was calculated by assuming it was spread in with 1 mm of water and converted to  $1.98 * 10^{-6} \text{ kg/cm}^3$ . The bromide is added on day six and not day five because it has to correspond with the output times. Because of this issue, the bromide had to be added over two days to get the model to run. The dispersivity in *mprops* also needed to be changed to allow solute transport. Dispersivity was estimated using (Gelhar, Welty, & Rehfeldt, 1992) and a value of approximately 10 % of the flow length. In *mprops*, the dispersivity was set to 50.

#### 4.2.3 Dual-domain

A dual-domain was added to the HGS model to represent macropores by dual-permeability. The set up of the dual-domain was done from the verification example by Gerke (Therrien, McLaren, Sudicky, & Panday, 2010). The dual-domain was added using the domain type *dual*, and the dual medium properties were specified in the *dprops* file. In *mprops* in the dual continuum flow conditions, the initial head is the same as for the porous medium, and the boundary condition at the bottom was set to free drainage.

Values for unsaturated Van Genuchten functions and dispersivities are from (Rosenbom, et al., 2009) while the interface unsaturated Van Genuchten functions are taken from the Gerke example (Therrien, McLaren, Sudicky, & Panday, 2010). Values for hydraulic conductivity in the *mprops* file was also initially taken from (Rosenbom, et al., 2009) but was subsequently lowered by manual calibration and the Van Genuchten parameters were also changed by manual calibration. Initially, the *dprops* file only had one zone from the entire model, but it was later divided into three zones, like the *mprops* file corresponding to the soil horizons. This allowed different macropore properties in different zones. The initial input data in the *dprops* file is shown in Table 6.

Table 6: Input data in the dprops file (dual-domain properties) used to simulate macropores in the dual-domain model.

<b>HGS model input data dual-domain</b>	
<b>Macropores (dprops)</b>	<b>Value</b>
Hydraulic conductivity [cm/day]	1000
Specific storage [ $cm^{-1}$ ]	1.0E-7
Porosity [%]	0.95
Volume fraction dual medium	0.05
First-order fluid exchange coefficient	0.3
Interface k	0.01
Longitudinal dispersivity [ $cm^{-1}$ ]	10
Transverse dispersivity [ $cm^{-1}$ ]	0.1
Vertical transverse dispersivity [ $cm^{-1}$ ]	2
Tortuosity	1
Bulk density	2.65
First-order mass exchange	0.15
<b>Unsaturated Van Genuchten functions</b>	
Residual saturation	0.01
Van Genuchten's alfa [ $cm^{-1}$ ]	0.1
Van Genuchten's beta [-]	2
<b>Interface unsaturated Van Genuchten functions</b>	
Residual saturation	0.10526
Van Genuchten's alfa [ $cm^{-1}$ ]	0.005
Van Genuchten's beta [-]	1.5

### 4.3 Inverse calibration

The inverse calibration of the HGS models was done with the calibration tool PEST (Doherty, 2018). It was set up with the master folder and three subfolders for running models. Due to limited computing power, it was not possible to use more than three subfolders. Initially, PEST was set up to calibrate on ten different parameters: hydraulic conductivity in all zones (k1, k2, and k3), Van Genuchten's  $\alpha$ , and  $\beta$  (a1, a2, a3, b1, b2, and b3) and drain conductance (drain). PEST was also set up to calibrate against observed pressure head (head) data in 275 cm b.g.s, observed drain data, and observed saturation (wsat) in the depths of 25 cm, 60 cm, 93 cm, 110 cm, 190 cm, and 210 cm b.g.s. The pressure head data was only measured once a month while the drain data and saturation were measured once a day, and the saturation was measured in six different depths. This means

there are 6 x 1095 observation data points for saturation while there are 1095 observed data points for drain and only less than 36 observed data points for pressure head data because a few months don't have useful measurements. To ensure the saturation data do not dominate the calibration because of the many data points, each group of data is assigned equal weight, resulting in each group contributing with 100 to the objective function making the total 300 at the beginning of the calibration. Before each parameter estimation run, a sensitivity analysis was run to identify parameter correlation. If two parameters correlate more than 0.9 %, the least sensitive parameter was excluded from the calibration to avoid convergence problems (Sonnenborg & Henriksen, 2005). When the calibration still would not converge, the specific parameters in the model that halted execution were examined to try to identify which parameter values caused the problems. This method, together with literature, was used to set parameter boundaries for all the model parameters to try to ensure a successful parameter estimation. It also proved necessary to fixate some of the parameters to ensure a successful parameter estimation. This was done by changing the term *log* in the controls file to *fixed* for parameters causing problems with the calibration.

Initially, in the manually calibrated model, the saturation data fit relatively good compared to the drain data, and especially the pressure head data had a bad fit. Changes in the group weighing also have an impact on the calibration and therefore in some model runs the weight of the saturation data was set to 25 while the weight for pressure head and drain was maintained at 100 to try and force the model to find a better fit for these data groups. A variety of weights, fixed parameters, and parameter boundaries was tried to get the best possible calibration.

Many inverse calibrations were completed unsuccessfully because the chosen parameters in the specific optimization caused the HGS model to not converged, and therefore the inverse calibration could not finish successfully. When this happened, the HGS model was investigated to try and determine which parameter values caused the model to crash and try and from that adapt the parameter boundaries in the .pst file to try to ensure a successful optimization. Due to limited computing power, each inverse calibration had a duration of more than 24 hours, and therefore it was not possible to run an unlimited number of calibrations, and several inverse calibrations were unsuccessful. In these cases, the last optimization, which also had the lowest objective function, was used in the HGS model. Even as the calibration was not completed successfully, this provided some useful data.

Solute transport was added to the model after calibration. The dual-domain model was also set up after the inverse calibration of the models with a single domain. Due to a lack of time, it was not possible to do inverse calibration on the dual-domain models.

The uncertainty limit for saturation data was estimated to 0.1, and the uncertainty for the drain was estimated to be a 10 % difference from average observed data (Sonnenborg & Henriksen, 2005).

Due to the significant value differences in the observed data på pressure head, it was difficult to determine an uncertainty limit, and therefore the RMSE values are only used relatively to evaluate the models against each other.

## 5 Results

Model A is the initial model that was manually calibrated and further developed and calibrated through the inverse calibration process. Model A, Model B, Model C, and Model D are all single-domain models only containing matrix and not macropores. Model B, Model C, and Model D are all results of inverse calibrations even though only Model B was calibrated successfully. The calibration for Model C and Model D did not finish successfully, and the parameter values used in these models were taken from the last successfully optimization run. Therefore, there are no data for the 95% confidence interval for the different parameter values used in these models. Model E is a dual-domain model where the second domain represents macropores. Model D is only manually calibrated. An overview of the different models is shown in Table 7.

Table 7: Overview of the different models.

<b>Model Overview</b>	
<b>Model</b>	<b>Description</b>
<i>Model A</i>	Initial model – Manually calibrated – Single domain
<i>Model B</i>	Inverse calibrated – Single domain 2 parameters fixed
<i>Model C</i>	Inverse calibration (not completed) – Single domain 2 parameters fixed and change in boundaries
<i>Model D</i>	Inverse calibration (not completed) – Single domain 2 parameters fixed and change in weights
<i>Model E</i>	Dual-domain – Manually calibrated Macropores

As a tool for comparison to support the visual assessment of the model's different statistics has been calculated for the data groups used in the assessment. Fbal [%] was calculated for the drainage, while RMSE was calculated for the pressure head and saturation. The results are shown in Table 8.

The water balance for each of the models are shown in Table 9. Inflow to the model happens by precipitation, whereas water leaves the model through free drainage, ET, and drains.

Table 8: Calculated model statistics for the different models.

<b>Model statistics</b>	<b>Model A</b>	<b>Model B</b>	<b>Model C</b>	<b>Model D</b>	<b>Model E</b>
<i>Fbal [%] (drainage)</i>	228.9	17.8	485.1	151.3	-
<i>RMSE (pressure head)</i>	133.6	128.6	106.4	67.3	374.2
<i>RMSE (wsat)</i>	0.16	0.26	0.18	0.31	0.38

Table 9: Water balance for the different models.

<b>Water Balance</b>	<b>Model A</b>	<b>Model B</b>	<b>Model C</b>	<b>Model D</b>	<b>Model E</b>
<i>Precipitation [cm<sup>-3</sup>]</i>	21236	21236	21236	21236	21236
<i>Free Drainage [cm<sup>-3</sup>]</i>	-4560	-6686	-2161	-2737	-979
<i>ET [cm<sup>-3</sup>]</i>	-15322	-14823	-17803	-14929	-13912
<i>Simple Drain [cm<sup>-3</sup>]</i>	-1246	-311	-2217	-952	0
<i>Total inflow [cm<sup>-3</sup>]</i>	21236	21236	21236	21236	21236
<i>Total outflow [cm<sup>-3</sup>]</i>	-21129	-21820	-22181	-18618	-14891
<i>Difference [%]</i>	0.5	2.7	4.4	14.1	42.6

### 5.1 Model A - Manual calibrated

After manual calibration, the parameters in Table 10 gave in the best result and were therefore used in Model A. This model was also used to set up inverse calibration, and a sensitivity analysis was made together with a parameter correlation coefficient matrix. The inverse calibration did not run, probably because of too large boundaries, which for all parameters were set from 1E-10 to 1E+10. The correlation matrix also showed a parameter correlation between b2 and K2 (Table 11). The sensitivity analysis shows that b2 and K2 are almost equally sensitive (Figure 14), but b2 is slightly more sensitive and was therefore fixed in further work with the inverse calibration. Because of experience from the manual calibration, also a2 was fixed because the model was very sensitive to this parameter, and changes in this parameter often caused problems with convergence. The sensitivity analysis also shows that parameter a2 has the highest relative sensitivity (Figure 14).

Table 10: Final parameter values used in Model A from manual calibration.

Calibration results	
Model A	
Parameter	Parameter value
<i>K1 [cm/day]</i>	10
<i>K2 [cm/day]</i>	10
<i>K3 [cm/day]</i>	0.05
<i>a1 [cm<sup>-1</sup>]</i>	0.030
<i>a2 [cm<sup>-1</sup>]</i>	0.036
<i>a3 [cm<sup>-1</sup>]</i>	0.030
<i>b1</i>	1.60
<i>b2</i>	1.55
<i>b3</i>	1.30
<i>Drain [cm<sup>3</sup> / day]</i>	10

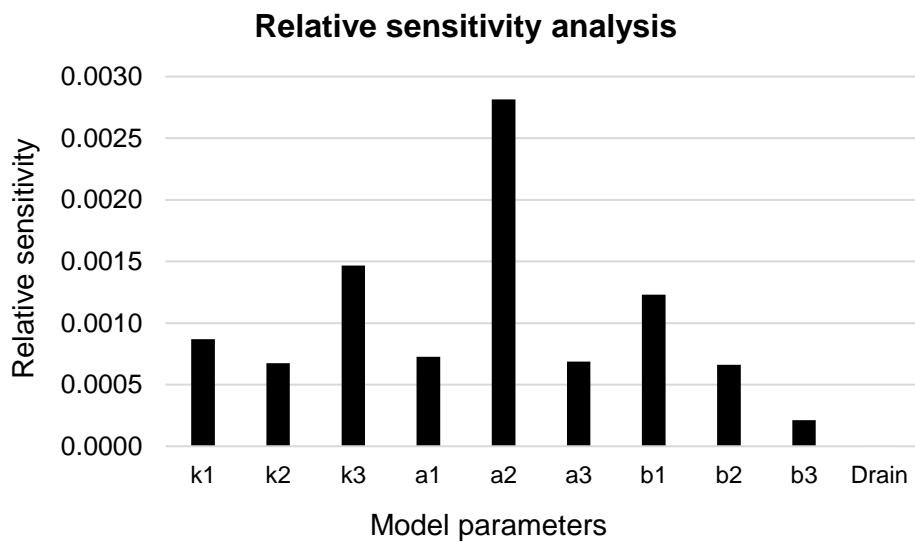


Figure 14: Sensitivity analysis of the parameters in Model A.

Table 11: Parameter correlation coefficient matrix for parameters in Model A. Values over 0.90 have been marked with red.

<b>Parameter correlation coefficient matrix</b>										
	<b>K1</b>	<b>K2</b>	<b>K3</b>	<b>a1</b>	<b>a2</b>	<b>a3</b>	<b>b1</b>	<b>b2</b>	<b>b3</b>	<b>Drain</b>
<b>K1</b>	1	-0.53	0.37	0.02	-0.41	-0.10	-0.46	0.38	-0.07	-0.01
<b>K2</b>	-0.53	1	-0.39	-0.25	0.64	0.12	0.58	-0.94	0.09	-0.60
<b>K3</b>	0.37	-0.39	1	0.03	-0.08	0.06	-0.10	0.32	-0.63	0.30
<b>a1</b>	0.02	-0.25	0.03	1	-0.15	-0.66	-0.34	0.21	0.27	0.35
<b>a2</b>	-0.41	0.64	-0.08	-0.15	1	-0.01	0.33	-0.63	-0.32	0.11
<b>a3</b>	-0.10	0.12	0.06	-0.66	-0.01	1	0.12	-0.06	-0.24	-0.27
<b>b1</b>	-0.46	0.58	-0.10	-0.34	0.33	0.12	1	-0.58	0.12	-0.41
<b>b2</b>	0.38	-0.94	0.32	0.21	-0.63	-0.06	-0.58	1	-0.06	0.64
<b>b3</b>	-0.07	0.09	-0.63	0.27	-0.32	-0.24	0.12	-0.06	1	-0.24
<b>Drain</b>	-0.01	-0.60	0.30	0.35	0.11	-0.27	-0.41	0.64	-0.24	1.00

The simulated data from Model A has been compared to the observed data for drainage, pressure head, and saturation is shown respectively in Figure 15, Figure 16, and Figure 17. The simulated drainage (Figure 15) is overall much too high and does not follow the dynamics of the flow very well. Where the observed drainage has smaller peaks of flow over a larger period, the simulated drainage has much higher peaks of flow over a shorter period. In some areas like from the 01-11-2001 to 01-03-2002, simulated drainage dynamics somewhat mimic the observed data, but the outflow is still much too high. The simulated pressure head (Figure 16) is overall much too low and does not at all mimic the dynamics of the observed data. Only when the observed pressure head is at its highest, the simulated data show a minimal peak.

The simulated saturation at 25 cm b.g.s. (Figure 17) does generally have a good fit for the observed data in regards to the dynamics. The values are overall a little lower than observed values, especially during the summer, whereas single peaks are simulated a little too high during the winter. The simulated data for saturation at 60 cm b.g.s, 93 cm b.g.s, 110 cm b.g.s, 190 cm b.g.s, and 210 cm b.g.s is shown in Appendix 1. For 60 cm b.g.s and 93 cm b.g.s, the simulated values are generally at too low compared to the observed values and for 110 cm b.g.s, 190 cm b.g.s, and 210 cm b.g.s the simulated values are generally a little higher than the observed values.

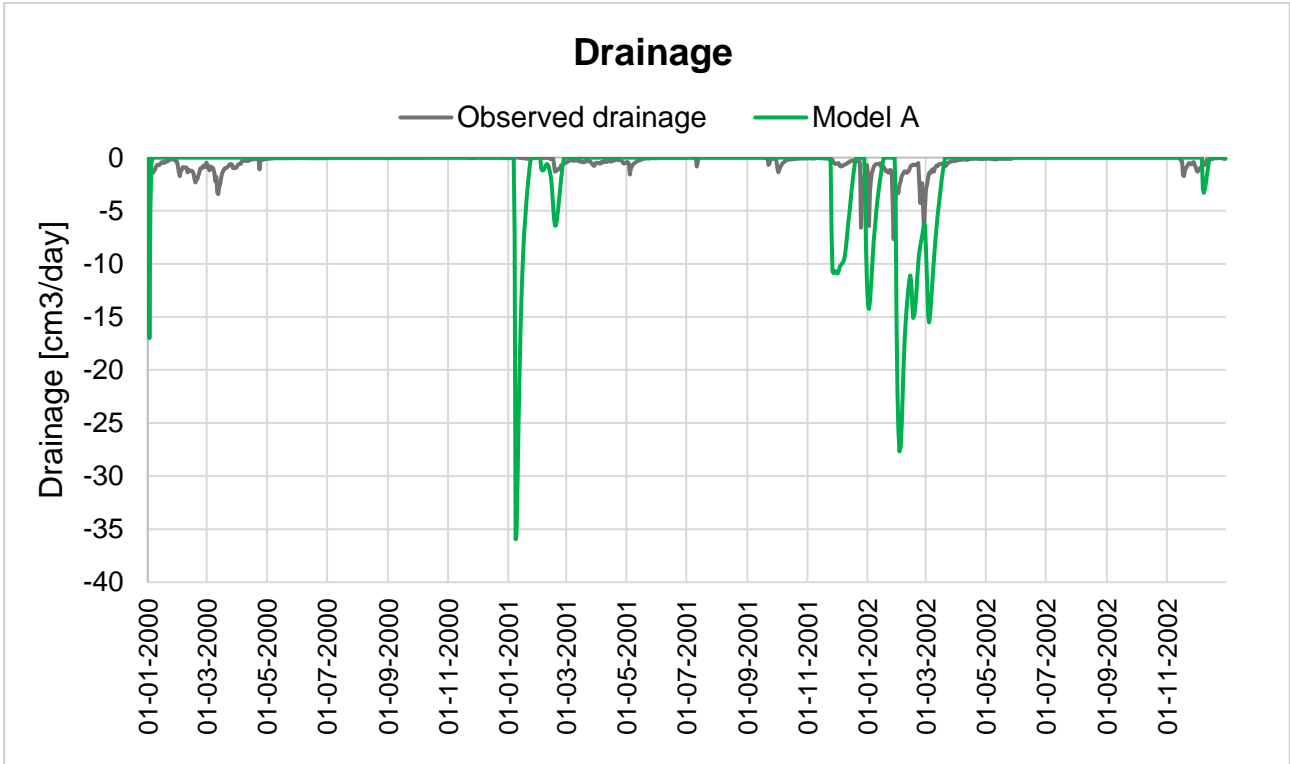


Figure 15: Simulated drainage (green line) from Model A and observed drainage (grey line).

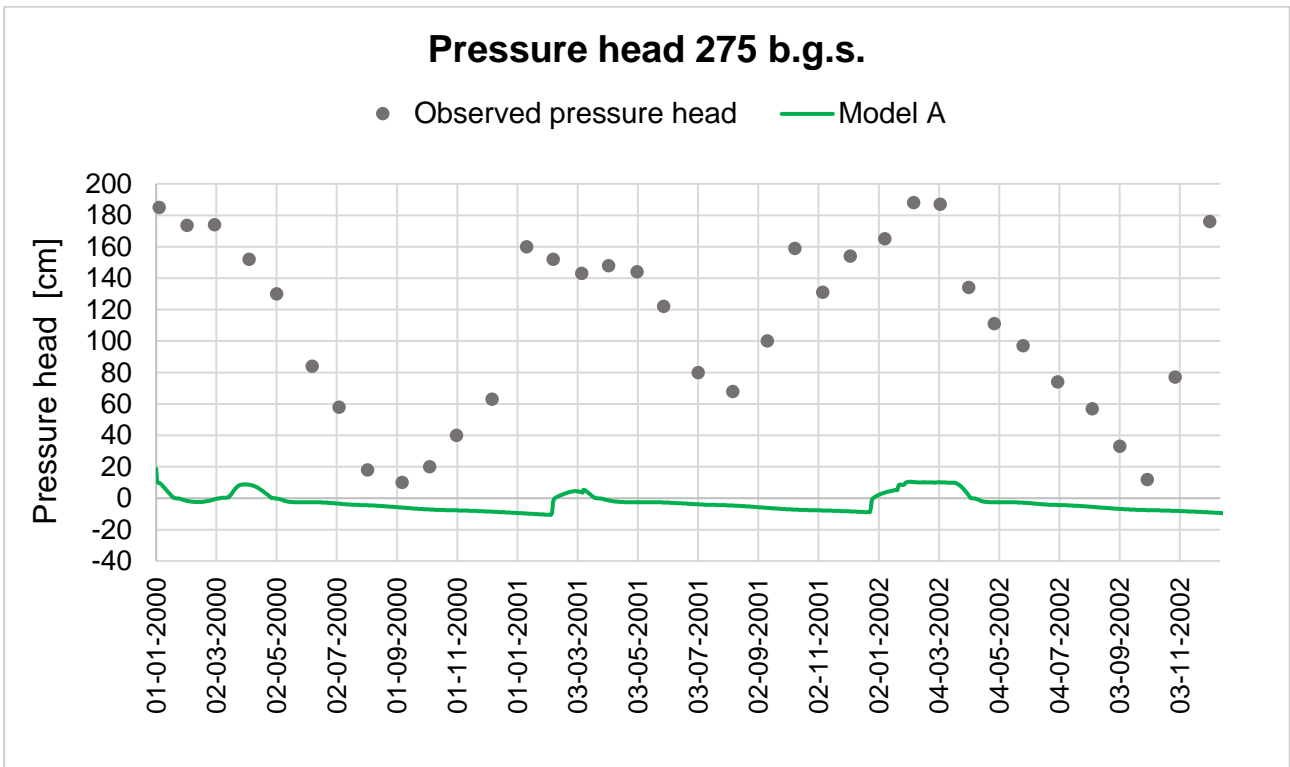


Figure 16: Simulated pressure head (green line) from Model A and observed pressure head (grey line).

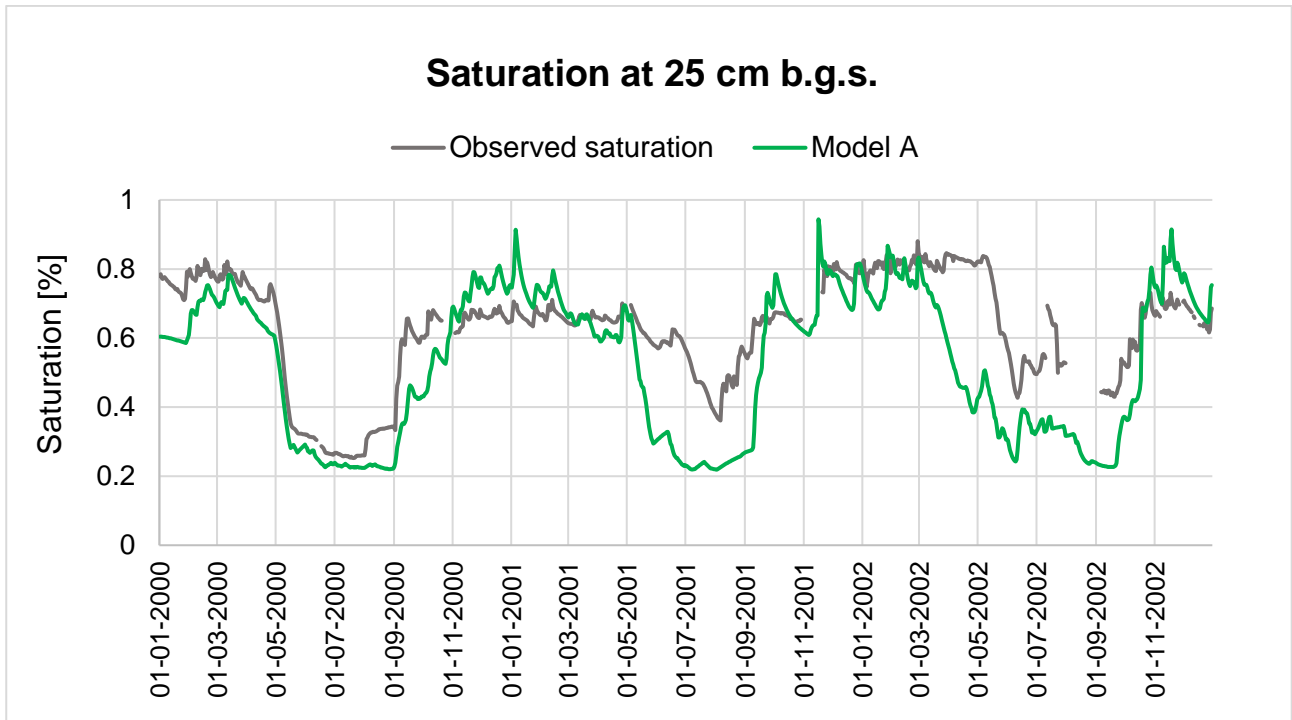


Figure 17: Simulated saturation (green line) from Model A at 25 cm b.g.s and observed saturation (grey line).

## 5.2 Model B - Inverse calibrated

Model B was made with parameters from inverse calibration, and the result of the calibration are shown in Table 12. In the inverse calibration of Model B, the same initial values were used as in Model A. However, the parameters  $a_2$  and  $b_2$  have been fixed. In this calibration, the boundaries are also much more narrow than for Model A (Appendix 1). The sensitivity analysis shows that  $k_3$  is the most sensitive parameter in this calibration, and the correlation matrix did not show a correlation between any of the parameters (Appendix 2).

The weight for the observed saturation data was lowered from 100 to 25 in this calibration to try and force the inverse calibration to find a better fit for drain and pressure head because the fit between the simulated and observed saturation already was relatively good in comparison to the pressure head and drainage. The assigned weights and the contribution to objective function after calibration are shown in Table 13.

Table 12: Final parameter values for Model B and 95 % Confidence interval found by inverse calibration.

Calibration results		95% Confidence Interval	
Model B			
Parameter	Parameter value	Lower bound	Upper bound
$K_1$ [cm/day]	28.74	8.58	96.28
$K_2$ [cm/day]	27.89	13.31	58.41
$K_3$ [cm/day]	0.175	0.17	0.19
$a_1$ [cm <sup>-1</sup> ]	0.058	0.05	0.07
$a_2$ [cm <sup>-1</sup> ]	Fixed at 0.036		
$a_3$ [cm <sup>-1</sup> ]	0.1	0.04	0.25
$b_1$	1.61	1.57	1.65
$b_2$	Fixed at 1.56		
$b_3$	1.37	1.07	1.75
Drain [cm <sup>3</sup> / day]	0.24	0.11	0.52

Table 13: Assigned weights and contribution to objective function after calibration.

<b>Objective function Model B</b>		
<b>Observation group</b>	<b>Weight</b>	<b>Contribution to objective function after calibration</b>
<i>Heads</i>	100	100.35
<i>Wsat</i>	25	25
<i>Drain</i>	100	1.5
<i>Total</i>	225	126.85

The results from Model B show that the calibration lowered the objective function from 225 to 126 but also that this change was only reached by lowering the contribution from drainage. The simulated drainage (Figure 18) shows that values fit much better than Model A, but the simulated data does not mimic the dynamics of the flow.

The simulated pressure head values (Figure 19) are almost similar to those in Model A and do not capture either the dynamics or the values of the observed data.

The simulated saturation values at 25 cm b.g.s. (Figure 20) are overall lower than the observed values but generally capture the dynamics. The simulated data for saturation at 60 cm b.g.s, 93 cm b.g.s, 110 cm b.g.s, 190 cm b.g.s, and 210 cm b.g.s are shown in Appendix 2. For 60 cm b.g.s, 93 cm b.g.s, and 110 cm b.g.s. the simulated values are generally too low compared to the observed values, and for 190 cm b.g.s and 210 cm b.g.s, the simulated values vary between being too low or too high compared to the observed values.

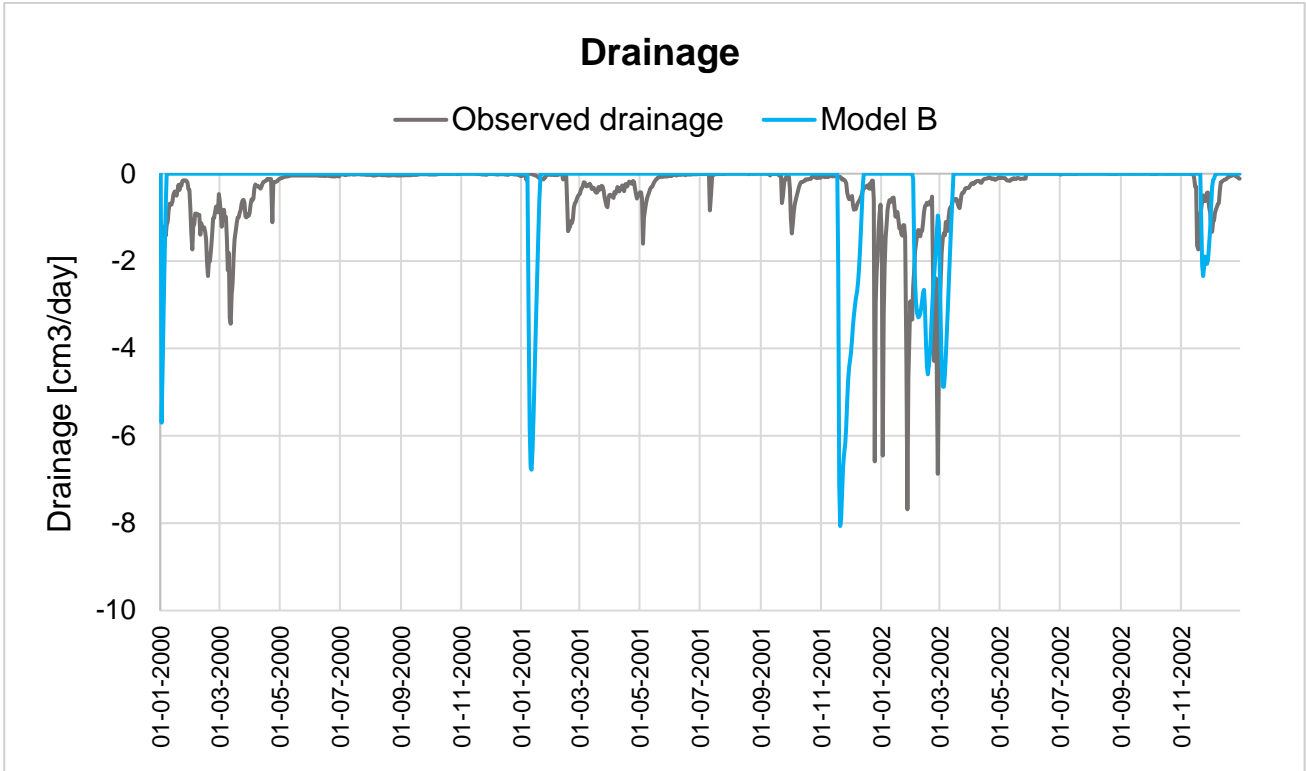


Figure 18: Simulated drainage (blue line) from Model B and observed drainage (grey line).

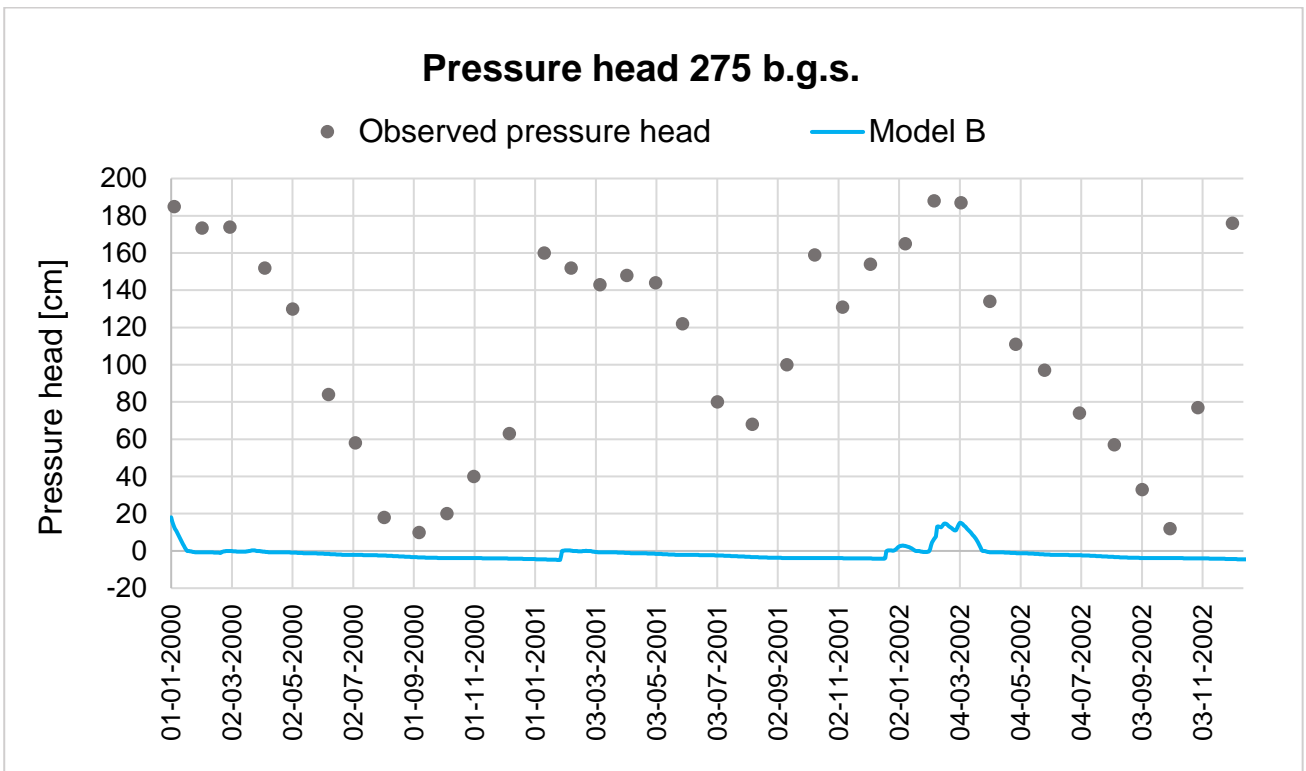


Figure 19: Simulated pressure head (blue line) from Model B and observed pressure head (grey line).

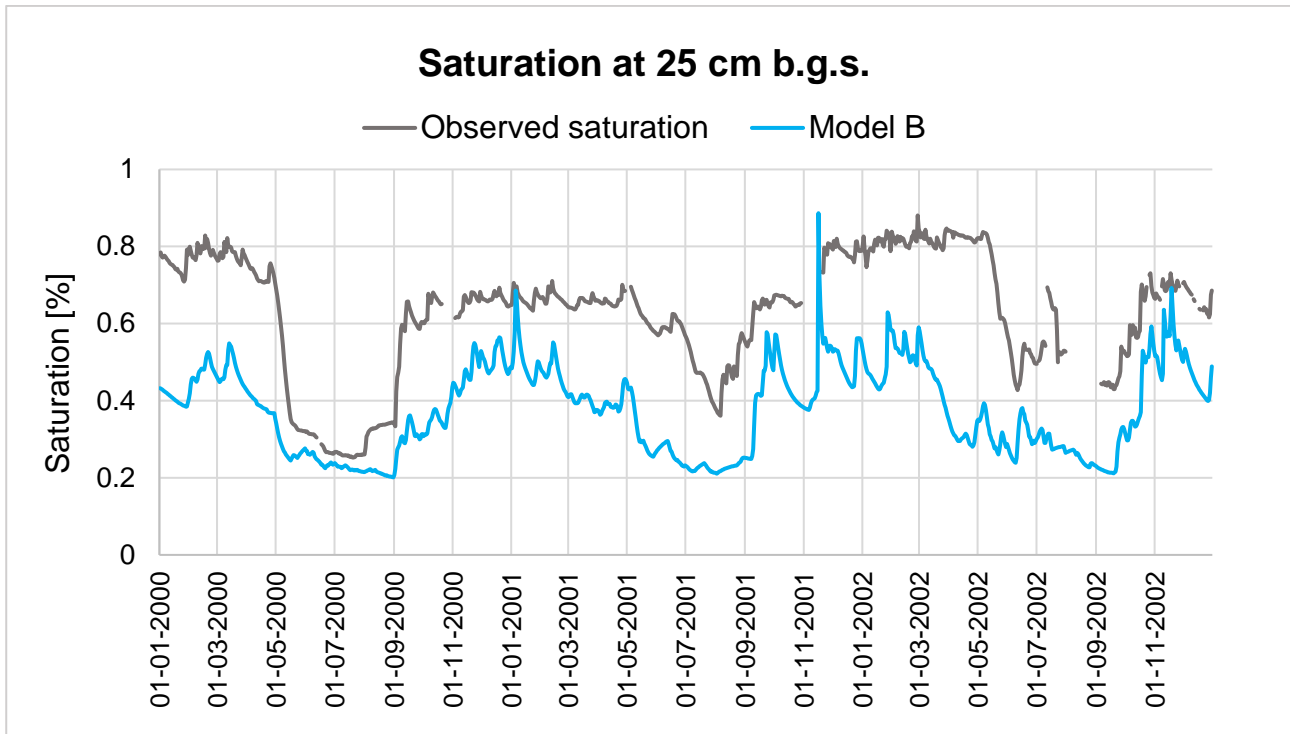


Figure 20: Simulated saturation (blue line) from Model B at 25 cm b.g.s and observed saturation (grey line).

### 5.3 Model C - Inverse calibrated (not completed)

Model C was made with parameters from inverse calibration, and the result of the calibration is seen in Table 14. In the Model C inverse calibration, the same initial values were used as in Model A, but the parameters  $a_2$  and  $b_2$  are fixed. In this calibration, the boundaries are also much more narrow than for Model A but wider than Model B (Appendix 3). The sensitivity analysis is the same as for Model B because the same initial values are used (Appendix 2) and show that  $k_3$  is the most sensitive parameter and that there is no correlation between any of the parameters (Appendix 2). The calibration did not finish successfully due to convergence problems with the HGS model probably because of too wide boundaries of the  $\alpha$  and  $\beta$  parameters. The values used in Model C were, therefore, taken from the last optimization, which resulted in the objective function in Table 15.

The weight for the observed saturation data is the same as for Model B. The assigned weights and the contribution to objective function after calibration are shown in Table 15.

Table 14: Final parameter values for Model C found by inverse calibration.

<b>Calibration results</b>	
<b>Model C (last optimization)</b>	
<b>Parameter</b>	<b>Parameter value</b>
$K_1$ [cm/day]	3026
$K_2$ [cm/day]	417
$K_3$ [cm/day]	0.024
$a_1$ [cm <sup>-1</sup> ]	0.016
$a_2$ [cm <sup>-1</sup> ]	Fixed at 0.036
$a_3$ [cm <sup>-1</sup> ]	0.14
$b_1$	1.49
$b_2$	Fixed at 1.56
$b_3$	1.51
Drain [cm <sup>3</sup> / day]	0.02

Table 15: Assigned weights and contribution to objective function after calibration.

<b>Objective function Model C</b>		
<b>Observation group</b>	<b>Weight</b>	<b>Contribution to objective function after calibration</b>
<i>Heads</i>	100	49.33
<i>Wsat</i>	25	25
<i>Drain</i>	100	0.94
<i>Total</i>	225	75.27

The results from Model C show that the calibration lowered the objective function from 225 to 75.27 but also that this change was reached primarily by lowering the contribution from pressure heads and only a minimal lowering of drainage.

The simulated drainage (Figure 21) shows that the values overall are much too high but that they fit the dynamics of the flow much better than Model A and Model B.

The simulated pressure heads (Figure 22) show that the values overall are lower than the observed values. Even though the simulated values are all lower than the observed values, the simulated values somewhat mimic the observed values. The peaks in the observed data are reproduced in the simulated data only in much lower values.

The simulated saturation data (Figure 23) shows that the values overall mimic the dynamics in the observed values. The simulated values are overall too high compared to the observed data. The simulated saturation in 60 cm b.g.s, 93 cm b.g.s, and 110 cm b.g.s show peaks where the values are too high, and otherwise, the values are too low, and the values only somewhat mimic the dynamics in the observed data (Appendix 3). In 190 cm b.g.s and 210 cm b.g.s, the simulated values are too high compared with the observed values, and the dynamics in the observed data are only minimal visible in the simulated data (Appendix 3).

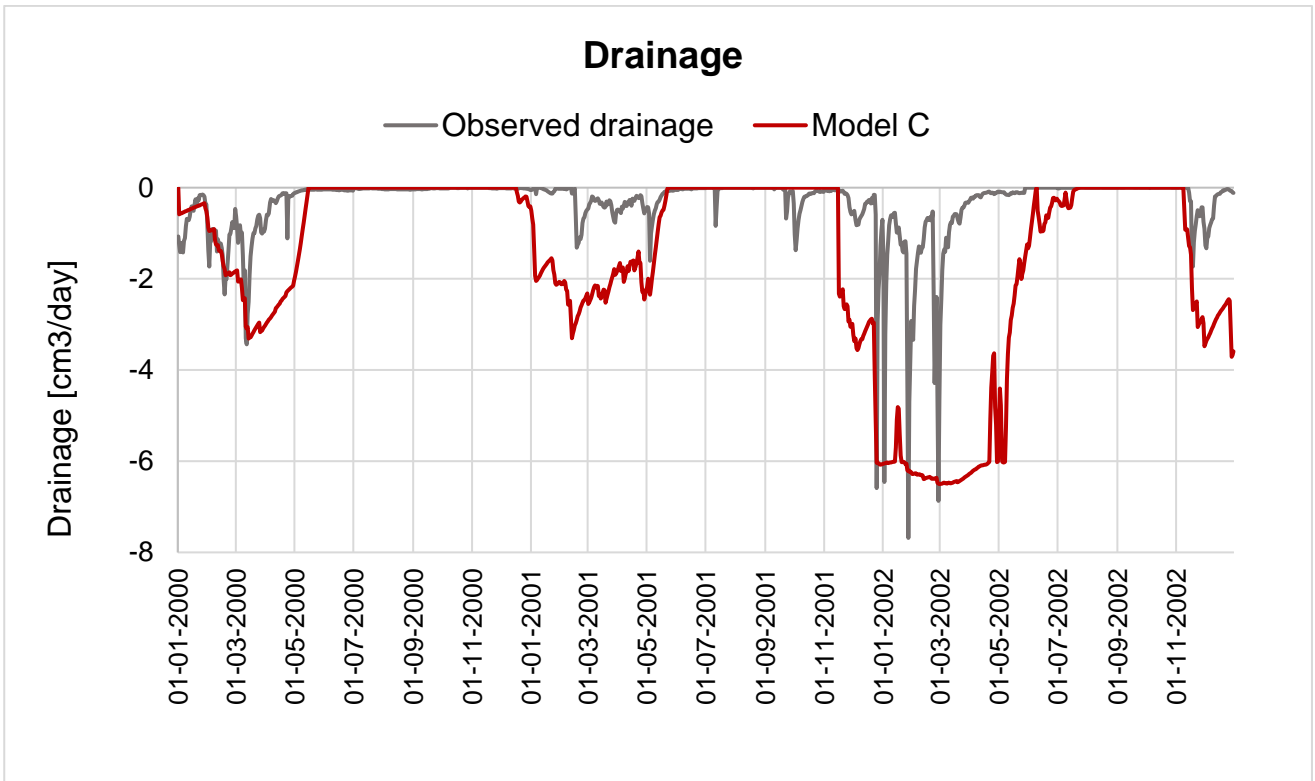


Figure 21: Simulated drainage (red line) from Model C and observed drainage (grey line).

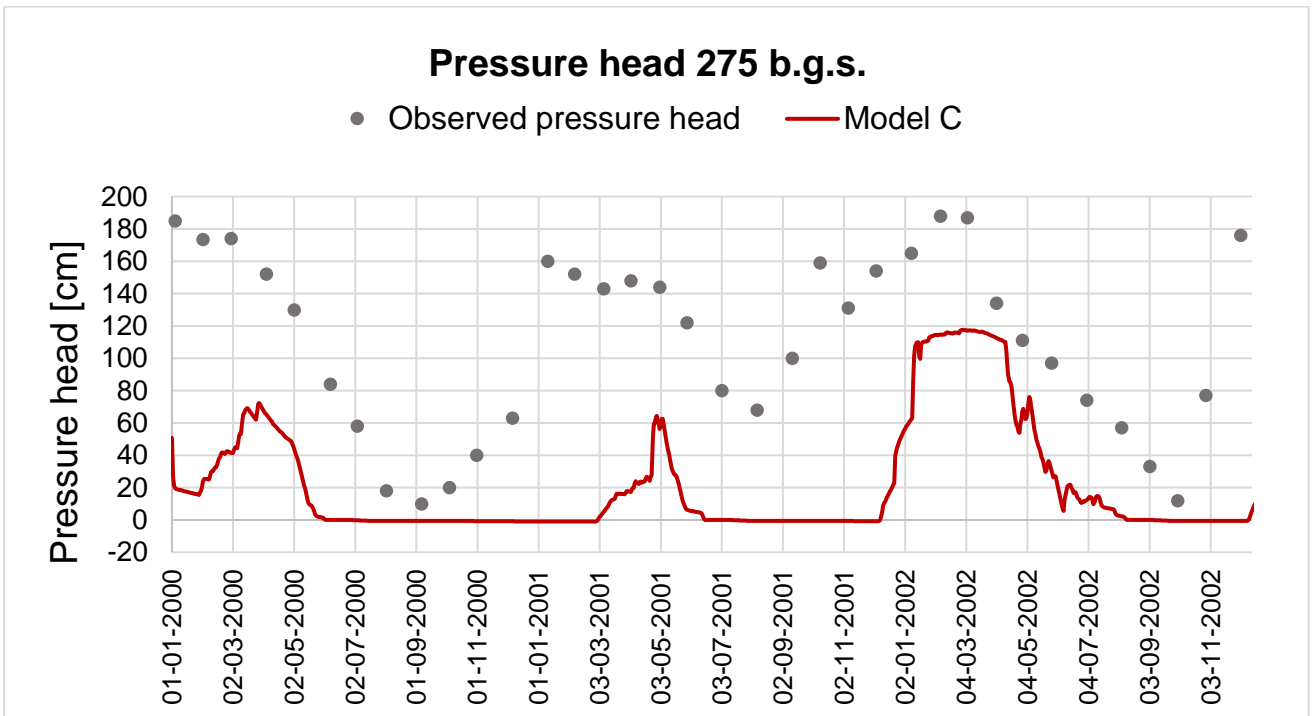


Figure 22: Simulated pressure head (red line) from Model C and observed pressure head (grey line).

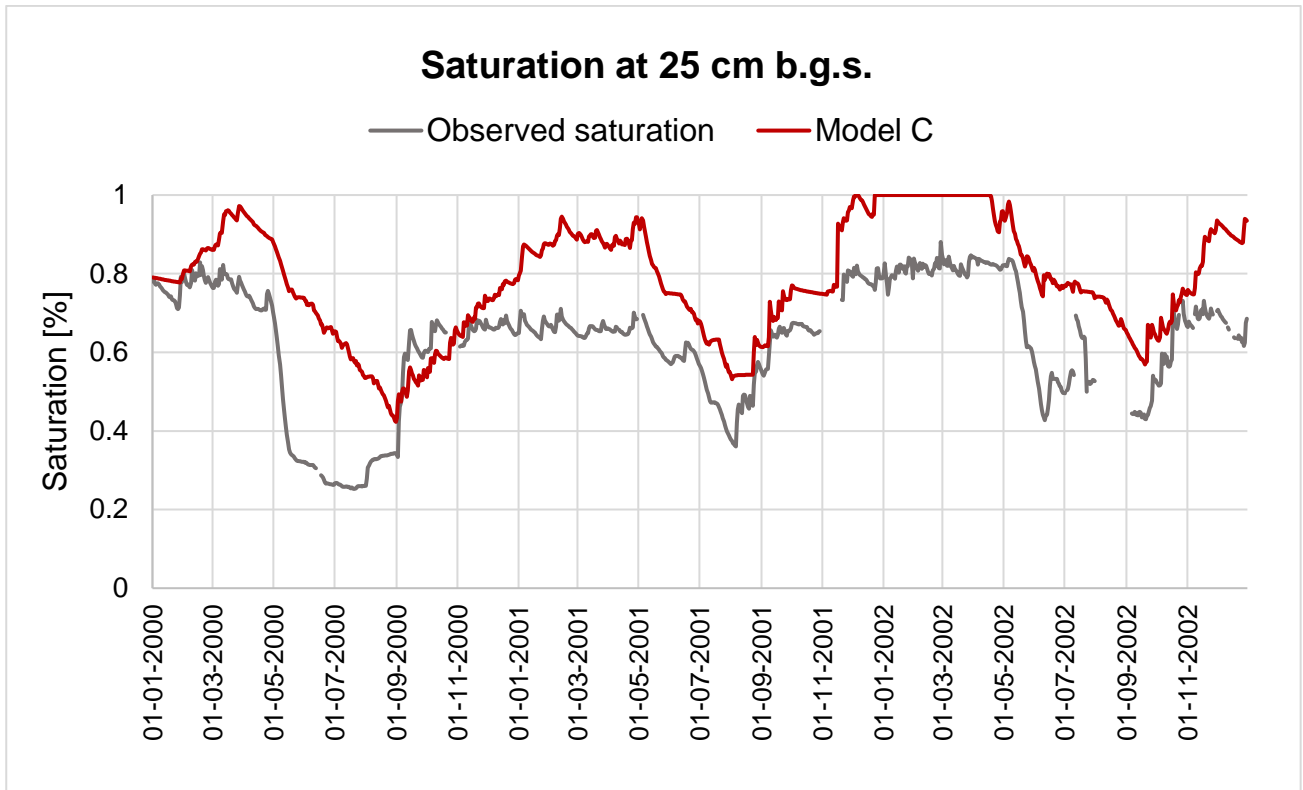


Figure 23: Simulated saturation (red line) from Model C at 25 cm b.g.s and observed saturation (grey line).

### 5.3.1 Model C - Validation

Model C was like Model B and Model D inverse calibrated against data from 01-01-2000 to 31-12-2002. Model C was after the calibration extended to include the period from 01-01-2003 to 31-12-2005. In Figure 24 (drainage), Figure 25 (pressure head), and Figure 26 (saturation), the calibration periods are shown with a red line and the validation periods with a blue line. The simulated values in the validation periods for both drainage, pressure head and saturation show the same tendencies as in the calibration period.

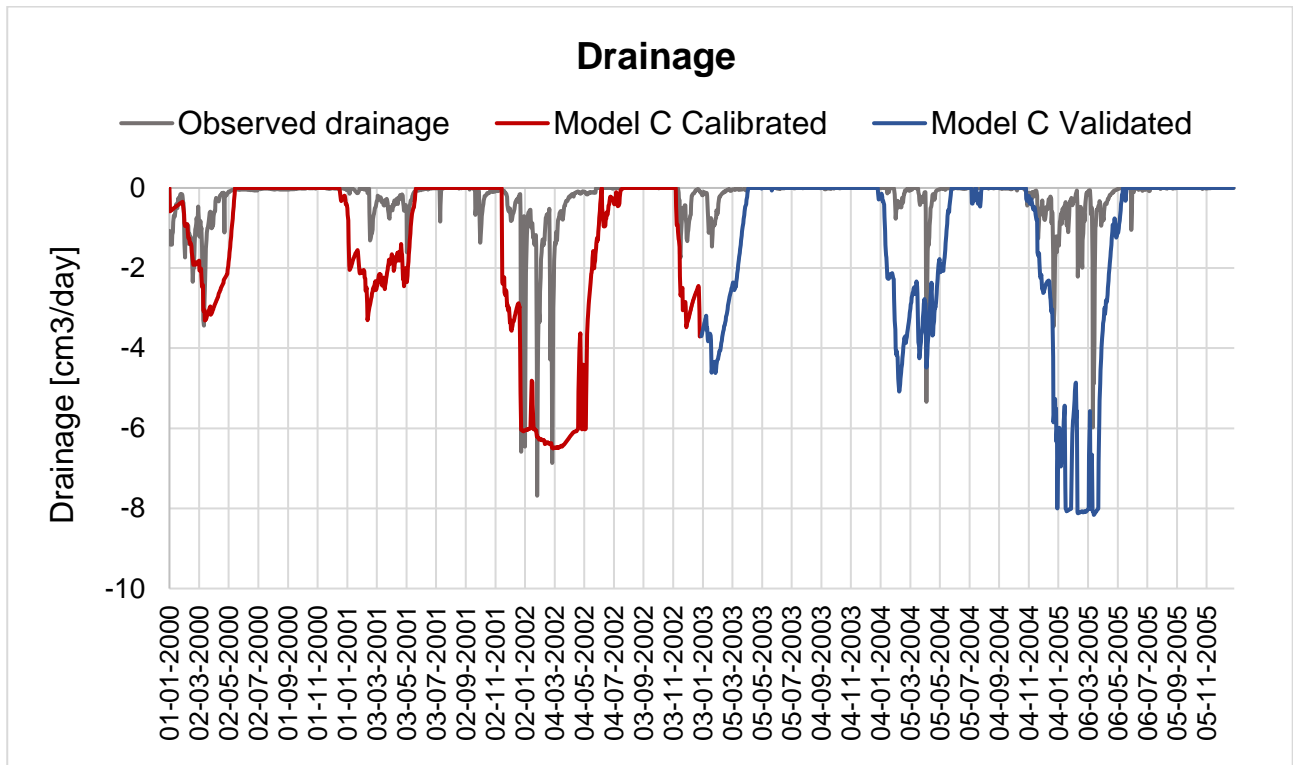


Figure 24: Simulated drainage (red and blue line) from Model C and observed drainage (grey line). The red line shows the calibration period, and the blue line shows the validation period.

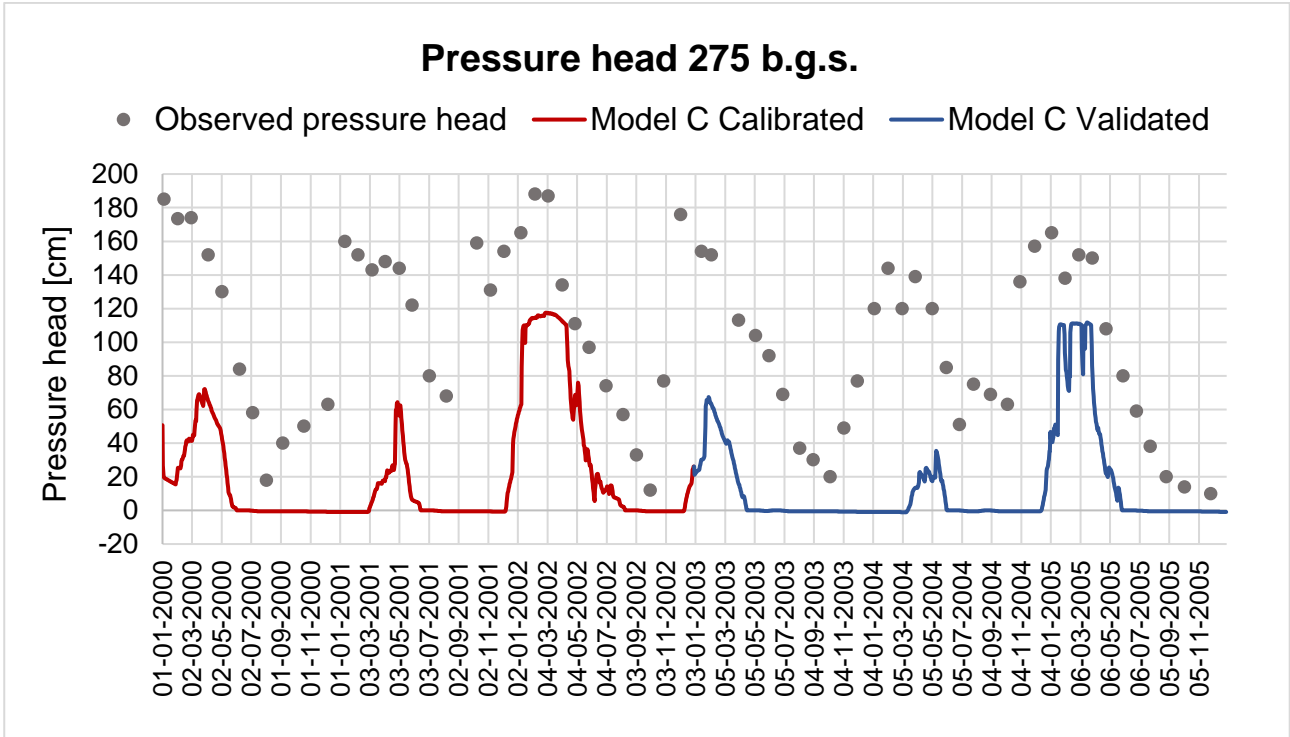


Figure 25: Simulated pressure head (red and blue line) from Model C and observed pressure head (grey line). The red line shows the calibration period, and the blue line shows the validation period.

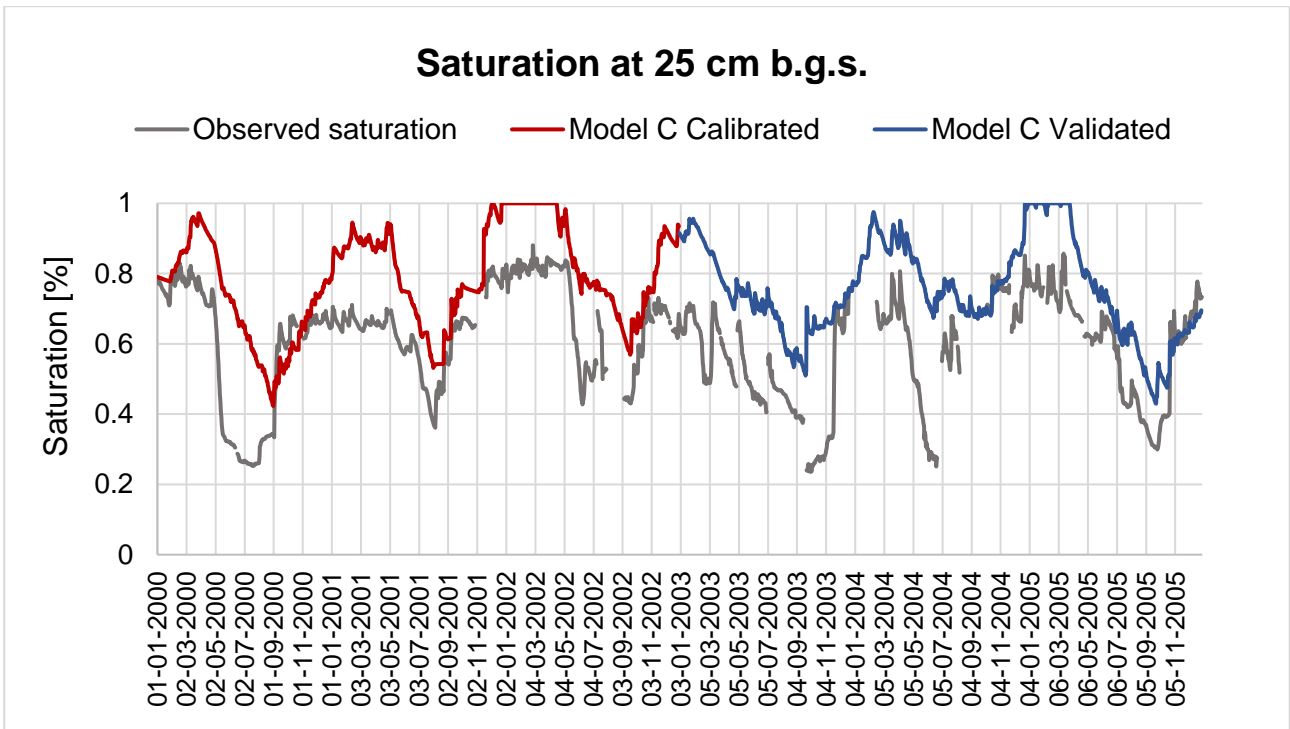


Figure 26: Simulated saturation (red and blue line) from Model C at 25 cm b.g.s and observed saturation (grey line). The red line shows the calibration period, and the blue line shows the validation period.

### 5.3.2 Model C - Solute transport

Model C was chosen to simulate solute transport at Faardrup. The solute transport simulations are compared to observations from suction cups at 100 cm b.g.s. (Figure 27), suction cups at 200 cm b.g.s (Figure 28), drains at 110 cm b.g.s., (Figure 29) and horizontal screen wells at 350 cm b.g.s. (Figure 30).

In Figure 27, the simulated bromide concentration at 100 cm b.g.s. is overall a little too high compared to the observed data. The simulated values show an increase in concentrations around 01-11-1999, where the observed data first show an increase around 01-01-2000. The simulated values also have a steeper breakthrough curve than the observed values. Around 02-08-2001, the simulated values show a peak in concentrations which is not present in observed data. However, except for this peak, the overall tendencies in the observed data are replicated in the simulated values.

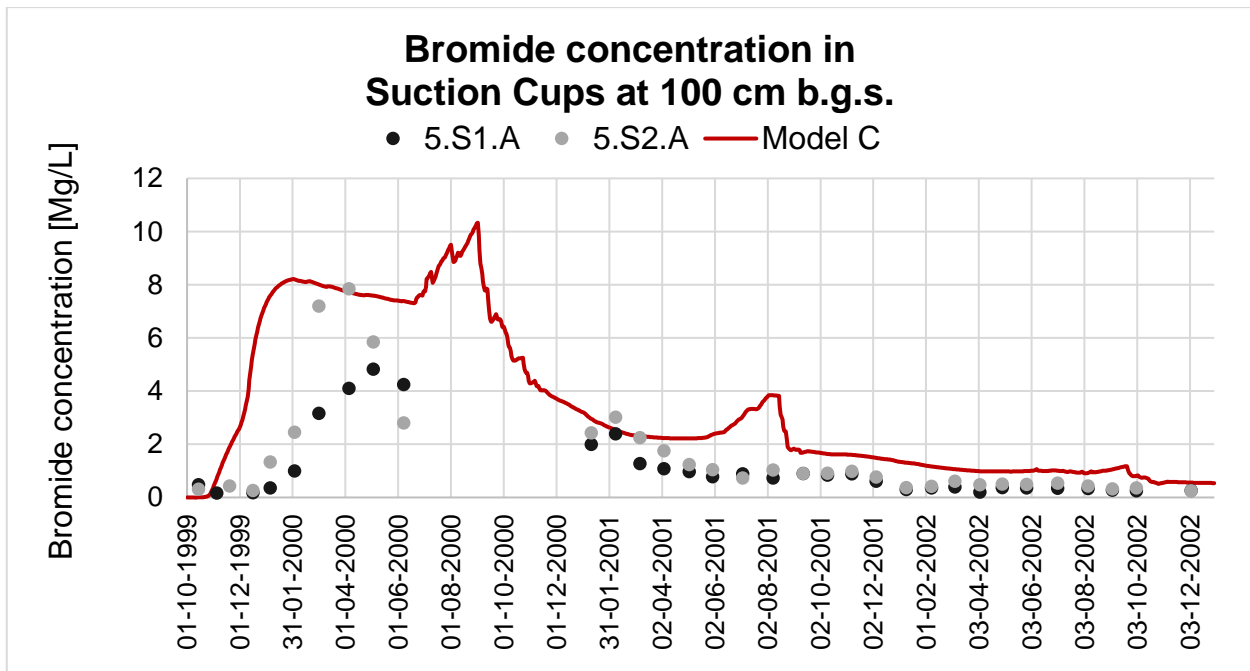


Figure 27: Simulated bromide concentrations at 100 cm b.g.s. (red line) from Model C and observed bromide concentrations (grey and black dots).

The simulated data in Figure 28 show that the breakthrough is less step in 200 cm b.g.s than in 100 cm b.g.s (Figure 27). The overall tendencies in the observed values seen in Figure 28 are over replicated by the simulated values. However, before 01-06-2000, the simulated values are too low compared to the observed values, and after 01-06-2000, the simulated values are too high.

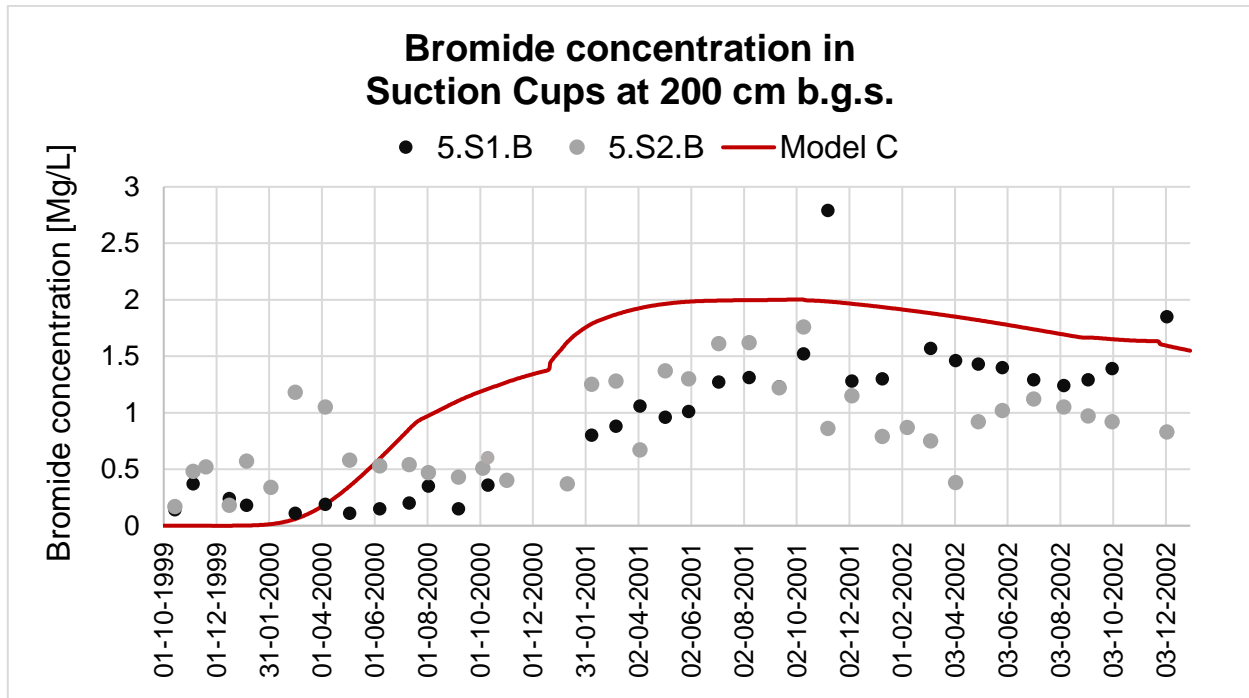


Figure 28: Simulated bromide concentrations at 200 cm b.g.s. (red line) from Model C and observed bromide concentrations (grey and black dots).

The simulated bromide concentrations in 110 cm b.g.s. are in Figure 29 compared to the observed bromide concentrations in the drain water. The simulated values are too high compared to the observed values and show two peaks in concentration that is not present in the observed data.

In 350 cm b.g.s. (Figure 30) the simulated concentrations are very low and generally lower than the observed values. The tendencies in the observed data are only minimal replicated in the simulated data.

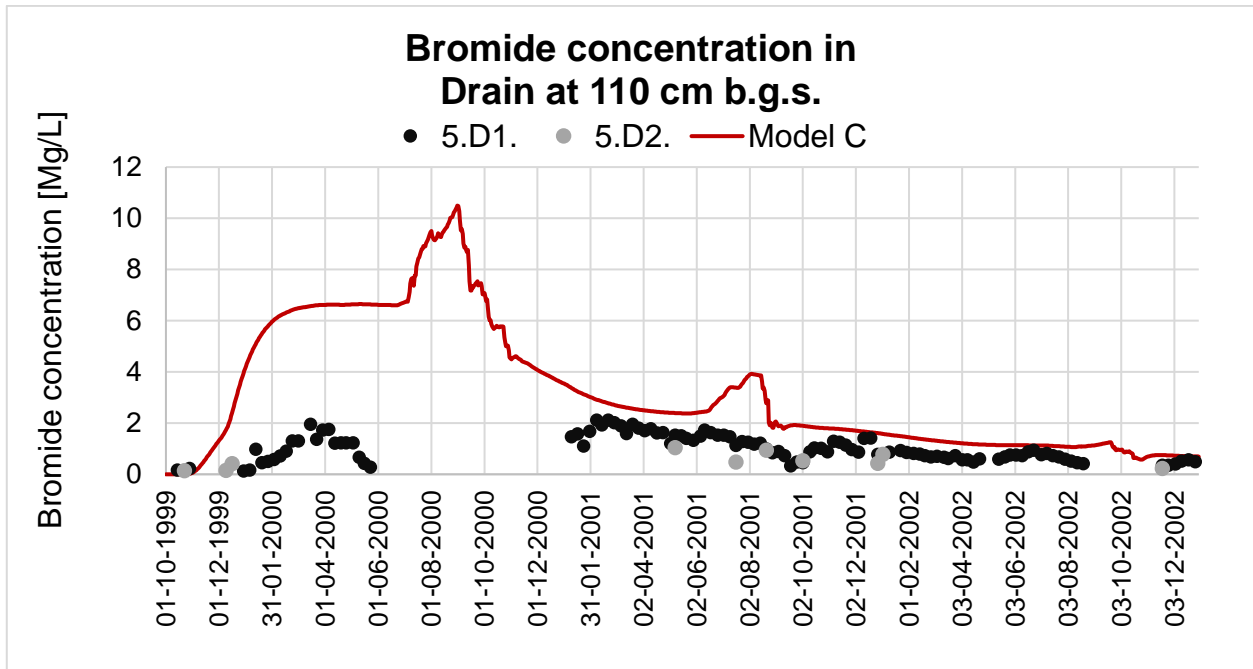


Figure 29: Simulated bromide concentrations at 110 cm b.g.s. (red line) from Model C and observed bromide concentrations (grey and black dots).

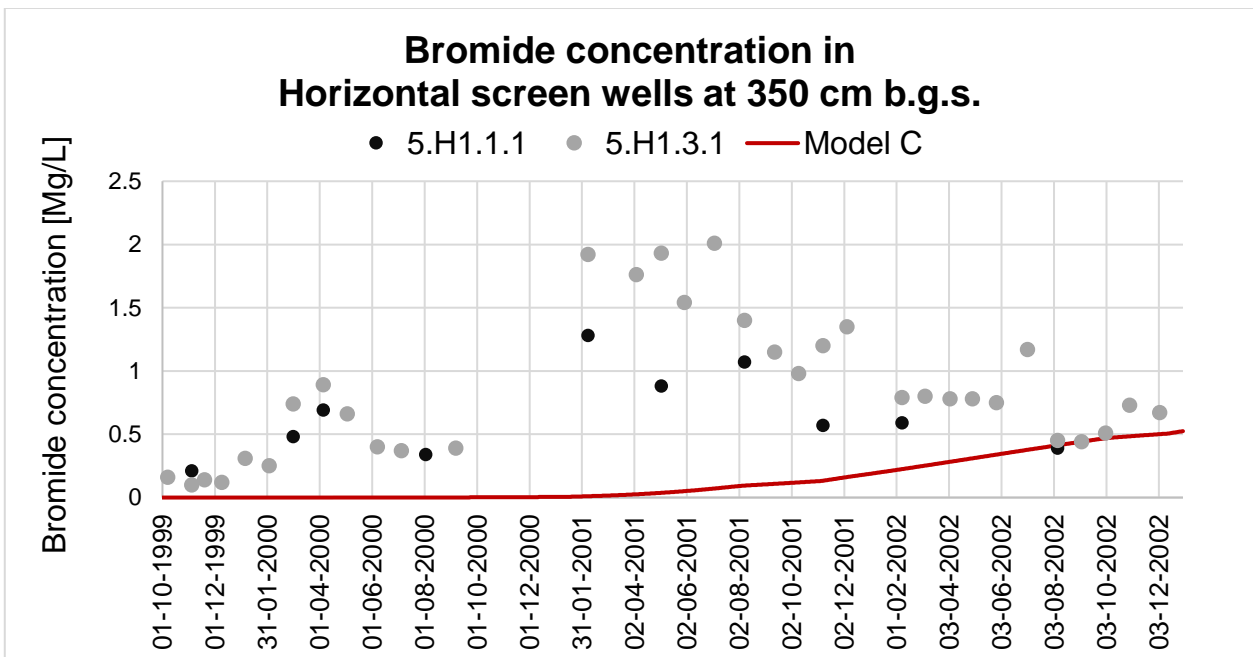


Figure 30: Simulated bromide concentrations at 350 cm b.g.s. (red line) from Model C and observed bromide concentrations (grey and black dots).

#### 5.4 Model D - Inverse calibrated (not completed)

Model D was made with parameters from inverse calibration, and the result of the calibration is seen in Table 16. In the Model D inverse calibration, the same initial values were used as in Model A except for the drain parameter that was lowered from 10 to 1. This was done because all the calibrations gave results with a much lower drain parameter than 10. The parameters  $a_2$  and  $b_2$  are still fixed at the same values as in the other models (Table 16). In this calibration, the boundaries are the same as for Model B (Appendix 2), but the weight was changed. The weight for the observed drain flow was lowered from 100 to 80. This was done to try and force a better fit on the pressure head data because the previous models have mostly lowered the contribution from the drain data (Table 17). The calibration did not finish successfully due to convergence problems with the HGS. The values used in Model D was, therefore, taken from the last optimization, which resulted in the objective function in Table 17.

Table 16: Final parameter values for Model D found by inverse calibration

<b>Calibration results</b>	
<b>Model D (last optimization)</b>	
<b>Parameter</b>	<b>Parameter value</b>
$K_1$ [cm/day]	2046
$K_2$ [cm/day]	495
$K_3$ [cm/day]	0.025
$a_1$ [cm <sup>-1</sup> ]	0.038
$a_2$ [cm <sup>-1</sup> ]	Fixed at 0.036
$a_3$ [cm <sup>-1</sup> ]	0.1
$b_1$	2.68
$b_2$	Fixed at 1.56
$b_3$	1.89
Drain [cm <sup>3</sup> / day]	0.003

Table 17: Assigned weights and contribution to objective function after calibration.

<b>Objective function Model D</b>		
<b>Observation group</b>	<b>Weight</b>	<b>Contribution to objective function after calibration</b>
<i>Heads</i>	100	25.3
<i>Wsat</i>	25	25
<i>Drain</i>	80	1.01
<i>Total</i>	205	51.3

The sensitivity analysis shows that  $k_3$  is the most sensitive parameter in this calibration, and the correlation matrix did not show a correlation between any of the parameters (Appendix 4).

The simulated drainage (Figure 31) shows that the values are very consistent with no peaks like the observed data and do not capture the dynamics of the observed flow. Overall the simulated values are too high except for the high peaks seen in the observed data where the simulated values are too low because the model does not mimic these peaks.

The simulated pressure heads (Figure 32) show that the values overall are lower than the observed values except for the last half of 2002, where the simulated overall are higher than the observed data. Generally, the simulated data mimic the dynamics of the observed data.

The simulated saturation data (Figure 33) shows that the values only somewhat mimics the dynamics in the observed values. The simulated values in 2000 are too low compared to the observed data where the simulated values in 2001 and 2002 are too high, and many simulated values reach 100 % saturation. This pattern is also seen in the simulated saturation values in 60 cm b.g.s, 93 cm b.g.s, 110 cm b.g.s, 190 cm b.g.s, and 210 cm b.g.s where the simulated values overall are too high compared to the observed values and often reach 100 % saturation (Appendix 4).

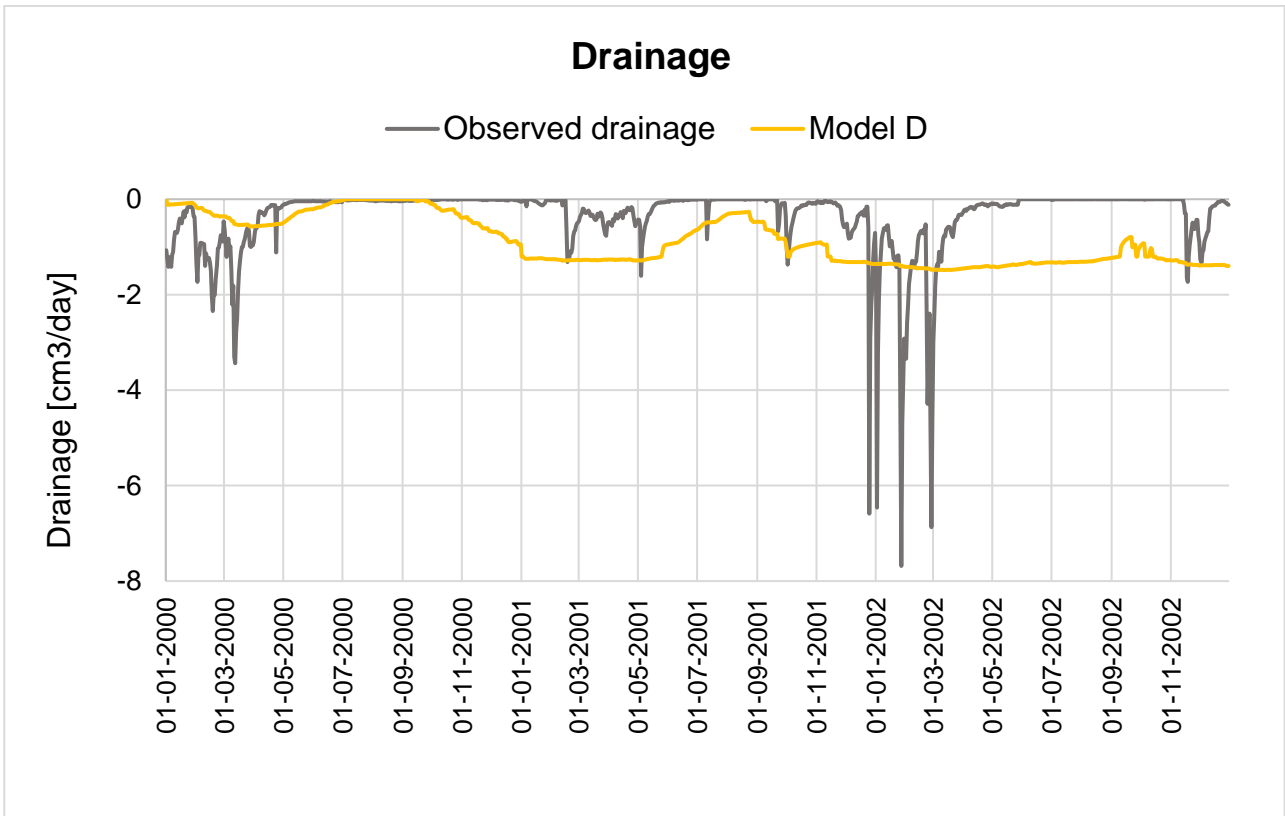


Figure 31: Simulated drainage (yellow line) from Model D and observed drainage (grey line).

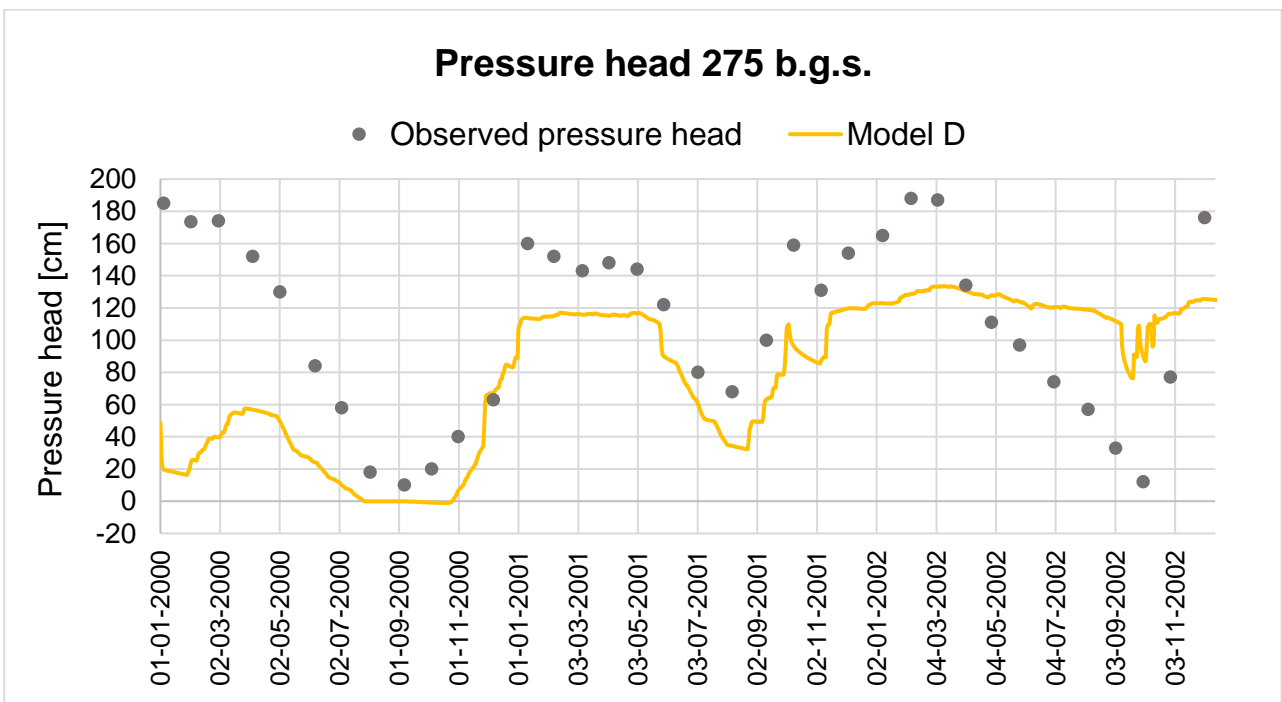


Figure 32: Simulated pressure head (yellow line) from Model D and observed pressure head (grey line).

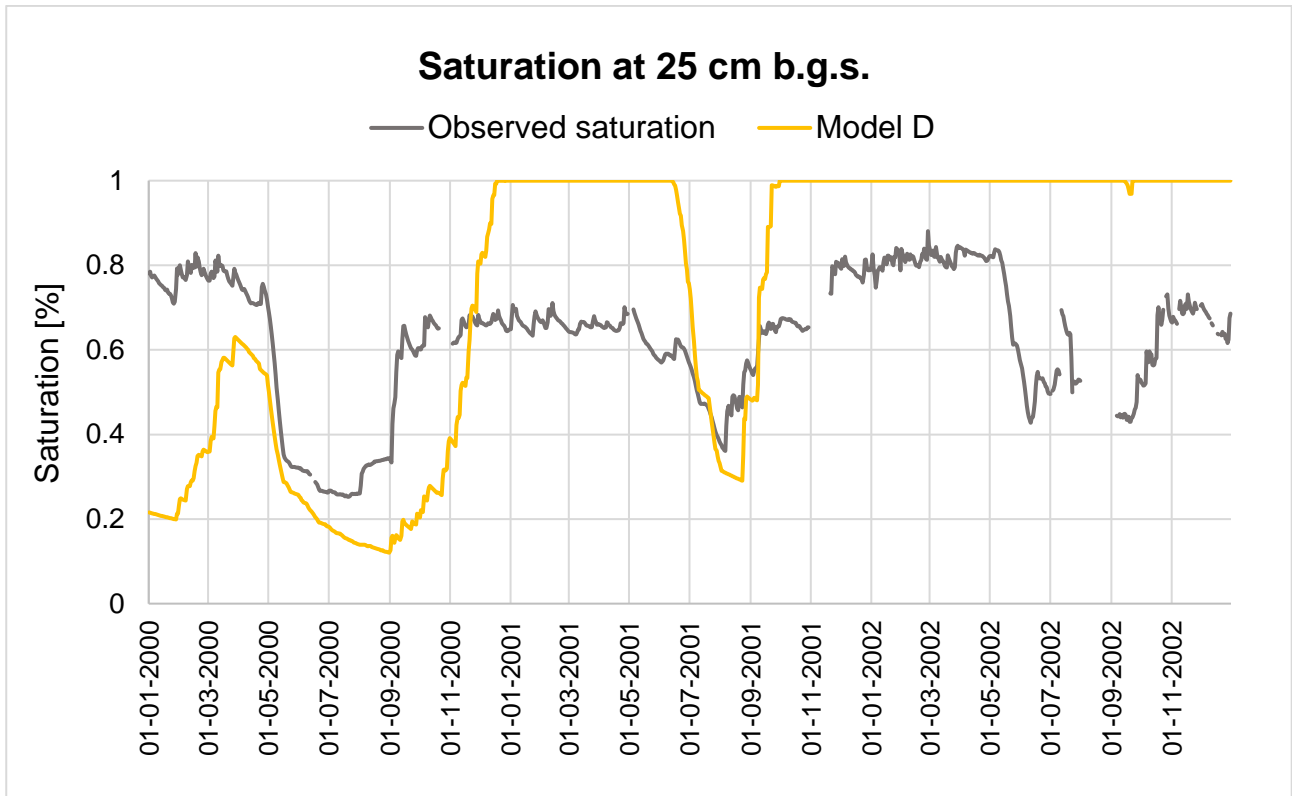


Figure 33: Simulated saturation (yellow line) from Model D at 25 cm b.g.s and observed saturation (grey line).

### 5.5 Model E - Dual-domain

Model E is a dual-domain model with the second domain representing macropores. Due to time limitations and difficulties with adding the second domain (macropores), Model E has only been calibrated manually. Model E is not fully developed, and therefore the results are only preliminary. The parameter values used in the best calibrated dual-domain model (Model E) are shown in Table 18.

Table 18: Parameter values for Model E found by manual calibration.

<b>Calibration results Model E</b>	
<b>Parameter</b>	<b>Parameter value</b>
<i>K1 [cm/day]</i>	1
<i>K2 [cm/day]</i>	0.2
<i>K3 [cm/day]</i>	0.0175
<i>a1 [cm<sup>-1</sup>]</i>	0.005
<i>a2 [cm<sup>-1</sup>]</i>	0.00293
<i>a3 [cm<sup>-1</sup>]</i>	0.00293
<i>b1</i>	2
<i>b2</i>	1.07442
<i>b3</i>	1.07442
<i>Drain [cm<sup>3</sup> / day]</i>	0.24

The simulated pressure heads are shown in Figure 34, and the values are much lower than the observed values. However, even though the values are much too low, they do overall mimic the dynamics of the observed values. The simulated values for saturation at 25 cm b.g.s. are shown in Figure 35. The dynamic of the observed data is overall present in the simulated data, but the fluctuations are a bit larger than in the observed data. When the observed data show high values, the simulated values are a little higher, and when the observed values are lowest, the simulated values are a bit lower. Model E does not simulate any drain outflow.

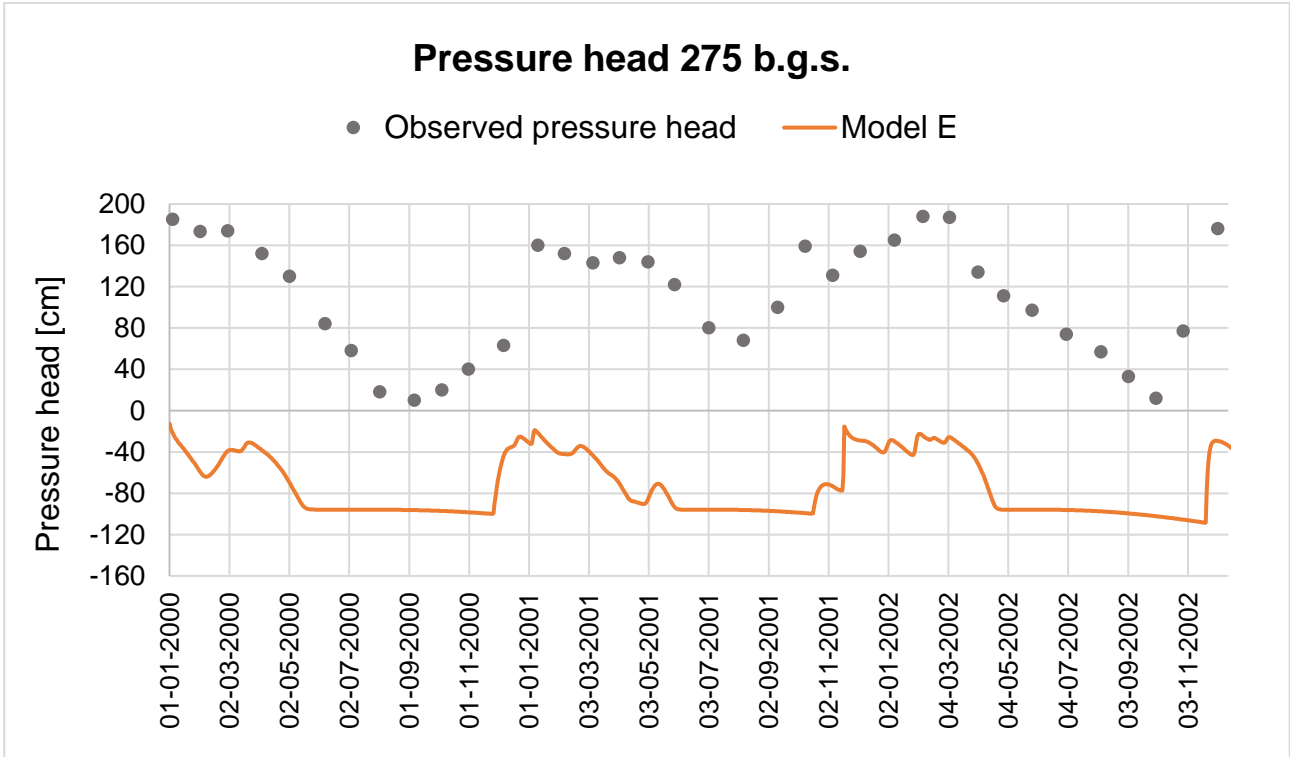


Figure 34: Simulated pressure head (orange line) from Model E and observed pressure head (grey line).

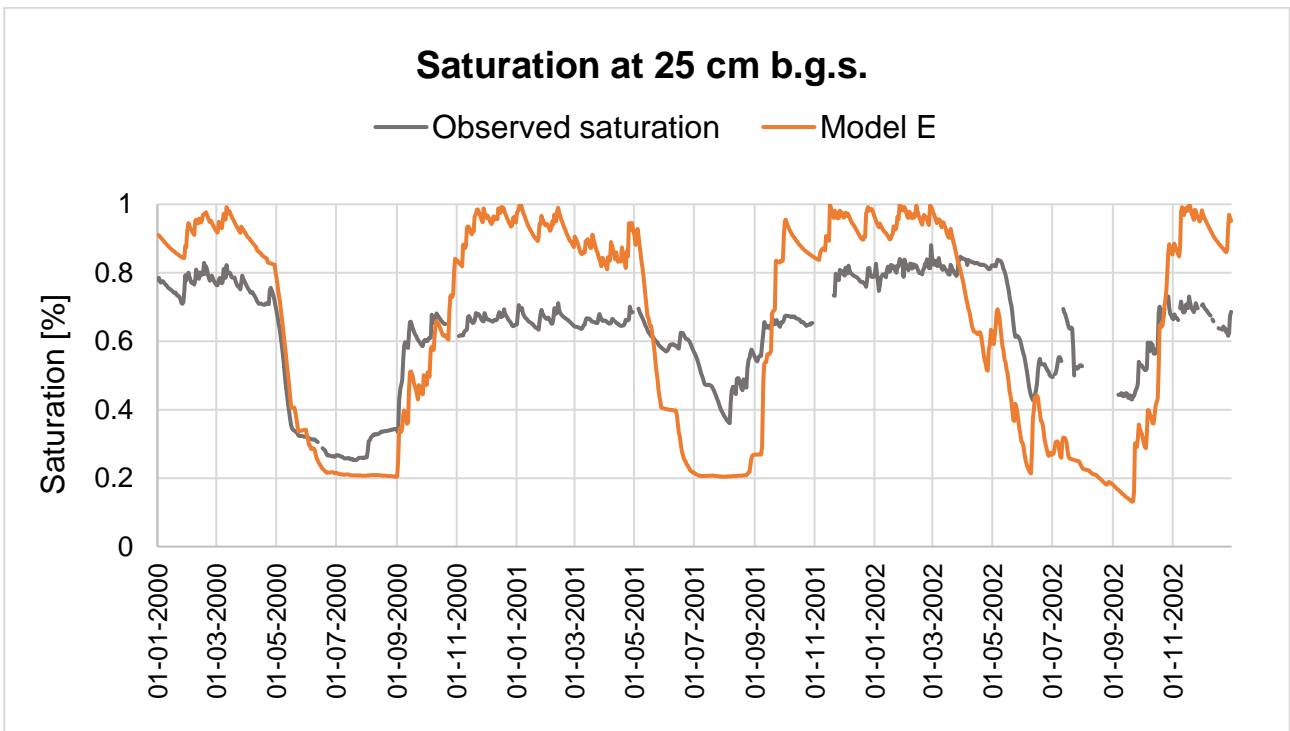


Figure 35: Simulated saturation (orange line) from Model E at 25 cm b.g.s and observed saturation (grey line).

## 6 Fieldwork

In connection to this project, a few field measurements were conducted at the Faardrup field site on the 30<sup>th</sup> of October, 2018. The measurements were conducted to estimate saturated hydraulic conductivity using the Guelph Permeameter Method (Wiltschut, u.d.). The Guelph Permeameter method is used to measure hydraulic conductivity above the water table in a relatively quick and easy way compared to other above water table methods and was there suitable for the fieldwork at Faardrup. This method is most optimal in the range between 15 to 75 cm below the soil surface (Mohsenipour & Shahid, 2016). It was the intention to do multiple measurements in the depths of 20 cm, 30 cm, 40, cm 50 cm and 60 cm, at different locations around the field. It was not allowed to carry out field measurements in the actual field to preserve the field, and therefore the measurements were conducted in the buffer zone around the field. Due to an unusually warm and dry summer (Damberg, 2018), the ground was very dry and hard, so it was almost impossible to dig the holes for the experiments with the handheld drill which was used. This resulted in only three measurements, one in the depth of 20 cm and two in the depth of 25 cm. The location of the field measurements can be seen in Figure 36, and the results can be seen in Table 19. The calculations were done in an excel sheet provided by Maiken Caroline Looms Zibar (KU) and are presented in Appendix 6.

It was also the intention to due filed measurement with a tension infiltrometer to measure unsaturated hydraulic conductivity (Eijkelkamp, u.d.). Even though multiple experiments were conducted, it was not possible to get the equipment to function correctly, and therefore it did not give useful data. Soil cores were also excavated for measurements of soil hydraulic test, but due to lack of time, these tests were not conducted.

Table 19: Location name and results of field measurements at the Faardrup field site.

<b>Field measurements</b>		
<b>Location</b>	<b>Depth b.g.s. [cm]</b>	<b>Hydraulic conductivity K [cm/day]</b>
L1	25	60.8
L2	25	24.8
L3	20	7.4

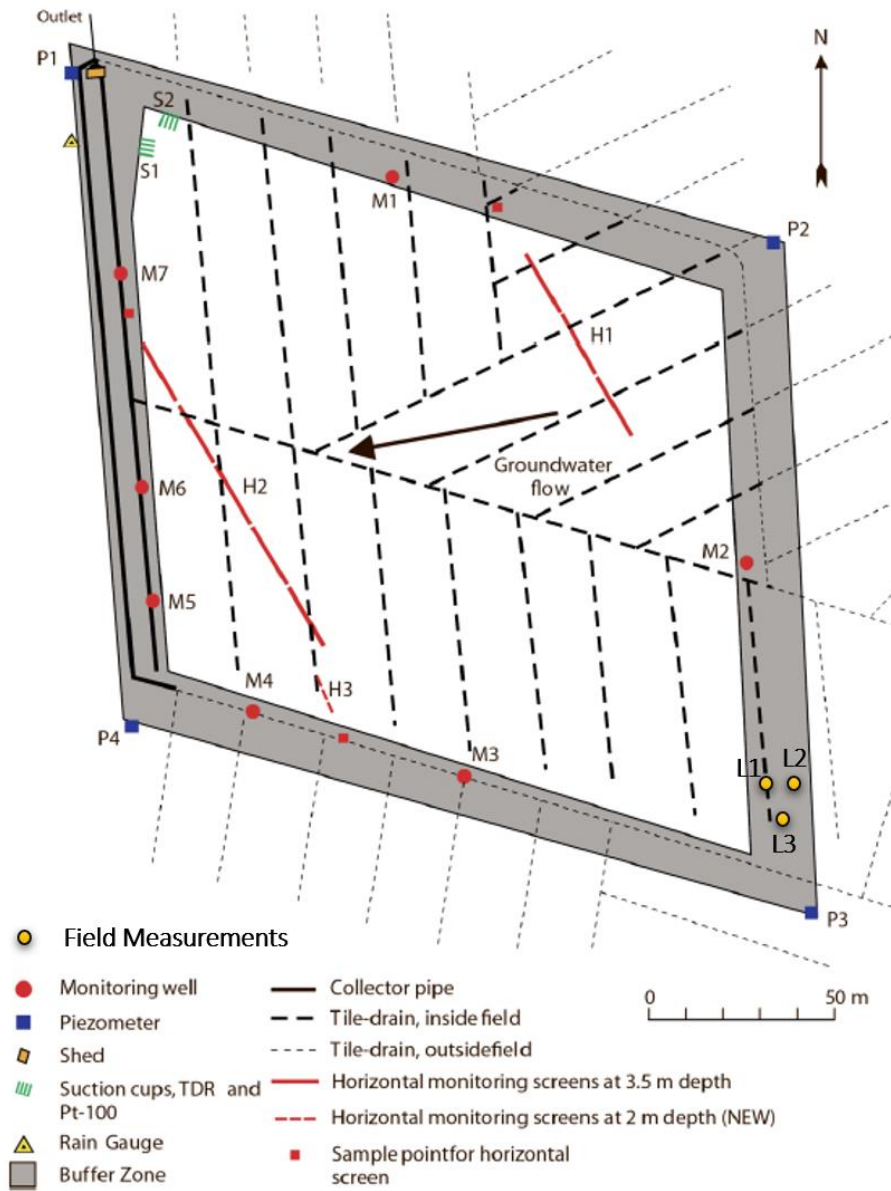


Figure 36: Overview of the technical installations at the Faardrup field site with the location of the field measurements (Lindhardt, et al., 2001).

## 7 Discussion

Model A, B, C, D, and E are all included in this report because they each have different properties, which make them important through the process of developing a useful model in HGS. The models contain a various range of values for hydraulic conductivity and Van Genuchten parameters  $\alpha$  and  $\beta$ . These models are all included because they contribute to determining which parameters and parameter values are needed to fit the simulated data to the observed data. As the different models show, this can be very difficult. Model A shows that fitting of the saturation (Figure 17) with the observed data is fairly easy and can be done by manual calibration. The problems arise when trying to simulate pressure head and drain values. Especially the pressure head values (Figure 16) are difficult to replicate with the model. The developed models have a tendency to simulate much too low pressured head values. This means that the simulated water table is located too deep compared to the observed water table. Therefore, the development of the HGS models has been focused around trying to simulate a more shallow water table. The too deep water table also caused problems with activations of the drains. In the first simulations, the drains were not activated, and there was no simulated drain outflow. Most of the water just left the model through the bottom of the model. To correct this, changes were made in the K-values (hydraulic conductivity) in the different horizons. Initially, the K-values given from MACRO was very high (Table 5), and these were lowered considerably. In zone 1, the K-values were lowered from 1615.2 cm/day to 10 cm/day, in zone 2 from 2668.8 cm/day to 10 cm/day and in zone 3 from 62.4 cm/day to 0.05 cm/day. Simulations showed that especially the lowering the K-value in zone 3 was very important for the performance of the model. The K-value in zone 3 had to be very low to get any drain outflow and a more shallow water table. This is evident in all the models where the K-value in zone 3 is much smaller than the values in zone 1 and 2. Zone 3 makes up most of the model, and it is would, therefore, also be expected to be one of the most essential parameters.

Changes alfa and beta values were also required to get the model to run. Simulations show that the model was very sensitive to changes in these parameters, and many simulations did not converge because of changes in these parameters. Alfa and beta values were therefore taken from (Carsel & Parrish, 1988). Model B shows that the inverse calibration also had trouble finding parameter values, which would result in higher pressure head values (Figure 19). Even though inverse calibration for Model B was successfully completed (Table 12), the results were not very useful. The objective function was only lowered by a better fit on the drain outflow. The pressure head values were equally bad as in Model A, and the fit with observed saturation was worse than Model A. The 95 % confidence intervals for the parameter values in Model B show large uncertainties in the vales overall with large bounds, but for K3 it has a quite narrow range. K3 is also the most sensitive parameter in the sensitivity analysis, and experience from the manual calibration shows that this value has a great

impact on the model. The overall fit of Model B altogether is very bad, and the only thing useful from this model was the drain value. It has a much lower value than Model A, and the simulated values are much closer to the observed values than in Model A.

Model B was also important because it showed that the inverse calibration with PEST could be achieved after many failed attempts with incomplete runs. The calibration was achieved by changing the parameter boundaries and assigned weights.

The wider range of boundaries in the inverse calibration for Model C (Appendix 3) resulted in an incomplete run, but the results were still useful. The objective function was lowered from 225 to 75.27 mostly by the drain contribution but also from the pressure head contribution. With the parameter values in model C, it was possible to get higher pressure head values (Figure 22). Even though the simulated values are still much too low, it is still possible to see the dynamics of the observed values in the simulated values.

Changes in the weights in Model E also resulted in an incomplete run, but the contribution from the pressure head to the objective function was lowered even more than in Model C (Table 17). Model D has the best fit with observed pressure head values (Figure 32) of all the models but the worst fit with observed drain and saturation values (Figure 31 and Figure 33).

Model A, B, C, and D show that it is difficult to get a fit with the observed data for saturation drainage and pressure head at the same time. When the saturation fits relatively good, the pressure head is very bad, and when the pressure head fits relatively good, then the drain outflow fits very badly. In Model D, where the pressure head fits relatively good, the rise in the water table that allows for these values also causes a much more continuous outflow of drain water and too high saturation values. This also includes drain outflow in periods with not observed drain outflow (Figure 31).

When comparing the simulated data with the observed data to evaluate the models, visual comparison cannot stand alone. RMSE was calculated for each of the models for both saturation and pressure head (Table 8). The RMSE values calculated for pressure head shows as well as the visual comparison that Model D has the best fit with regards to observed pressure head data. The RMSE for Model D is 67.3 cm, where it for Model A and B are respectively 133.6 cm and 128.6 cm. These large values are consistent with the visual comparison as well. Model C, which somewhat mimics the dynamic in the observed pressure head values, has a slightly lower RMSE value of 106.4 cm. Because of the large variation in the observed values, it was difficult to estimate an accepted uncertainty limit. One possible value limit could be a maximum variation of 50 cm, and here all the models would fall outside.

For drainage, the Fbal value was calculated (Table 8), and an accepted uncertainty of a variation of 10% was decided on. Again non of the models fall with this limit. Model B is closest to the limit with a variation of 17.8 %, but the visual comparison shows that even with values close to the observed data, the dynamics of the observed data are not captured at all. Both models A, C, and D have Fbal values far above 100 %, with Model C having the highest value of 485.1 %. The visual comparison of the models shows that Model C (Figure 21) captures the dynamics of the flow best of all the models even though the simulated values are too high and have the highest Fbal value.

For saturation, the RMSE was calculated, and an accepted uncertainty of 0.1 was decided on. Again non of the models fall within this limit. Model A has the best fit on saturation with an RMSE value of 0.16. This also corresponds with the visual comparison. Model C has the next best fit with an RMSE of 0.18. Model B and D have RMSE values of 0.26 and 0.31.

The estimated Van Genuchten parameters  $\alpha$  and  $\beta$  vary slightly from model to model. In zone 1  $\alpha$  varies from 0.016 cm to 0.058 cm and defines the soil type as silt, loam, or sand clay loam. In zone 2, the values for  $\alpha$  are all 0.036 cm because the parameter was fixed and defines the soil type as loam. In zone 3  $\alpha$  ranges from 0.014 cm to 0.1 cm and defines the soil type as silt, loam, or loamy sand. Model C has the lowest  $\alpha$  values, while Model B has the highest values. The low  $\alpha$  values in Model C are possible one of the reasons why this model performs better in regards to pressure head values than Model B because soils with lower  $\alpha$  values have a stronger hold on the water, which seems to be needed to build up the pressure head. For the parameter  $\beta$ , the values are quite similar in models A, B, and C with values from 1.30 to 1.61 defining the soil types in all zones as silt, loam, or clay loam. Model D has slightly higher values for with the value 2.68 in zone 1 and 1.89 in zone 3, defining the soil types sand and sandy loam. Like  $\alpha$ ,  $\beta$  was fixed at 1.56, which defines the soil type loam. In the inverse calibration, a small range of boundaries for  $\alpha$  and  $\beta$  was necessary to avoid crashing the model. However, this might have prevented the more optimal values to be identified because they were outside the boundary limits.

The K-values are the values that vary most from model to model. In zone 1, the highest K-value is found in Model C at 3026 cm/day. In Model D the values are a bit lower at 2046 cm/day, and in Model A and B, they are much lower with values of 10 cm/day and 29 cm/day. In zone 2, the K-values in Model A and B are almost the same values as in zone 1, and in Model C and D, the values are 417 cm/day and 495 cm/day. In zone 3 the K-values are much lower at values from 0.05 cm/day to 0.175 cm/day. Model C and D show the same tendencies with high values in zone 1, lower values in zone 2, and the lowest values in zone 3. The high K-values in zone 1 and zone 2 in Model C could explain the high drain outflow. The models all agree that the highest K-values are found in zone one and the lowest in zone 3. Because zone 3 makes up most of the model, the K-value in zone 3 is also

one of the most sensitive parameters, and changes in this value largely affect the results of the model.

The fieldwork conducted to estimate hydraulic conductivity in 20 to 25 cm b.g.s. shows values from 7.4 to 60.8 cm/day. The measurements were done very close to each other and indicate that there exists a variation in the hydraulic conductivity values in the same depth across the field. This could be caused by whether the measurements are done where larger macropores exist.

Water balance for each of the models are shown in Table 9 and is useful when looking at how the water leaves the models. The amount of water leaving the models by ET is relatively similar, with values from 14.823 cm<sup>3</sup> to 17.803 cm<sup>3</sup>. The set-up for ET is the same for each model, so the differences in ET are likely caused by differences in the matrix properties determining how fast the precipitation can infiltrate the soil. The more interesting differences are seen in the drain outflow and the free drainage. Free drainage is the water leaving the model through the bottom of the model. This value is much higher for Model A and B than for Model C and D. This corresponds with the experiences from the simulations, which showed that too much water was leaving Model A and B to build up pressure head in the column. In Model C and D, where some meaningful pressure head values were achieved, much less water leaves the models through free drainage. In Model C, 2161 cm<sup>3</sup> water leaves the model through the bottom, and for Model D the amount is 2737 cm<sup>3</sup>. The values for Model A and B are 4560 cm<sup>3</sup> and 6686 cm<sup>3</sup>. The small number for free drainage in Model C could also be connected to a large amount of water, leaving the model through the drains. In the observed data, the drainage is 379 cm<sup>3</sup> water, and in Model C it is 2217 cm<sup>3</sup> which also explains the high RMSE value for drains in Model C. Model B is close to the observed value with 311 cm<sup>3</sup> of water leaving through the drains, but again the visual comparison of the simulated and observed values show a very poor resemblance in terms of the dynamics of the flow. The water balance shows that most of the water leaves the model through ET. Therefore, the amount of water entering the model and participating in the flow is only 6413 cm<sup>3</sup> out of a precipitation of 21236 cm<sup>3</sup>. This trend is also seen in the rest of the model with slight variations (Table 9).

None of the models falls within any of the set uncertainty limits for either simulated pressure head, drainage, or saturation. Despite this, one of the models had to be selected to simulate solute transport and validation. Based on an overall assessment of Model A, B, C, and D, Model C is estimated to be the best of the four single-domain models. In this decision, both the model statistics, the visual comparison, the water balance, and the objective function from the PEST calibrations were considered. Even though Model C has the highest deviation from the observed drain values, the fit of the drain dynamics is weighted higher in this decision. Model D has a better fit with observed

pressure head values, but because of the very poor fit with observed drain values, Model C is preferred over Model D.

The validation performed on Model C (Figure 24, Figure 25, and Figure 26) show that the model produces similar results when using other data than the ones used in the calibration. Validation of the other models would not be very useful since the poor fit of the simulated data would make it hard to link trends in the simulated data to the observed data.

When interpreting the solute transport results from Model C (Figure 27, Figure 28, Figure 29, and Figure 30), it is important to consider the overall fit of the model. Even though Model C in many areas varies from the observed data, the simulation of solute transport is relatively good. For the suction cups in 100 cm, the simulated bromide values are in the same magnitude as the observed values only slightly higher. For suction cups in 200 cm, the values are also in the same magnitude with values lower in one period and higher in another period. The values are as expected higher closer to the soil surface because it has not been dispersed as much. The simulated peak in concentration is also steeper and occur sooner at 100 cm b.g.s than 200 cm b.g.s. Unfortunately, there is a gap in the observation data right where the concentration peak 100 cm b.g.s, and it can therefore not be estimated if this also is the case. The too-high simulated concentrations seen 100 cm b.g.s could be caused by too high hydraulic conductivity in zone 1 and 2. With lower K-values in zone 1 and 2 the bromide could be delayed and diluted more before reaching 100 cm b.g.s. In the same way, the too low simulated concentrations at 350 cm b.g.s compared to the water from horizontal wells could be caused by too low hydraulic conductivity in zone 3. The higher observed values at 350 cm b.g.s could also be caused by the lack of macropores in the model. Macropores can lead to preferential flow and result in deeper infiltration of higher concentrations than flow exclusively in the matrix would (Šimůnek & van Genuchten, 2017). Some precautions must also be taken when comparing the simulated concentration with the observed concentration from the drains and horizontal wells. In the drain, the concentration is measured in the drain water and not directly in the water within the soil. If this makes, any difference is hard to determine but needs to be considered. Because Model C does not contain macropores, it is possible that the relatively good results could have been generated on a wrong and uncertain foundation. Nevertheless, it does show that the model is equipped to simulate solute transport in a fairly simple manner.

Model A, B, C, and D are all single domain models and consist only of a porous matrix domain. This may be the cause of the difficulties with the performance of the models. It is described in (Šimůnek & van Genuchten, 2017) that the uniform flow patterns usually predicted with the Richards equations are not consistent with the variably saturated flow in many agricultural soils, such as Faardrup. The presence of macropores in the soil at Faardrup field site may result in preferential flow where some

of the water flow in the macropores and thereby bypass a fraction of the porous matrix. The single-domain models were, therefore, never expected to fully replicate the observed data because the models do not describe a very crucial part of the conditions at the field site. To simulate the observed data at Faardrup, the model would need to be a dual-permeability model with one domain representing the porous matrix and one domain representing the macropores. The model's A, B, C, and D are apparently too simple to simulate the flow at the field site.

Model E is a dual-domain model with macropores as the second domain. Model E was not fully developed and only manually calibrated. The preliminary results show problems with the build-up of water in the column resulting in no drain outflow and much too low pressure head values (Figure 34). Even though the pressure head values are much too low, the tendencies seen in the observed data are visible in the simulated values. The dynamics seen in the observed saturation data are also seen in the simulated saturation data (Figure 35), but the values are either slightly too high or slightly too low. Due to the more complex dual-domain model, the simulation time was much longer than the single-domain models. The manual calibrations were, therefore, only conducted with a handful of different values for hydraulic conductivity and  $\alpha$ . The preliminary results from Model E indicate that the K-values and  $\alpha$  values had to be much lower than in the single-domain models. The model does not seem to have the same sensitivity to changes in the  $\alpha$  and  $\beta$  values, which caused many problems with the other models. The next step in the development of Model E would be an inverse calibration with PEST, but this was not achieved due to lack of time. With further development, this model would be expected to simulate flow at Faardrup better than Model A, B, C, and D because it incorporates macropores.

## 8 Conclusion

Five models have been developed in HGS: Four single-domain models (Model A, B, C, and D) and one dual-domain model (Model E).

Model A was manually calibrated and did only produce somewhat acceptable results in regard to saturation values with an RMSE of 0.16, which was the lowest of all the models.

Neither Model A nor Model B resulted in any useful data in regard to simulated pressure heads with RMSE values of 133.6 cm and 128.6 cm. Model C and D are much better at simulating pressure head with RMSE values of 106.4 cm and 67.3 cm. However, Model C has problems with simulating too high drain outflow values resulting in a 485.1% difference between observed and simulated average drain output. Model C has problems with the dynamics of the drain outflow and to high saturation values resulting in an RMSE value of 0.31.

Model B, C, and D were inverse calibrated with PEST, but only the calibration of Model B was completed successfully due to problems with convergence. However, the calibration did produce some useful results used to develop Model C and D. In spite of the issues caused by convergence problems, PEST proved to be a useful tool for inverse calibration of the HGS models.

It was assessed from an overall evaluation of all single-domain models, that Model C was the most useful, and it was therefore subsequently used to simulate solute transport. The results from the solute transport must be analyzed with caution since the performance of Model C is insufficient.

The difficulties with the single-domain models are likely caused by the lack of macropores in the model setup. The second domain in Model E represents macropores, which is an important feature at Faardrup field site. Model E was only calibrated manually and developed to the point where it produces preliminary results. Further work with Model E would include inverse calibration with PEST to give a better estimation of model parameters.

When using a model for any form of practical use like simulating flow or infiltration of pesticides, it is important to have confidence in the model. None of the models in this project fall within any of the decided accepted uncertainty limits. None of the produced models have a satisfying fit on all observed values and parameters and would not yet be suitable for practical use.

## 9 Future work

Further work with this project would include:

- Further development of the dual-domain model by investigations of model parameters to ensure model performance. This would also include further investigation of the model set-up and if other set-up options can produce more accurate results.
- Inclusion of more model parameters in the manual calibration of the dual-domain model like the unsaturated Van Genuchten functions and interface unsaturated Van Genuchten functions both for macropores (in *dprops*).
- Inverse calibration of the dual-domain model
- Adding solute transport to the dual-domain model, and possibly further develop the model to simulate the transport of different pesticides.
- Extending the simulation period. Observation data from Faardrup exist for almost 20 years, and therefore the model could be extended to include all these years.

**Acknowledgments**

I would like to thank my supervisor, Karsten Høgh Jensen (KU), for support and guidance throughout this project. I would also like to thank my co-supervisor, Annette E. Rosenbom (GEUS), for support and the providing of data to my project. I would also like to give a special thanks to my co-supervisor, Sachin Karan (GESU), for much technical support in the development of the HGS model and the set-up of the PEST calibration. Finally, I would also like to thank René Therrien for providing access to the HGS program and assistance in the development of the HGS model.

## References

- Aquanty. (2015). *HGS Reference Manual*. Aquanty inc.
- Benson, G., & Sawangsuriya, A. (February 2014). Estimating van Genuchten Parameters  $\alpha$  and  $n$  for Clean Sands from Particle Size Distribution Data. *Geotechnical Special Publication*.
- Carsel, R., & Parrish, R. (1988). Developing Joint Probability Distributions of Soil Water Retention Characteristics. *Water Resources Research vol. 24, No 5*, s. 755-769.
- Damberg, H. P. (2018). *DMI*. Hentet fra <https://www.dmi.dk/nyheder/2018-nyeste/2018-det-mest-toerkeramte-aar-i-danmark-i-99-aar/>
- Doherty, J. (7th Edition 2018). PEST Model-Independent Parameter Estimation. *Watermark Numerical Computing*.
- Eijkelkamp. (u.d.). *Operating instructions: 09.09 Tension Infiltrometer*.
- Fitts, C. (2012). *Groundwater Science* (2. Edition udg.). Academic Press.
- Gelhar, L., Welty, C., & Rehfeldt, K. (July 1992). A critical review of data on field-scale dispersion in aquifers. *Water Resources Research*, s. 1955-1974.
- Haverkamp, R., Debionne, S., Angulo-Jaramillo, R., & de Condappa, D. (2017). Soil Properties and Moisture Movement in the Unsaturated Zone. I J. Cushman, & D. Tartakovsky (Red.), *The Handbook of Groundwater Engineering* (s. 149-189). CRC Press.
- Hendriks, M. (2010). *Introduction to Physical Hydrology*. OXFORD UNIVERSITY PRESS.
- Kristensen, K., & Jensen, S. (1975). A Model for Estimating Actual Evapotranspiration from Potential Evapotranspiration. *Nordic Hydrology*, 6(3), 170-188.
- Larsbo, M., Roulier, S., Stenemo, F., Karsteel, R., & Jarvis, N. (2005). An Improved Dual-Permeability Model of Water Flow and Solute Transport in the Vadose Zone. *Vadose Zone Journal* 4, s. 398-406.
- Larsen, G., & Sand-Jensen, K. (2017). *Naturen i Danmark - Geologien*. Gyldendal.
- Lindhardt, B., Ablidtrup, C., Vosgerau, H., Olsen, P., Torp, S., & Iversen, B. (2001). *The Danish Pesticide Leaching Assessment Programme Monitoring Results May 1999–June 2016*. GEUS.
- Miljøstyrelsen. (2020). *Drikkevand*. Hentet fra <https://mst.dk/natur-vand/vand-i-hverdagen/drikkevand/>

- Mohsenipour, M., & Shahid, S. (2016). ESTIMATION OF SATURATED HYDRAULIC.
- Nimmo, J. (2004). Porosity and Pore Size Distribution. *Encyclopedia of Soils in the Environment: London, Elsevier*, v. 3, s. 295-303.
- Nimmo, J. (2009). Vadose Water. *Encyclopedia of Inland Waters*, s. 766-777.
- Rosenbom, A., Haarder, E., Badawi, N., Gudmundsson, L., von Platten-Hallermund, F., & ., .. (2017). *The Danish Pesticide Leaching Assessment Programme: Site Characterization and Monitoring Design*. GEUS.
- Rosenbom, A., Therrien, R., Refsgaard, J., Jensen, K., Ernsten, V., & Klint, K. (2009). Numerical analysis of water and solute transport in variably-saturated fractured clayey till. *Journal of Contaminant Hydrology*, s. 137-152.
- Šimůnek, J., & van Genuchten, M. (2017). Contaminant Transport in the Unsaturated Zone: Theory and Modeling. I J. Cushman, & D. Tartakovsky (Red.), *The Handbook of Groundwater Engineering* (s. 203-235). CRC Press.
- Sonnenborg, T., & Henriksen, H. (2005). *Håndbog i Grundvandsmodellering*. GEUS.
- Therrien, R., McLaren, R., Sudicky, E., & Panday, S. (October 2010). HydroGeoSphere A Three-dimensional Numerical Model Describing Fully-integrated Subsurface and Surface Flow and Solute Transport. *Groundwater Simulations Group*.
- Thorling, L., & Kjøller, C. (2020). *GEUS Grundvandsovervågning*. Hentet fra GEUS: <https://www.geus.dk/vandressourcer/overvaagningsprogrammer/grundvandsovervaagning/>
- Tuller, M., & Or, D. (2005). Water Retention and Characteristic curve. *Elsevier*.
- Wiltschut, H. (u.d.). *Operating Instructions for determining the hydraulic conductivity in the field by a permeameter with ball-cock*. Hentet fra <https://bodengutachten-wiltschut.de/>

## Appendix

### Appendix 1 - Model A

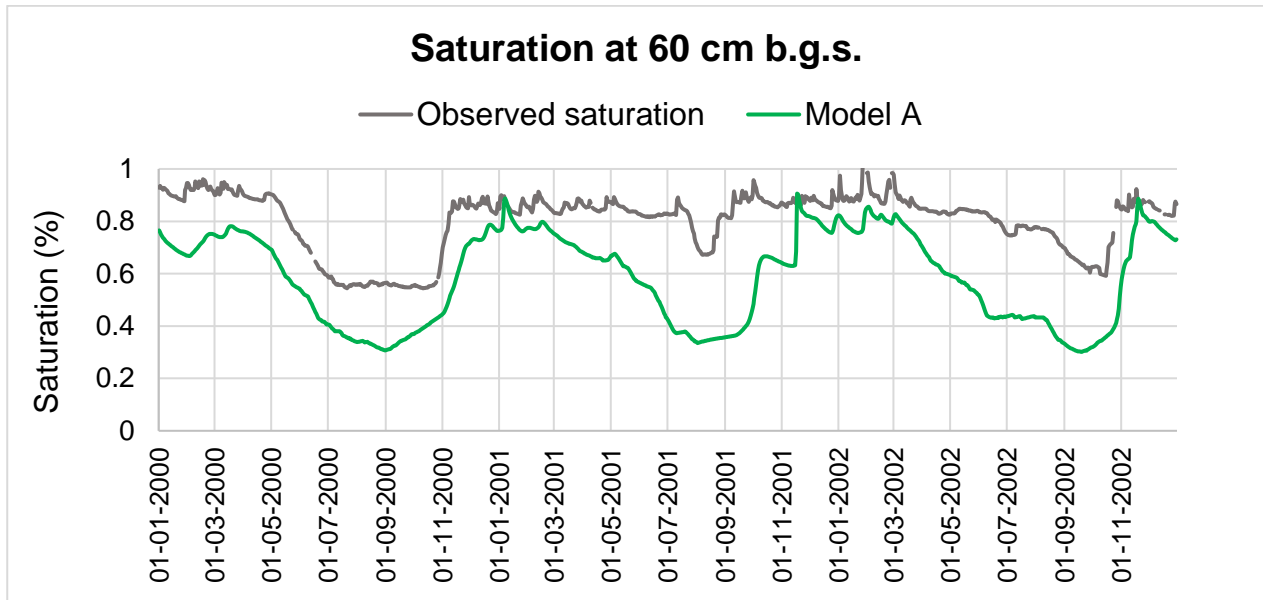


Figure 37: Simulated saturation (green line) from Model A at 60 cm b.g.s and observed saturation (grey line).

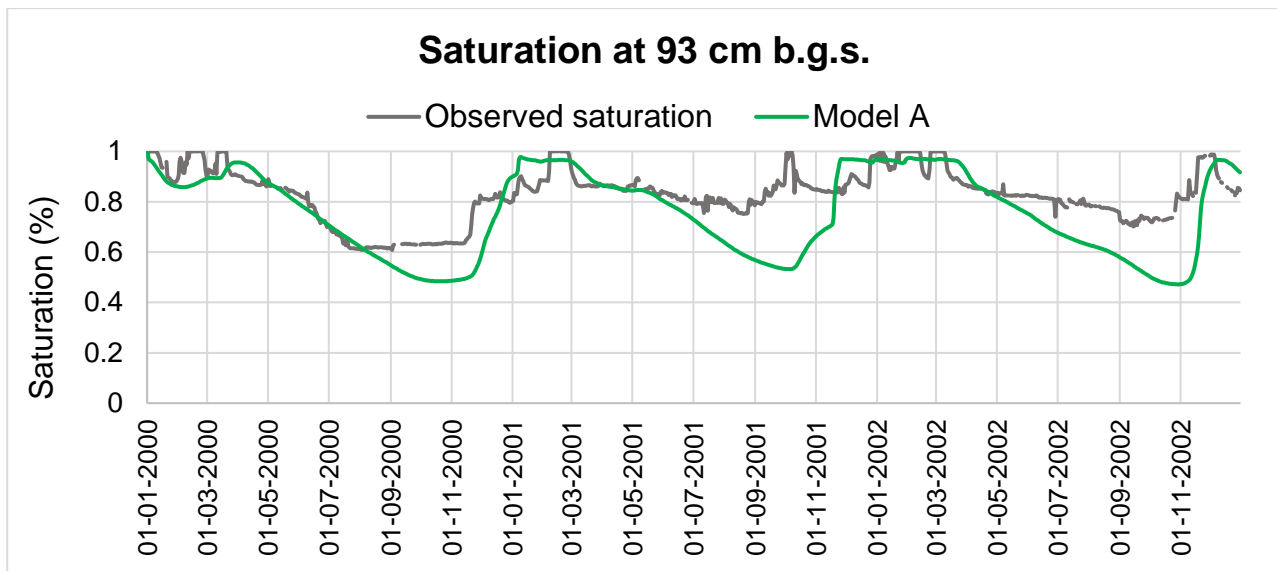


Figure 38: Simulated saturation (green line) from Model A at 90 cm b.g.s and observed saturation (grey line).

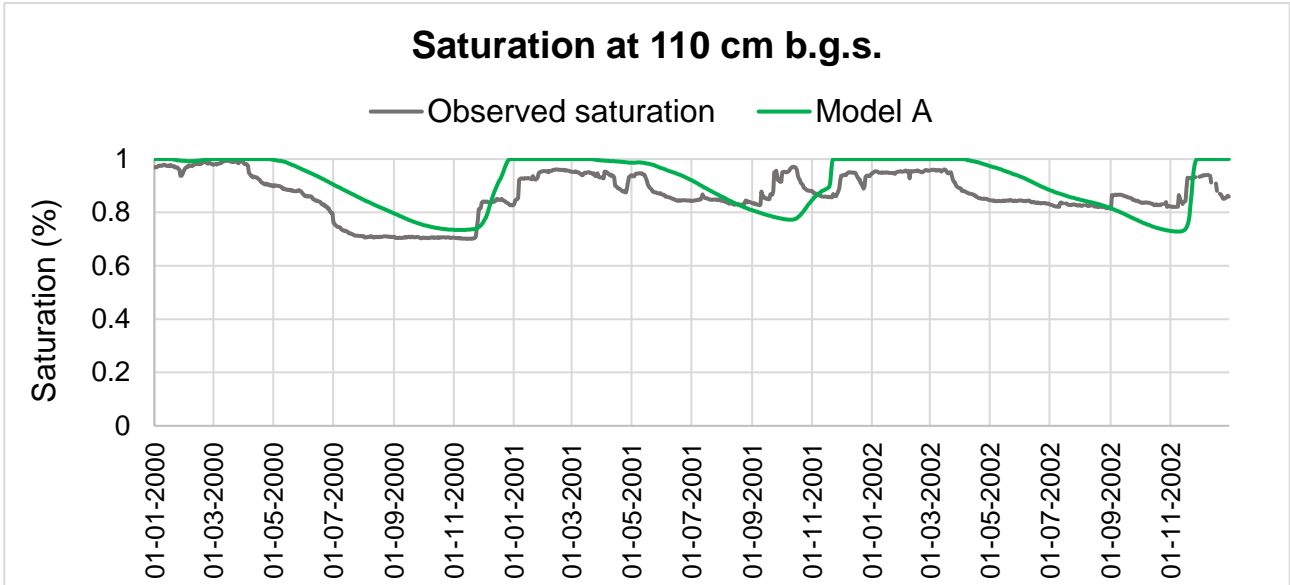


Figure 39: Simulated saturation (green line) from Model A at 110 cm b.g.s and observed saturation (grey line).

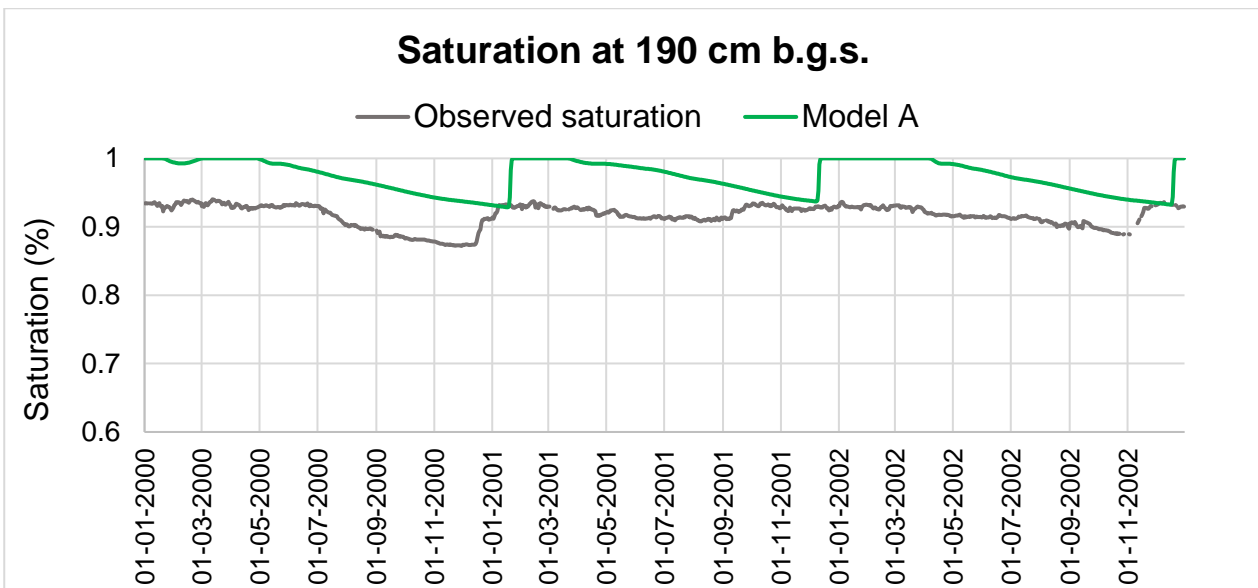


Figure 40: Simulated saturation (green line) from Model A at 190 cm b.g.s and observed saturation (grey line).

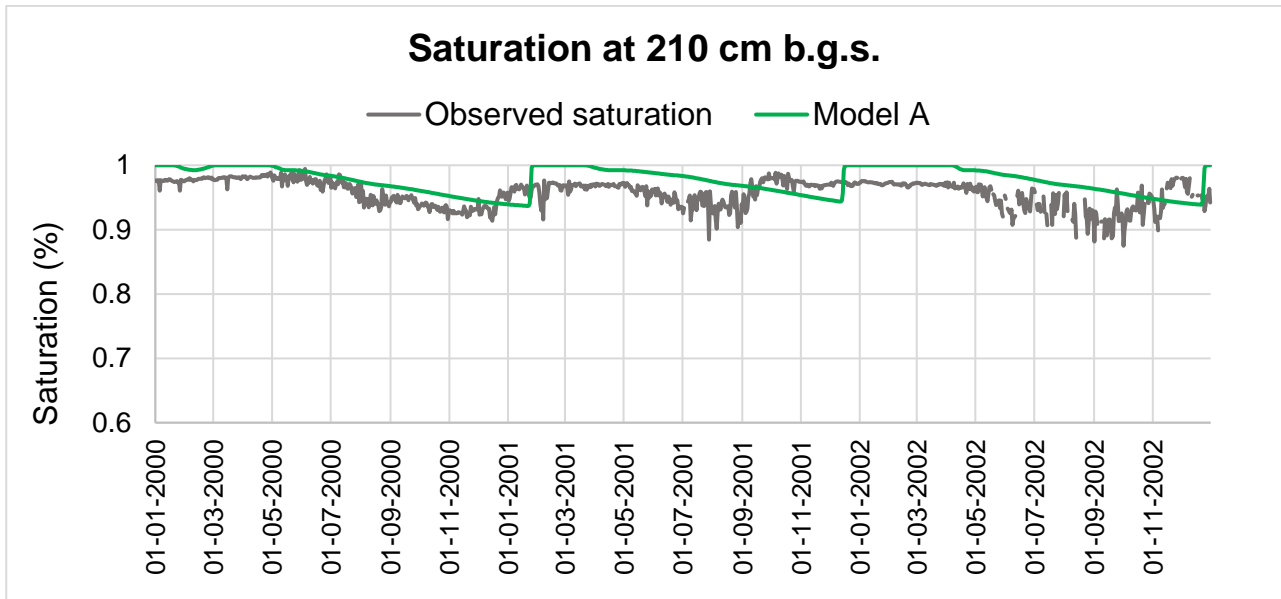


Figure 41: Simulated saturation (green line) from Model A at 210 cm b.g.s and observed saturation (grey line).

**Appendix 2 - Model B**

Parameter definitions:-

Name	Trans-formation	Change limit	Initial value	Lower bound	Upper bound
k1	log	factor	10.0000	1.000000E-10	4000.00
k2	log	factor	10.0000	1.000000E-10	4000.00
k3	log	factor	5.000000E-02	1.000000E-10	1000.00
a1	log	factor	7.500000E-02	3.700000E-02	0.145000
a2	fixed	na	3.600000E-02	na	na
a3	log	factor	7.500000E-02	1.600000E-02	0.100000
b1	log	factor	1.89000	1.61000	2.68000
b2	fixed	na	1.56000	na	na
b3	log	factor	1.89000	1.37000	1.89000
drain	log	factor	10.0000	1.000000E-10	100.000

Figure 42: Parameters values and parameter boundaries used in the inverse calibration of Model B. Screenshot from the PEST .pst file.

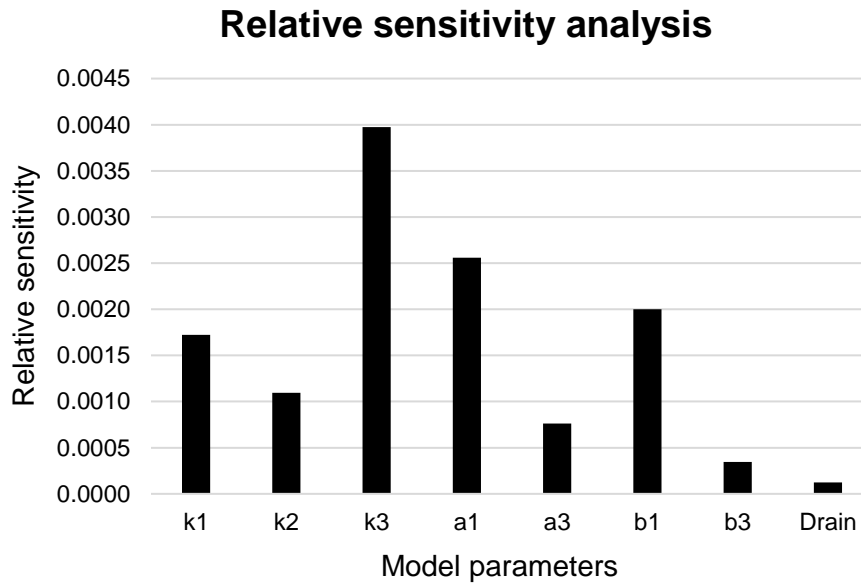


Figure 43: Sensitivity analysis of the parameters in Model B.

**Parameter correlation coefficient matrix**

	<b>K1</b>	<b>K2</b>	<b>K3</b>	<b>a1</b>	<b>a3</b>	<b>b1</b>	<b>b3</b>	<b>Drain</b>
<b>K1</b>	1	-0.45	0.61	-0.24	-0.41	0.11	0.05	4.7E-03
<b>K2</b>	-0.45	1	-0.09	0.32	-0.26	0.14	0.24	-0.46
<b>K3</b>	0.61	-0.09	1	-0.63	-0.38	0.02	-0.47	-0.22
<b>a1</b>	-0.24	0.32	-0.63	1	0.05	-0.07	0.63	0.08
<b>a3</b>	-0.41	-0.26	-0.38	0.05	1	-0.41	-0.08	0.15
<b>b1</b>	0.11	0.14	0.02	-0.07	-0.41	1	0.48	-0.03
<b>b3</b>	0.05	0.24	-0.47	0.63	-0.08	0.48	1	0.14
<b>Drain</b>	4.7E-03	-0.46	-0.22	0.08	0.15	-0.03	0.14	1

Figure 44: Parameter correlation coefficient matrix for parameters in Model B.

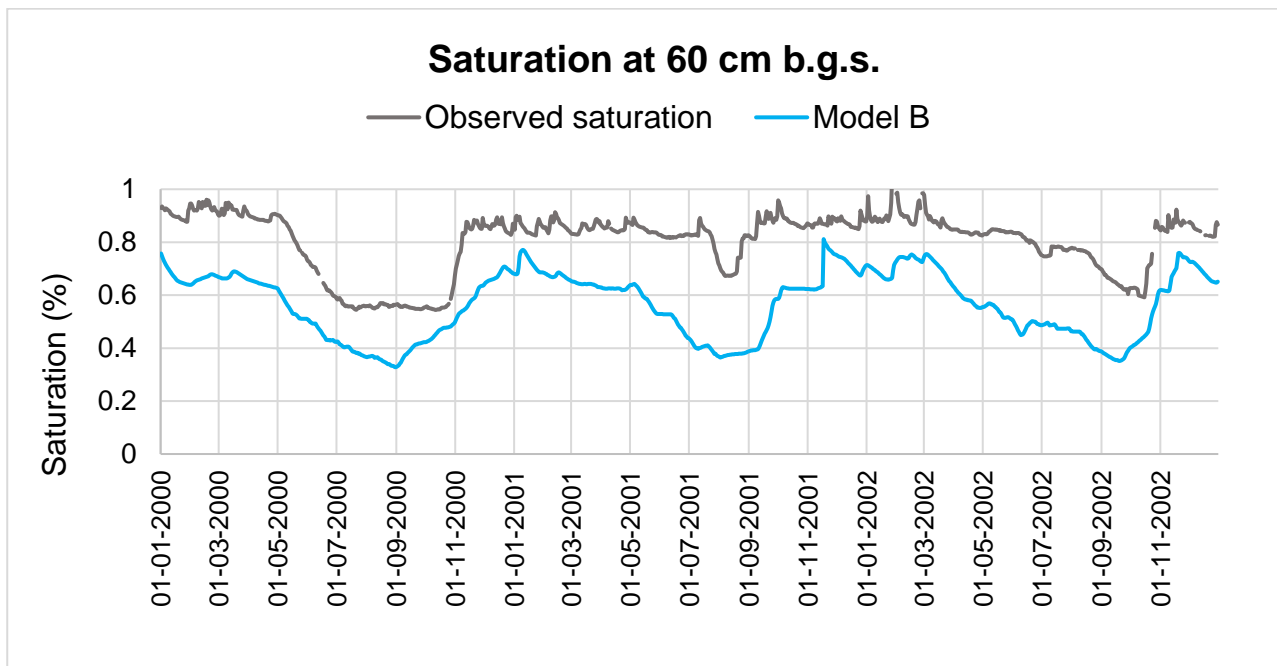


Figure 45: Simulated saturation (blue line) from Model B at 60 cm b.g.s and observed saturation (grey line).

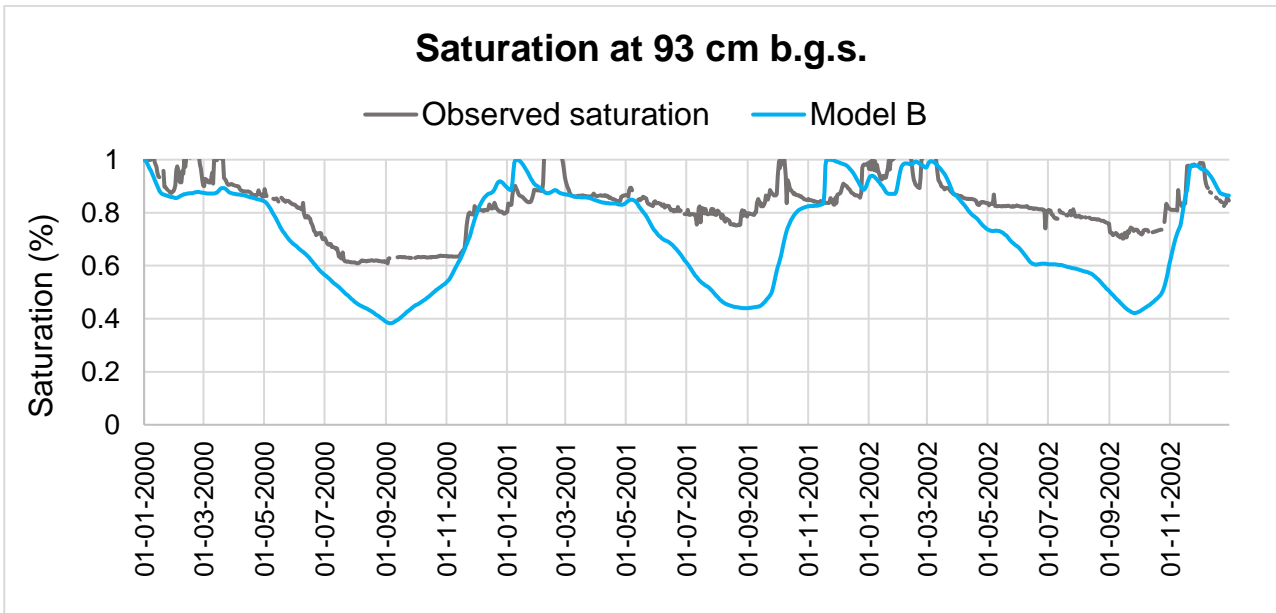


Figure 46: Simulated saturation (blue line) from Model B at 93 cm b.g.s and observed saturation (grey line).

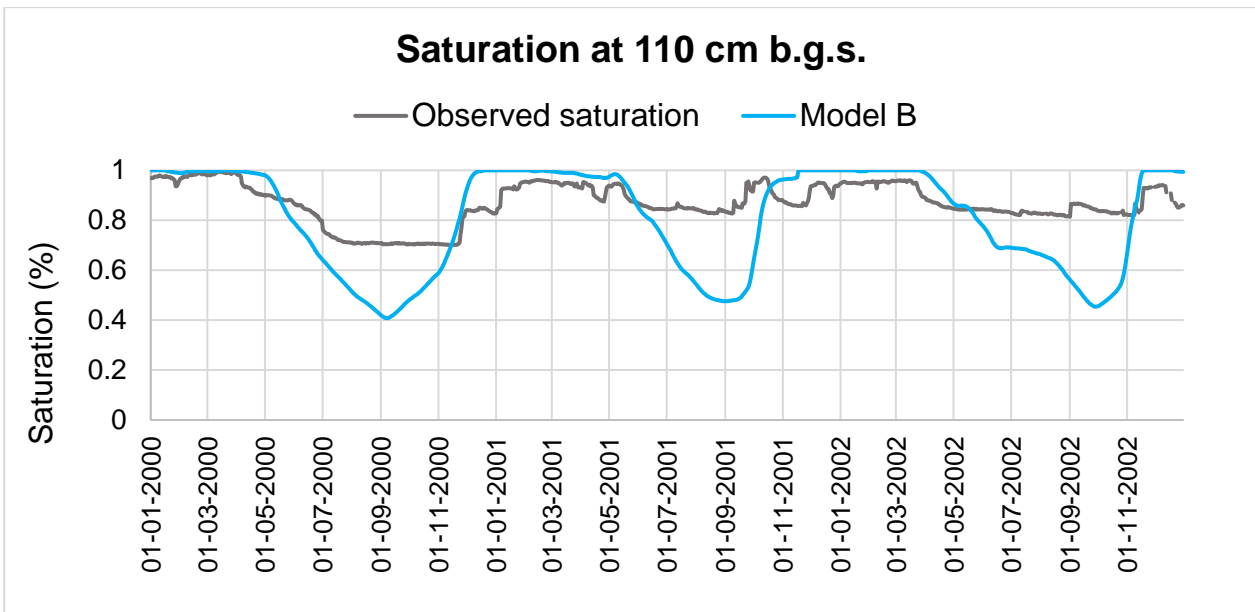


Figure 47: Simulated saturation (blue line) from Model B at 110 cm b.g.s and observed saturation (grey line).

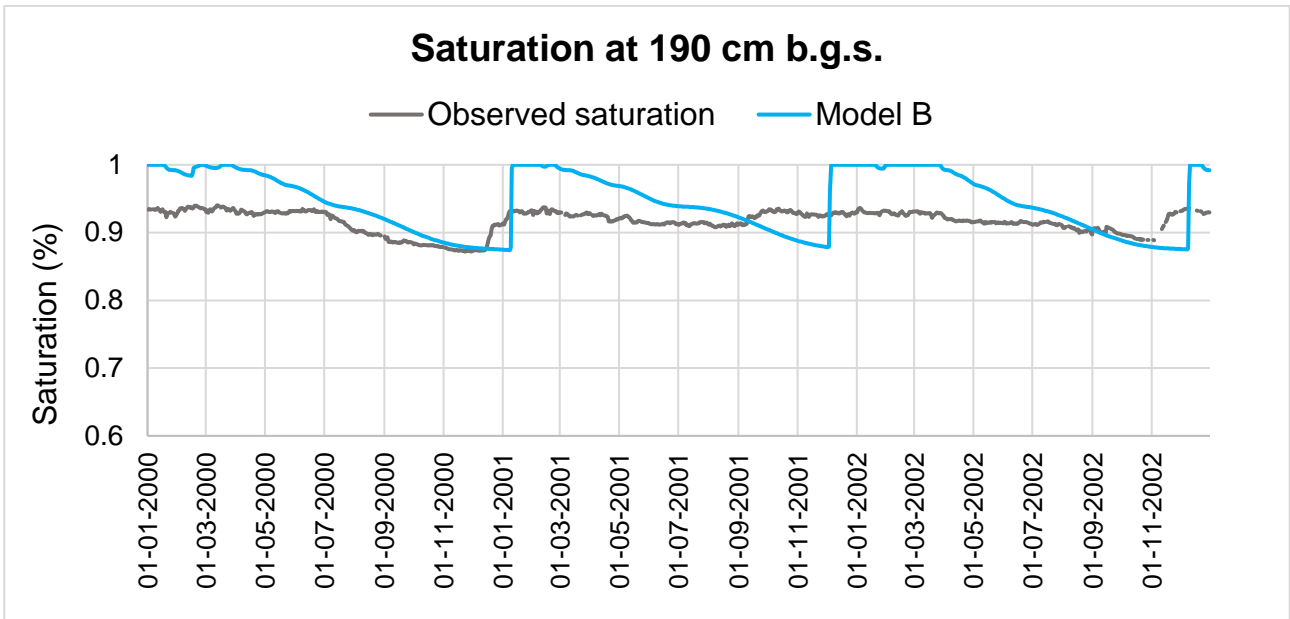


Figure 48: Simulated saturation (blue line) from Model B at 190 cm b.g.s and observed saturation (grey line).

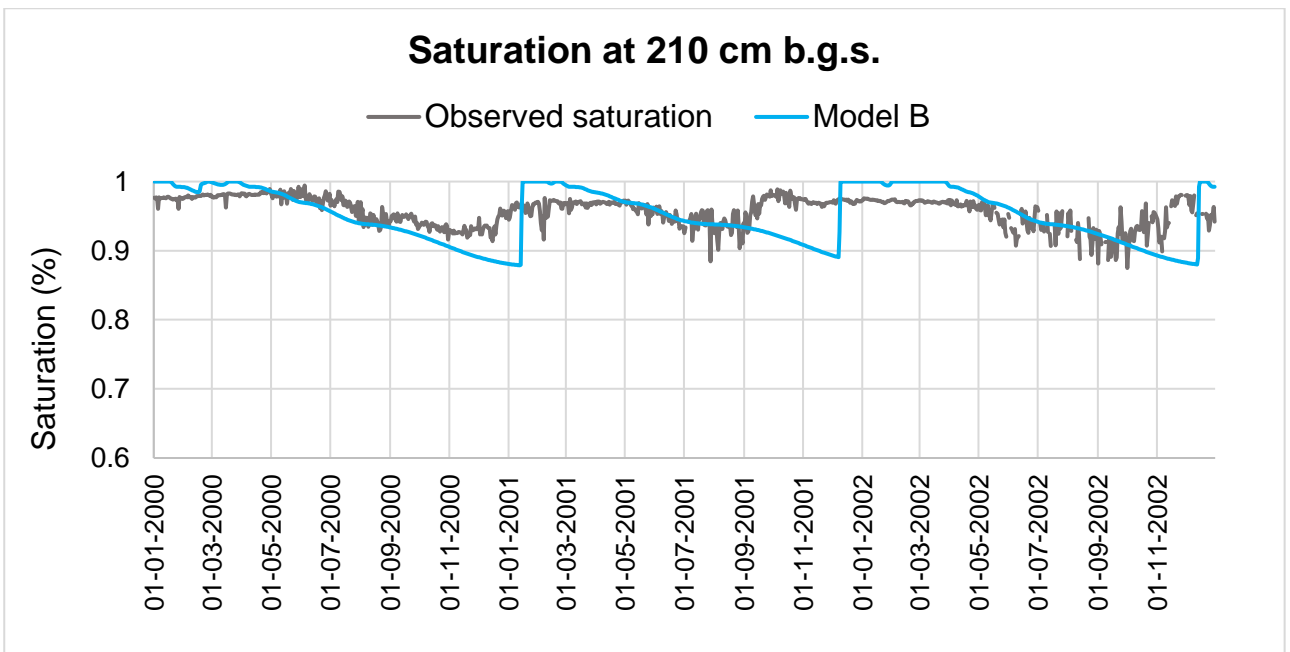


Figure 49: Simulated saturation (blue line) from Model B at 210 cm b.g.s and observed saturation (grey line).

**Appendix 3 - Model C**

Parameter definitions:-

Name	Trans-formation	Change limit	Initial value	Lower bound	Upper bound
k1	log	factor	10.0000	1.000000E-10	4000.00
k2	log	factor	10.0000	1.000000E-10	4000.00
k3	log	factor	5.000000E-02	1.000000E-10	1000.00
a1	log	factor	7.500000E-02	1.600000E-02	0.145000
a2	fixed	na	3.600000E-02	na	na
a3	log	factor	7.500000E-02	1.600000E-02	0.145000
b1	log	factor	1.89000	1.37000	2.68000
b2	fixed	na	1.56000	na	na
b3	log	factor	1.89000	1.37000	2.68000
drain	log	factor	10.0000	1.000000E-10	50.0000

Figure 50: Parameters values and parameter boundaries used in the inverse calibration of Model C. Screenshot from the PEST .pst file.

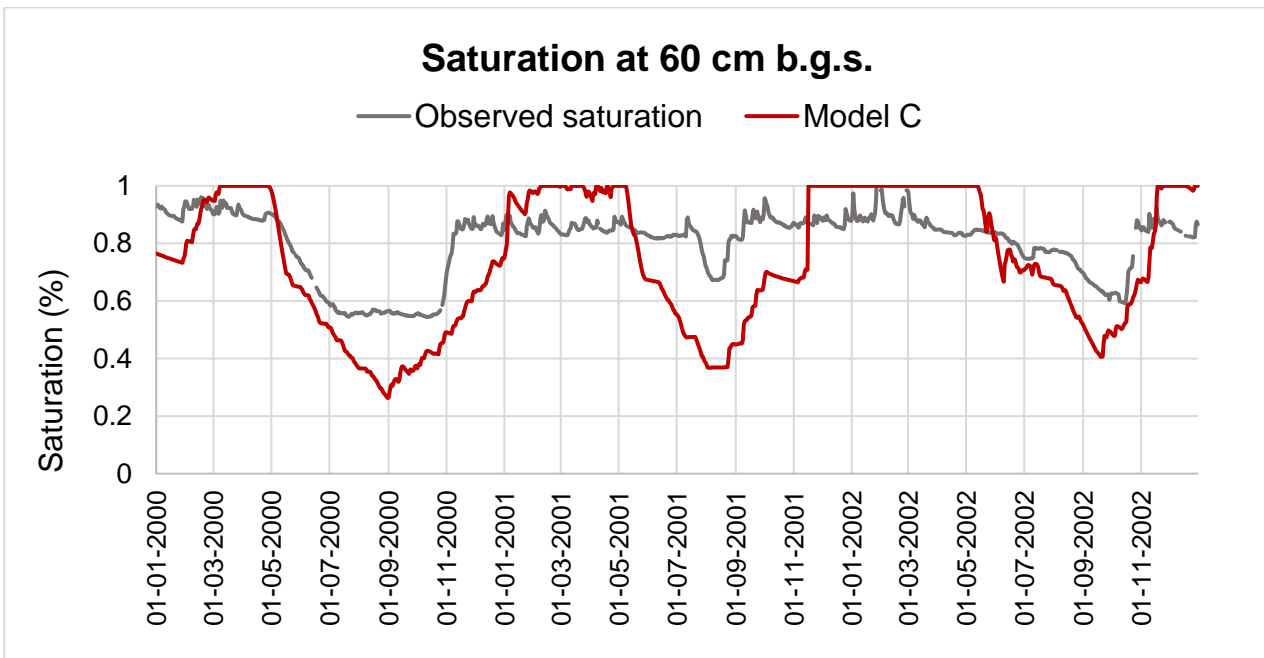


Figure 51: Simulated saturation (red line) from Model C at 60 cm b.g.s and observed saturation (grey line).

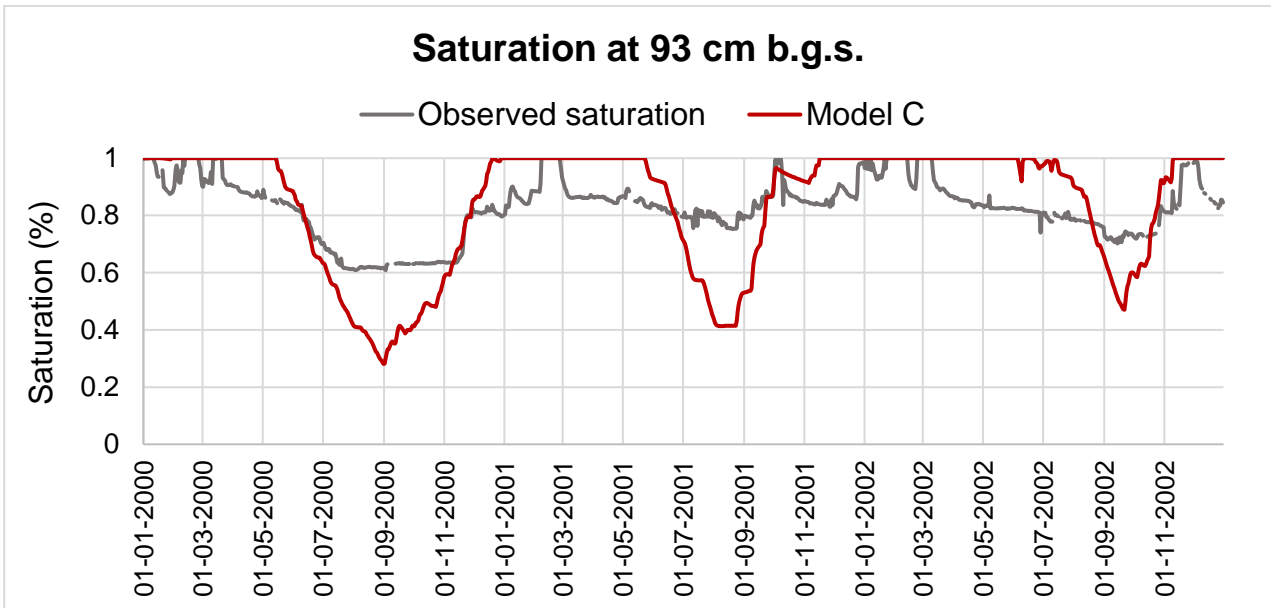


Figure 52: Simulated saturation (red line) from Model C at 93 cm b.g.s and observed saturation (grey line).

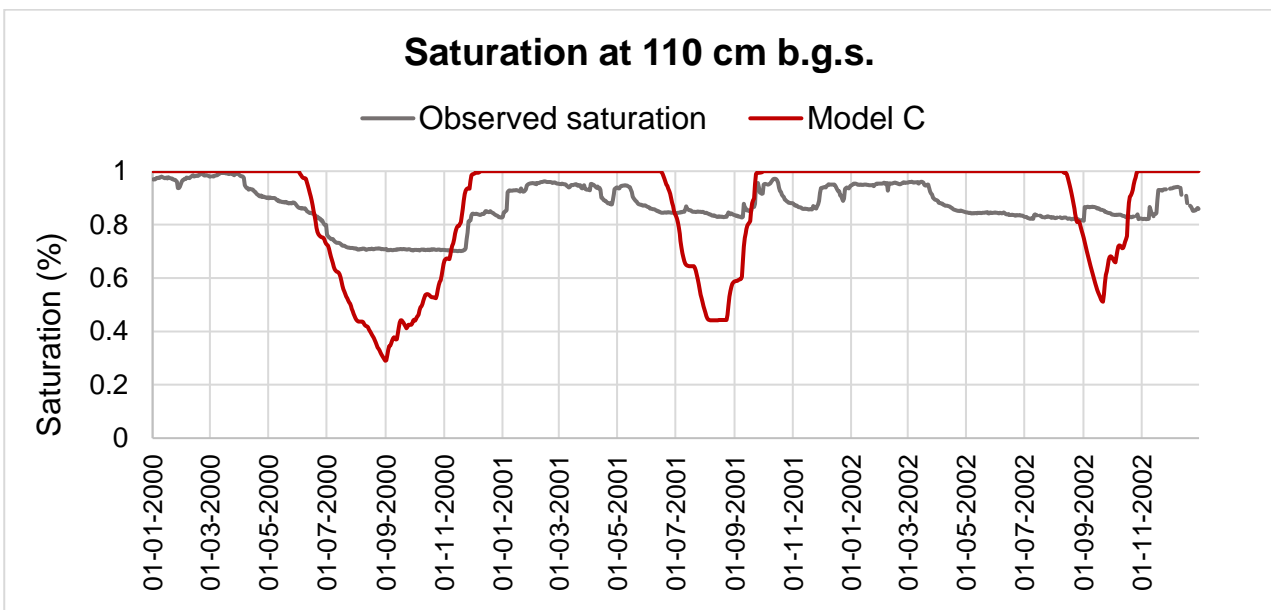


Figure 53: Simulated saturation (red line) from Model C at 110 cm b.g.s and observed saturation (grey line).

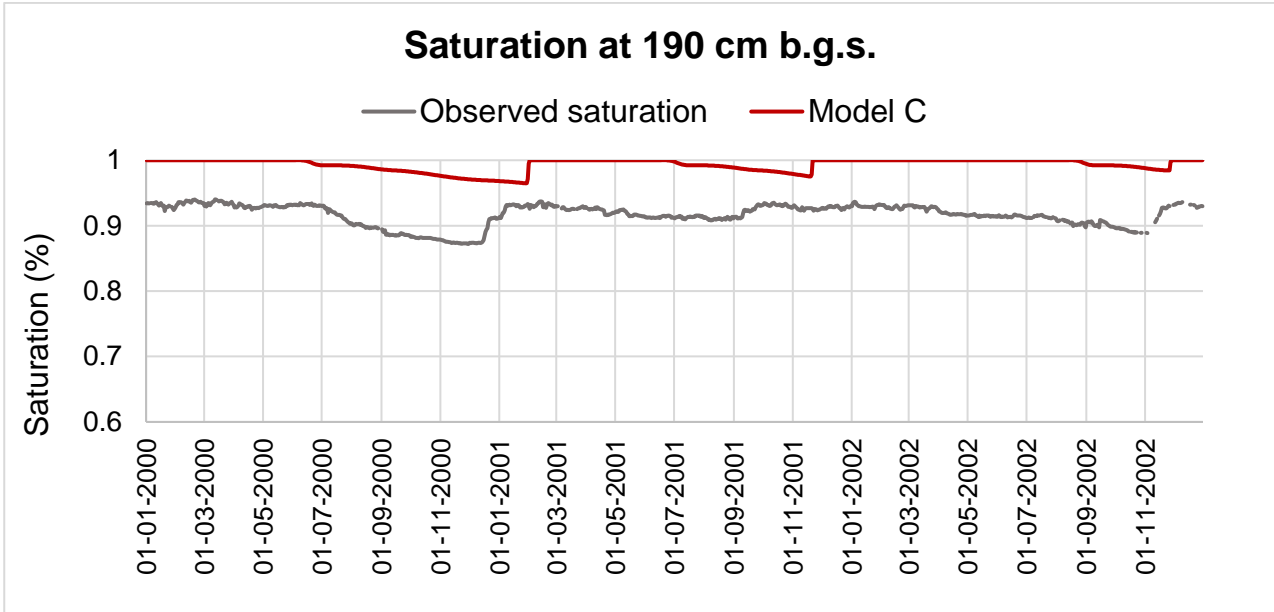


Figure 54: Simulated saturation (red line) from Model C at 190 cm b.g.s and observed saturation (grey line).

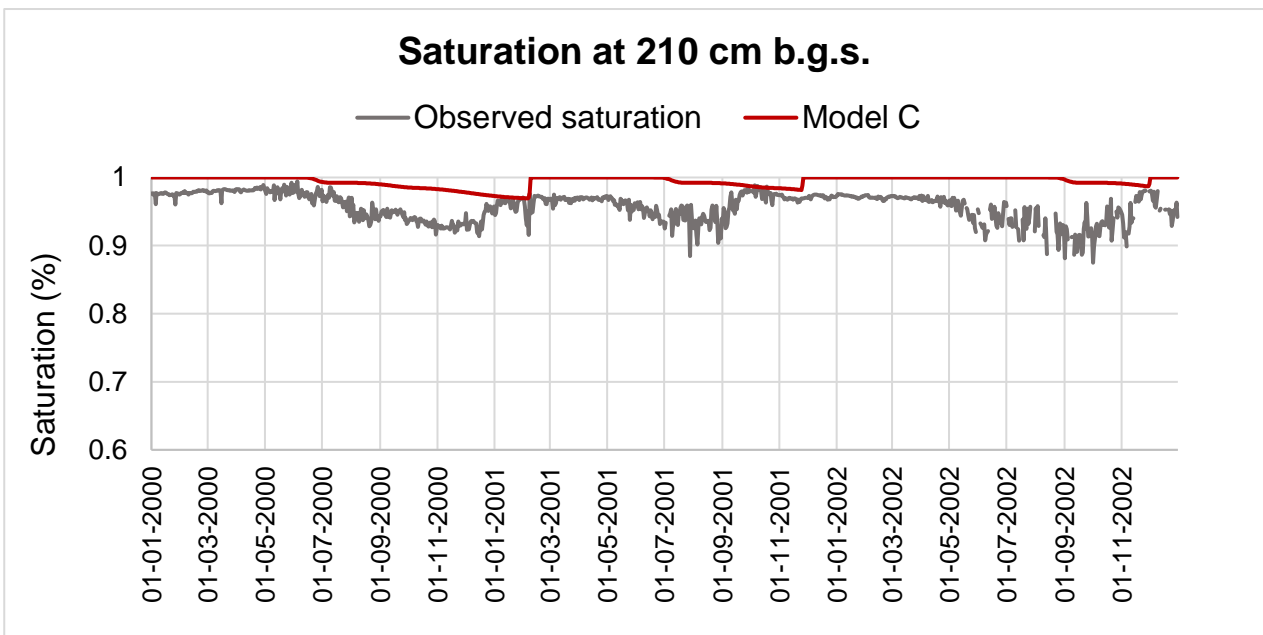


Figure 55: Simulated saturation (red line) from Model C at 210 cm b.g.s and observed saturation (grey line).

### Appendix 4 - Model D

Parameter definitions:-

Name	Trans-formation	Change limit	Initial value	Lower bound	Upper bound
k1	log	factor	10.0000	1.000000E-10	4000.00
k2	log	factor	10.0000	1.000000E-10	4000.00
k3	log	factor	5.000000E-02	1.000000E-10	1000.00
a1	log	factor	7.500000E-02	3.700000E-02	0.145000
a2	fixed	na	3.600000E-02	na	na
a3	log	factor	7.500000E-02	1.600000E-02	0.100000
b1	log	factor	1.89000	1.61000	2.68000
b2	fixed	na	1.56000	na	na
b3	log	factor	1.89000	1.37000	1.89000
drain	log	factor	1.00000	1.000000E-10	100.000

Figure 56: Parameters values and parameter boundaries used in the inverse calibration of Model D. Screenshot from the PEST .pst file.

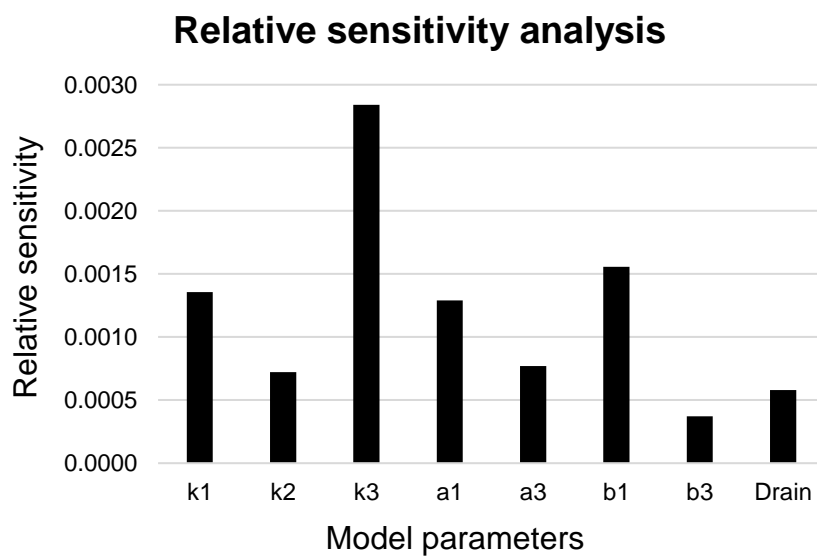


Figure 57: Sensitivity analysis of the parameters in Model D.

**Parameter correlation coefficient matrix**

	<b>K1</b>	<b>K2</b>	<b>K3</b>	<b>a1</b>	<b>a3</b>	<b>b1</b>	<b>b3</b>	<b>Drain</b>
<b>K1</b>	1	-0.75	0.56	-0.56	-0.06	0.20	-0.08	0.20
<b>K2</b>	-0.75	1	-0.40	0.51	-0.20	-0.16	0.15	-0.35
<b>K3</b>	0.56	-0.40	1	-0.71	-0.26	0.27	-0.42	0.13
<b>a1</b>	-0.56	0.51	-0.71	1	0.02	-0.44	0.16	-0.14
<b>a3</b>	-0.06	-0.20	-0.26	0.02	1	-0.19	0.20	-0.12
<b>b1</b>	0.20	-0.16	0.27	-0.44	-0.19	1	0.53	0.26
<b>b3</b>	-0.08	0.15	-0.42	0.16	0.20	0.53	1	0.26
<b>Drain</b>	0.20	-0.35	0.13	-0.14	-0.12	0.26	0.26	1

Figure 58: Parameter correlation coefficient matrix for parameters in Model D.

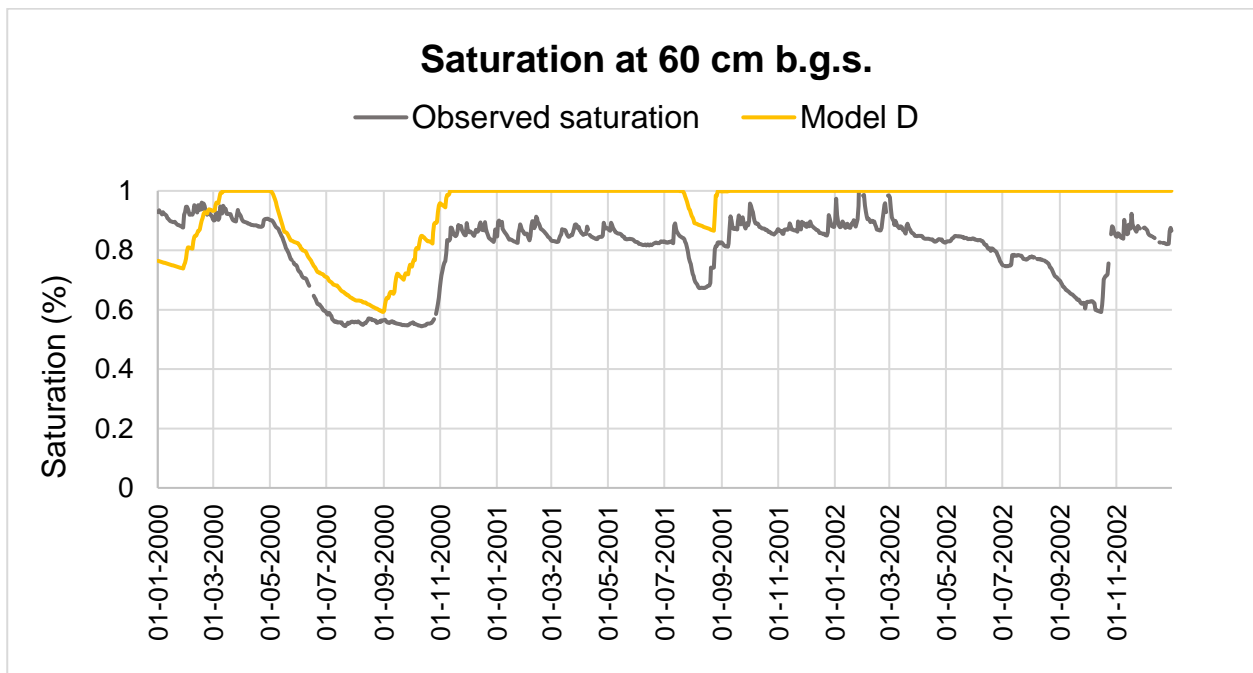


Figure 59: Simulated saturation (yellow line) from Model D at 60 cm b.g.s and observed saturation (grey line).

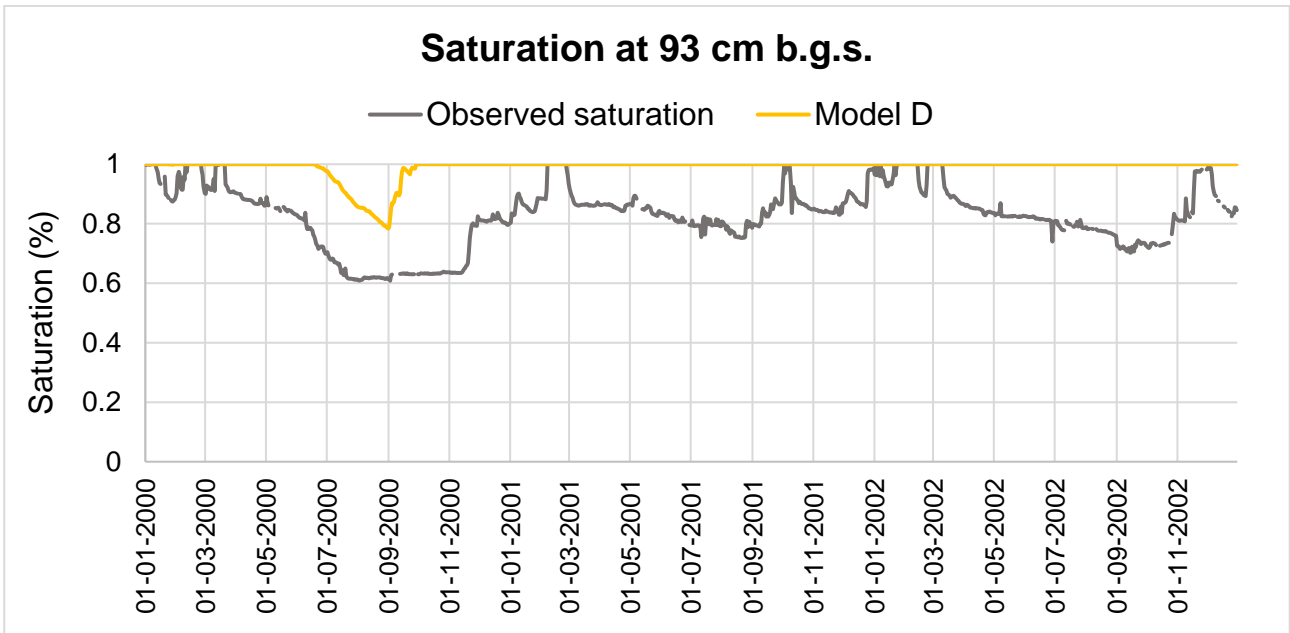


Figure 60: Simulated saturation (yellow line) from Model D at 93 cm b.g.s and observed saturation (grey line).

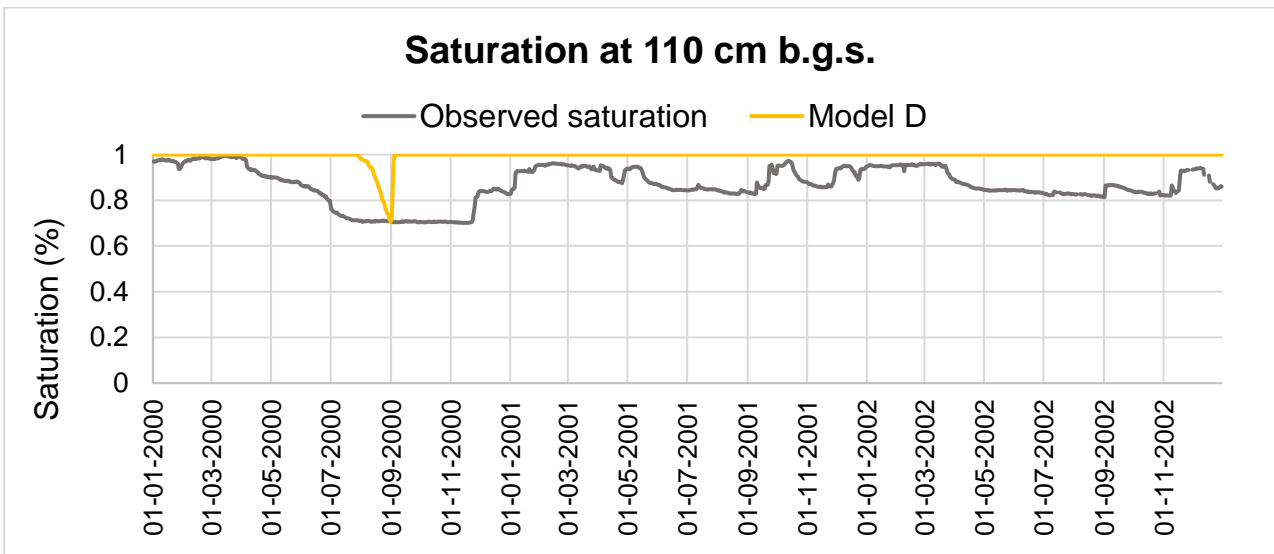


Figure 61: Simulated saturation (yellow line) from Model D at 110 cm b.g.s and observed saturation (grey line).

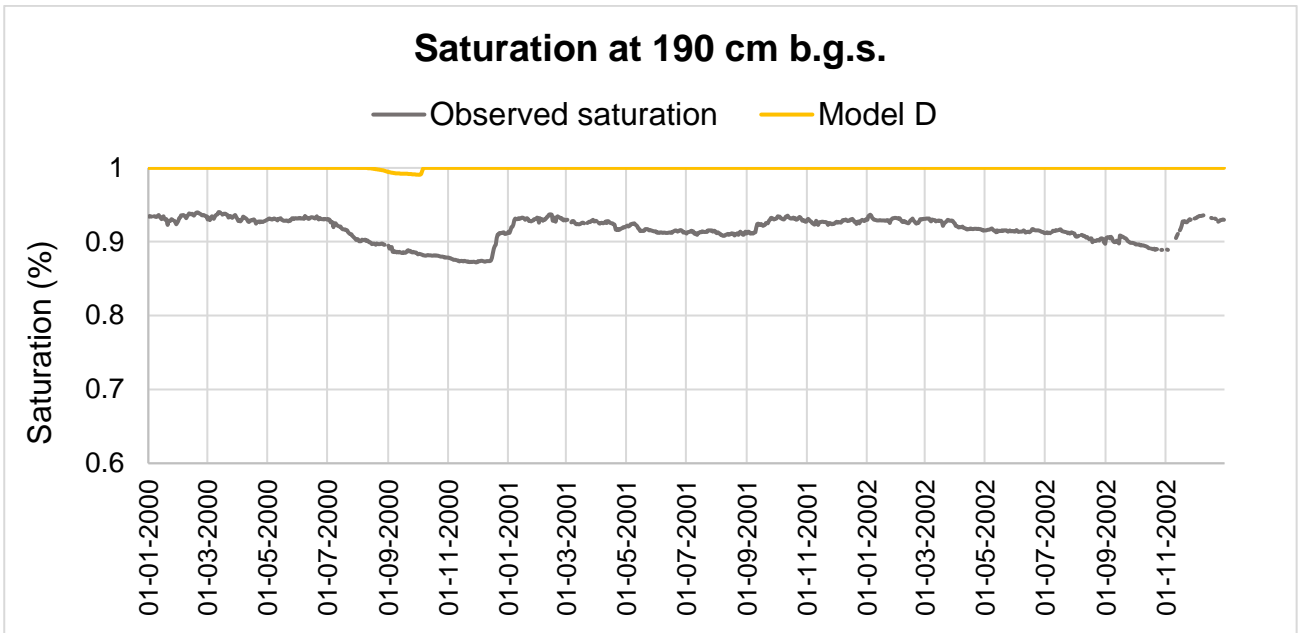


Figure 62: Simulated saturation (yellow line) from Model D at 190 cm b.g.s and observed saturation (grey line).

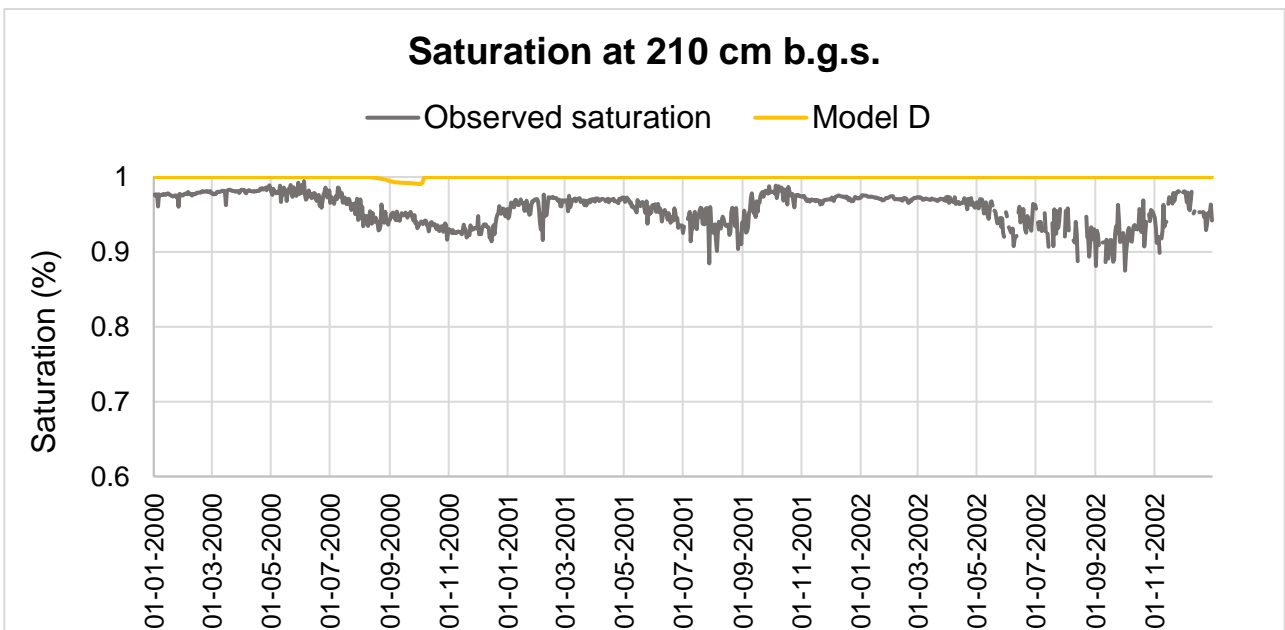
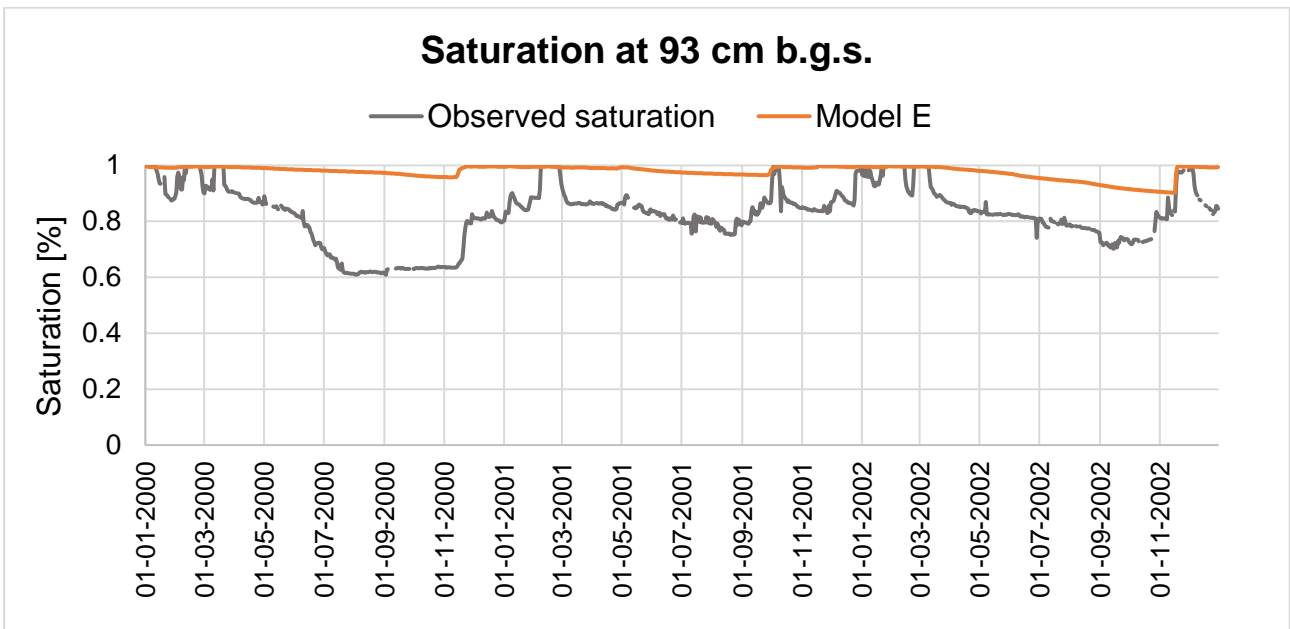
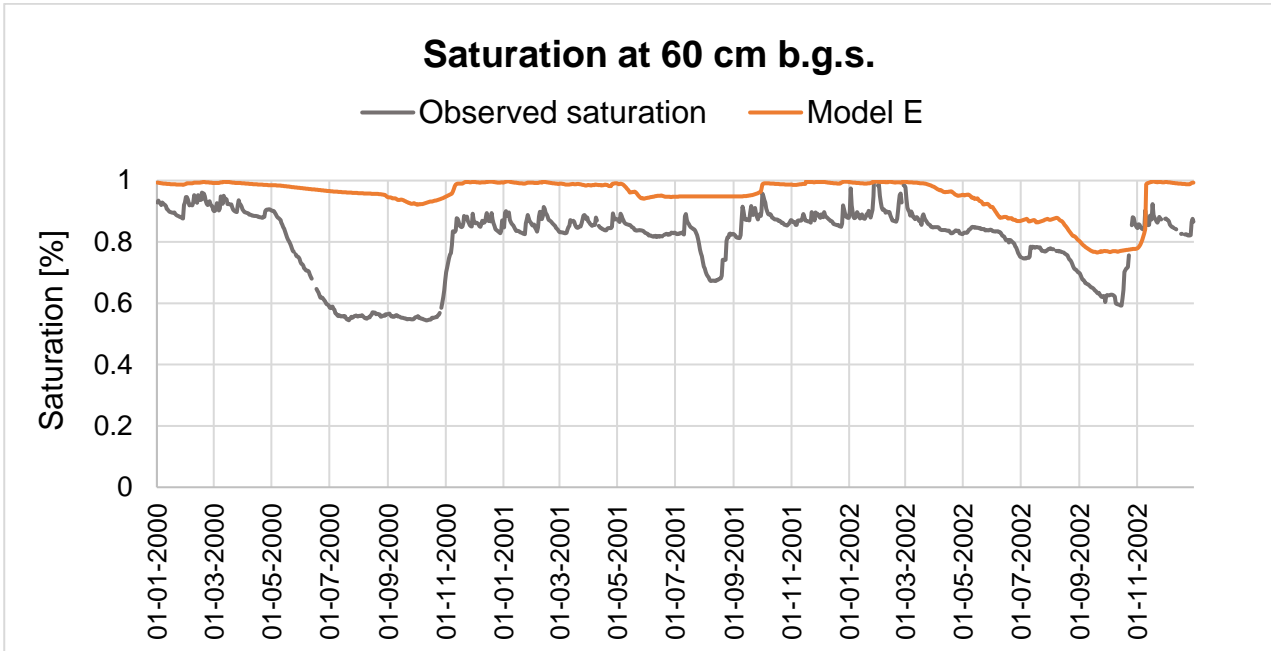
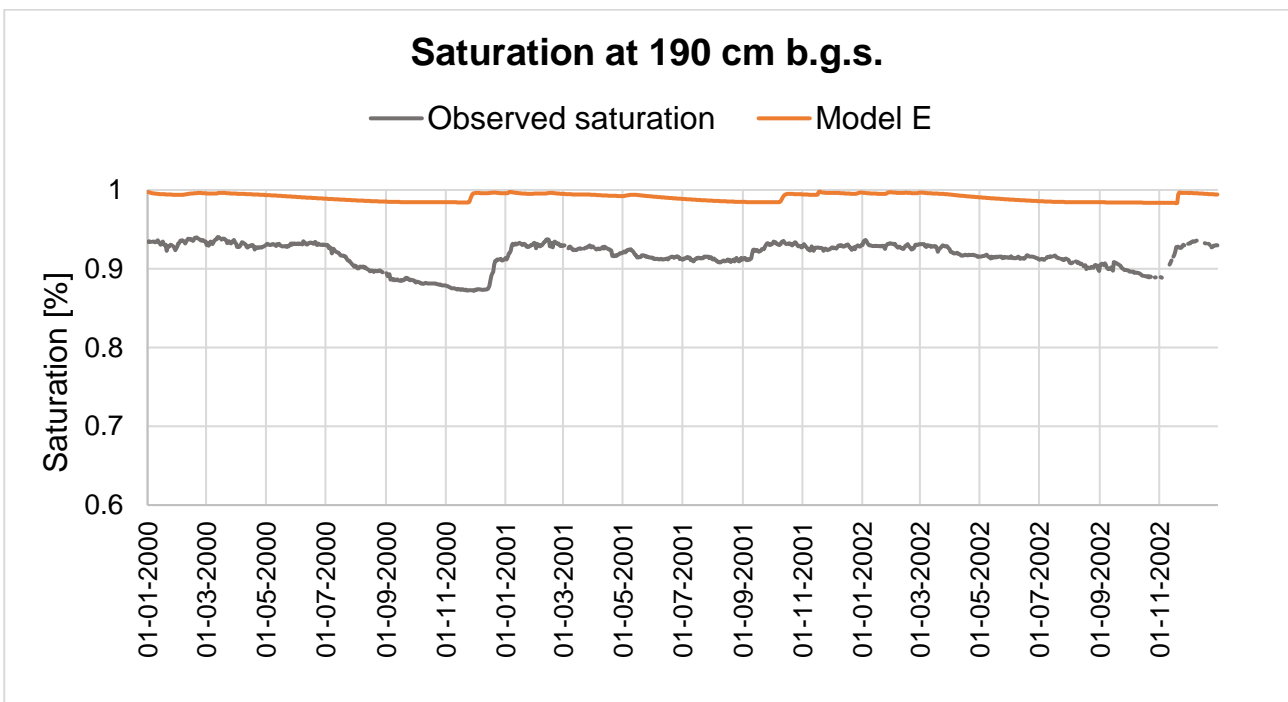
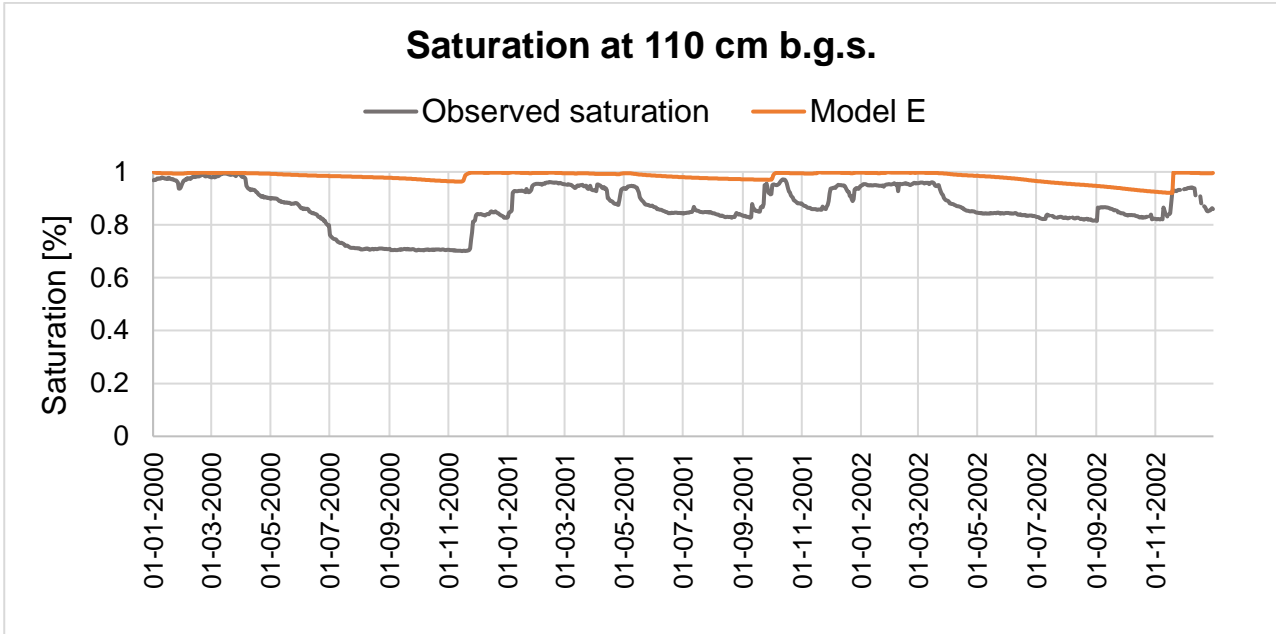
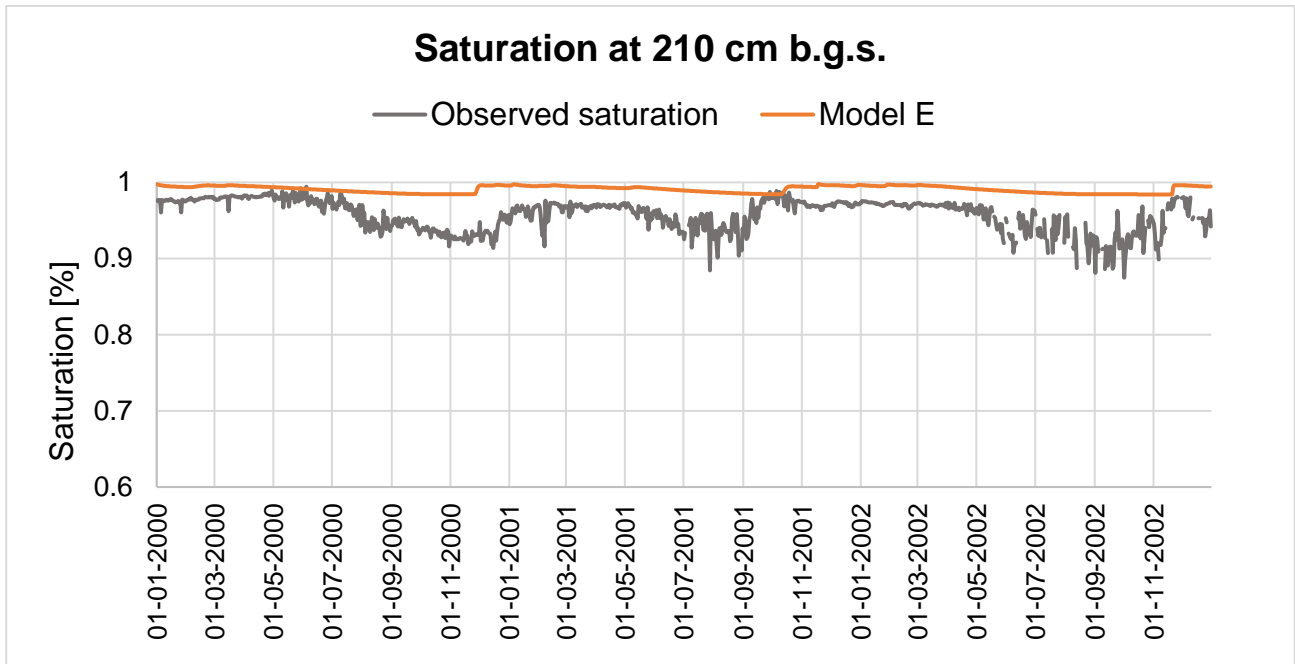


Figure 63: Simulated saturation (yellow line) from Model D at 210 cm b.g.s and observed saturation (grey line).

Appendix 5 - Model E







Appendix 6 - Fieldwork

Calculation sheets for the well permeameter method:

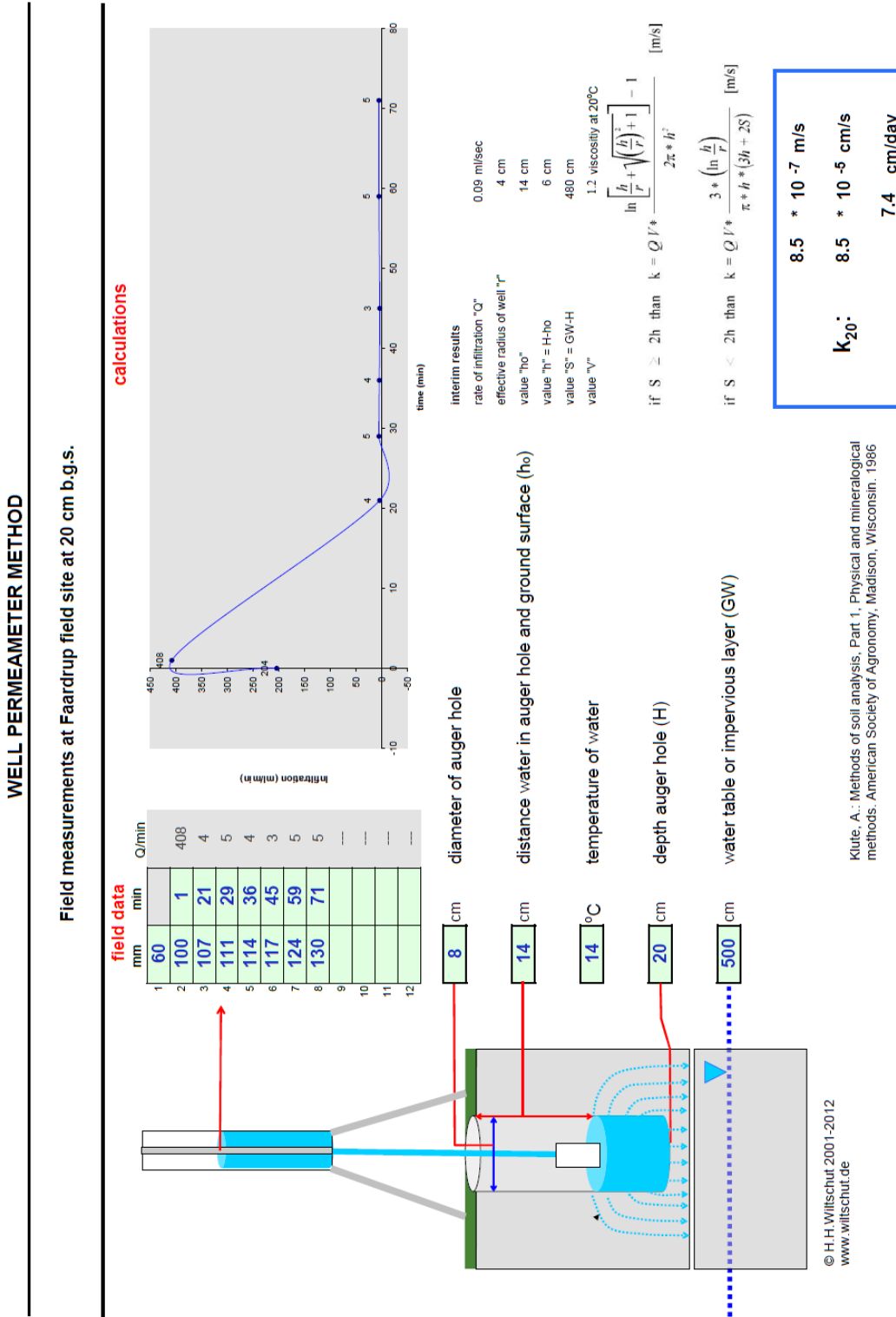
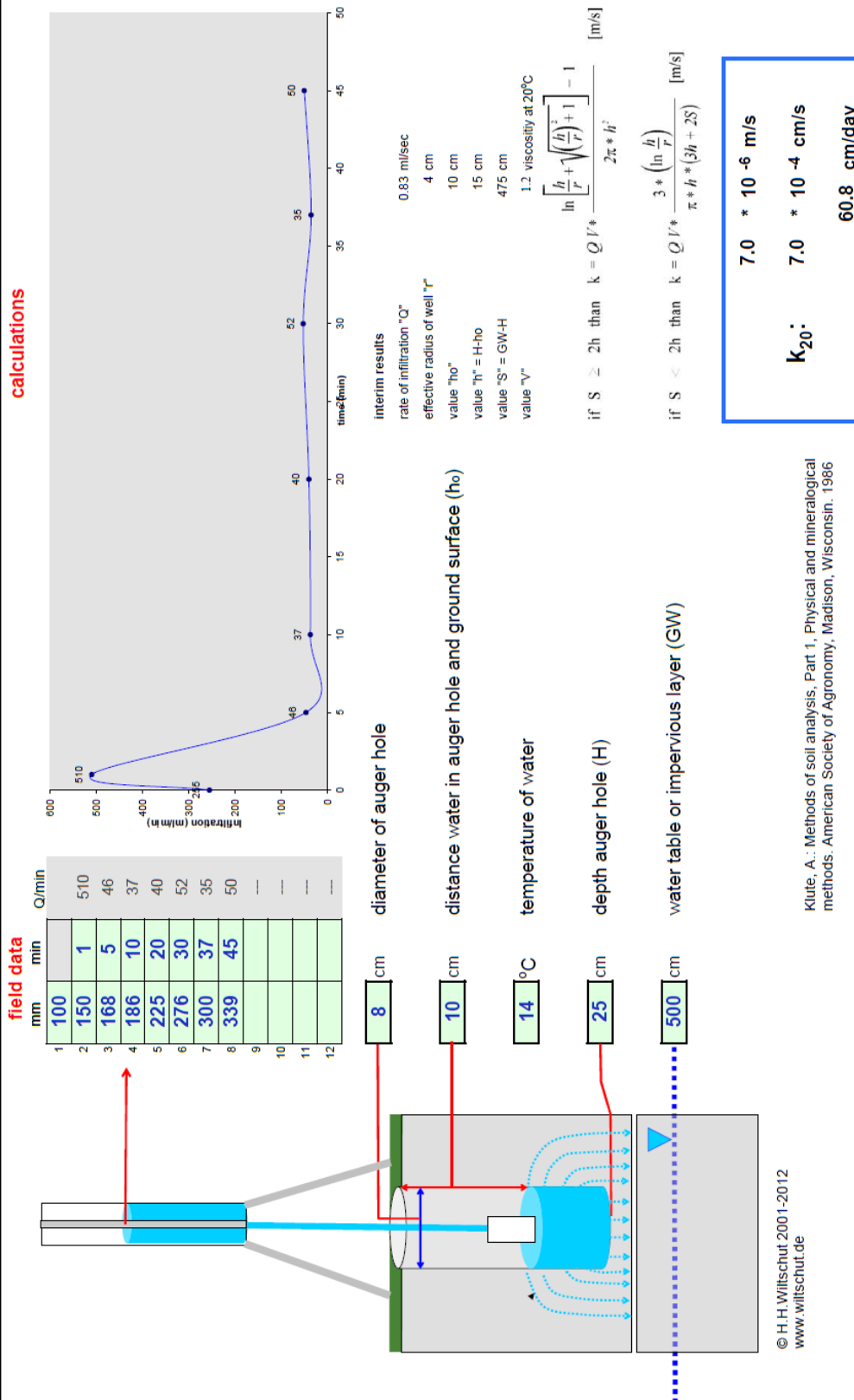


Figure 64: Calculation sheet for the permeameter measurements at location L3.

WELL PERMEAMETER METHOD

Field measurements at Faardrup field site at 25 cm b.g.s. (1)



© H.H.Wiltschut 2001-2012  
www.wiltschut.de

Klute, A.: Methods of soil analysis, Part 1, Physical and mineralogical methods. American Society of Agronomy, Madison, Wisconsin. 1986

Figure 65: Calculation sheet for the permeameter measurements at location L2.

**WELL PERMEAMETER METHOD**

Field measurements at Faardrup field site at 25 cm b.g.s. (2)

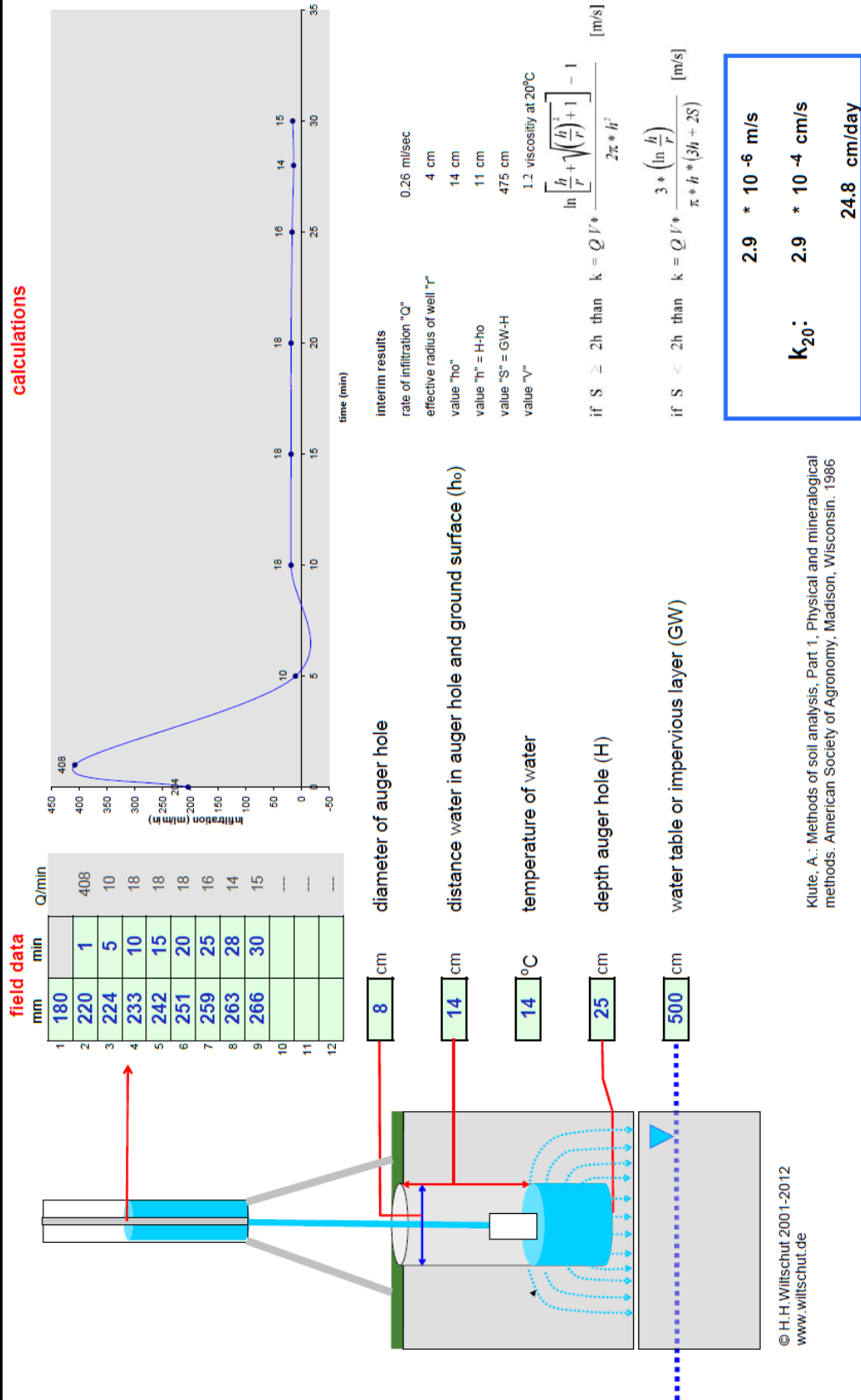


Figure 66: Calculation sheet for the permeameter measurements at location L1.

## Appendix 7 - Input files to HydroGeoSphere

In the development of the models in HGS, the following input files were produced for each of the models.

- u\_1d.grok (the model file)
- u\_1d.mprops (matrix properties)
- u\_1d.etprops (evapotranspiration properties)
- u\_1d.oprops (overland flow properties)
- u\_1d.dprops (dual properties)

The input files for Model A, Model B, Model C, Model D, and Model E has been submitted to supervisor Karsten Høgh Jensen (KU) .